Summer 8-15-2017

Numerical Methods for Nonlinear Optimal Control Problems and Their Applications in Indoor Climate Control

Runxin He
Washington University in St. Louis

Washington University in St. Louis

School of Engineering and Applied Science

Department of Electrical & Systems Engineering

Dissertation Examination Committee:
Humberto Gonzalez, Chair
Ramesh Agarwal
ShiNung Ching
Zachary Feinstein
Jr-Shin Li

Numerical Methods for Nonlinear Optimal Control Problems and Their Applications in Indoor Climate Control

by

Runxin He

A dissertation presented to
The Graduate School
of Washington University in
partial fulfillment of the
requirements for the degree
of Doctor of Philosophy

August 2017
Saint Louis, Missouri

Contents

List of Tables . . . . . **v**

List of Figures . . . . . **vi**

Acknowledgments . . . . . **viii**

Abstract . . . . . **x**

1 Introduction **1**
1.1 Indoor computational fluid dynamic model 2
1.2 Optimal control for HVAC system 3
1.3 Estimators for HVAC system 6
1.4 Numerical algorithm to nonlinear optimal control 8
1.5 Contributions of this work 10
1.6 Organization of the dissertation 12

2 Notations and CFD Model **13**
2.1 Notations 13
2.2 PDE-based CFD model 14

3 HVAC System's Efficiency Improvement via Zoned Control **21**
3.1 Problem statement 21
3.2 Numerical implementation 22
3.2.1 FEM Discretization 23
3.2.2 Optimal Control Discretization 25
3.3 Simulations 25
3.3.1 Nonlinear Navier-Stokes Model 27
3.3.2 Linearized Navier-Stokes model 30
3.4 Chapter conclusion 31

4 Gradient-Based Estimation of Indoor Air Flow and Geometry Configurations via PDE-based CFD Model **33**
4.1 Optimization problem statement 34
4.2 Costate-based gradient computation 36
4.2.1 Adjoint equations and Fréchet derivatives 37

4.2.2 Gradient-Based Optimization Algorithm . . . 39
4.3 Simulations . . . 40
4.3.1 Probabilistic estimation method . . . 41
4.3.2 Estimation using three thermostats . . . 43
4.3.3 Estimation using only one thermostat . . . 44
4.3.4 Memory usage comparison . . . 47
4.4 Chapter conclusion . . . 48

5 MPC for Indoor Thermal Comfort via PDE-based CFD Model . . . 49
5.1 Problem statement . . . 50
5.1.1 Framework of the MPC for indoor comfort . . . 50
5.1.2 CFD model and building configurations . . . 50
5.1.3 Predicted Mean Vote Index and Its Approximation . . . 54
5.1.4 Optimization Problem and Model Predicted Control . . . 57
5.2 Methods . . . 59
5.2.1 Adjoint Equations of CFD model . . . 60
5.2.2 Fréchet Derivatives of optimization problems . . . 61
5.2.3 Gradient-Based Optimization Algorithm . . . 63
5.3 Simulations . . . 67
5.3.1 Simulation with different door configurations and target locations . . . 68
5.3.2 Simulation with different personal variables related to PMV . . . 72
5.3.3 Memory and time usage analysis . . . 73
5.4 Chapter conclusion . . . 75

6 Numerical Synthesis of Pontryagin Optimal Control Minimizers Using Sampling-Based Method . . . 77
6.1 Problem statement . . . 78
6.2 Optimal conditions for optimal control . . . 81
6.2.1 Optimality Functions . . . 81
6.2.2 Gradient descent methods for relaxed problems . . . 84
6.3 Synthesis of relaxed optimal inputs . . . 88
6.3.1 Vector field representation . . . 88
6.3.2 Sampled-Based Synthesis . . . 90
6.4 Simulation results . . . 92
6.4.1 Constrained LQR . . . 93
6.4.2 Quadrotor helicopter . . . 96
6.5 Chapter conclusion . . . 98

7 Numerical Sampling-based Method to Pontryagin Optimal Control Minimizers in State-constrained Problems . . . 101
7.1 Problem statement . . . 101
7.1.1 Preliminaries . . . 102

7.1.2 Conceptual optimal control problem . . . 103
7.2 Optimality conditions for optimal control . . . 106
7.2.1 Optimality functions . . . 107
7.2.2 Gradient descent methods for relaxed problems . . . 110
7.3 Synthesis of relaxed optimal inputs . . . 113
7.3.1 Vector field representation . . . 114
7.3.2 Sampled-based synthesis . . . 115
7.3.3 Parallel computation . . . 119
7.4 Simulations . . . 122
7.4.1 Plan attack angle control . . . 122
7.4.2 Indoor thermal comfort control . . . 125
7.5 Chapter conclusion . . . 129

8 Conclusions . . . 130
8.1 Summary and conclustions . . . 130
8.2 Future directions . . . 131

Appendix A Proofs in Chapter 2 . . . 133

Appendix B Derivations in Chapter 4 . . . 141
B.1 Derivation of adjoint equations . . . 141
B.2 Derivation of Fréchet derivatives . . . 142

Appendix C Proofs in Chapter 5 . . . 144
C.1 Existence of Lagrange Multipliers . . . 144
C.2 Proof of Fréchet Derivatives . . . 148
C.3 Convergence of the Algorithm . . . 157
C.4 Finite Element Approximation . . . 158

Appendix D Proofs in Chapter 7 . . . 166

References . . . 174

Vita . . . 185

List of Tables

3.1 Properties for FEM basis. 23

List of Figures

3.1 Results of the experiments in section 3.3.1. Walls are shown in shaded black, and heaters are shown in shaded blue. Values are in [°C] with respect to T_A. 28
3.2 Air flow of the experiment in section 3.3.1 with target area Ω, i.e., the whole apartment. Average air speed in the apartment is 0.11[m/s]. Walls are shown in shaded black. Two outlets and one inlet of the HVAC system are marked as Γ_o, Γ'_o and Γ_i respectively. 29
3.3 Results of the experiments in section 3.3.1 and 3.3.2. Columns: (A) nonlinear model with zoned control, (B) nonlinear model without zoned control, (C) linearized model with zoned control. Each column shows the median (red line), mean (red box), and first-to-third quartiles (blue box). 29
3.4 Absolute error in temperature distribution, with respect to *FEniCS* simulation, for the linearized model in section 3.3.2, at time t_f with target area Ω_z. Values are in [°C]. 31

4.1 Floor plan of the apartment simulated in section 4.3. 42
4.2 Results of the experiments in section 4.3.2. Columns: (B) Banks and Bihari's method, (G) Gradient-based method, algorithm 1. 43
4.3 Initial temperature π_0 in [°C] with respect to T_A. 45
4.4 Estimation error of π_0 by Banks and Bihari's method, when all doors are closed. 45
4.5 Estimation error of π_0 by gradient-based method, algorithm 1, when all doors are closed. 46
4.6 Results of the experiments in section 4.3.3. Columns: (B) Banks and Bihari's method, (G) Gradient-based method, algorithm 1. 46
4.7 Memory usage in [GB] of the experiments in Sec. 4.3.4. 47

5.1 Single temperature loop control for HVAC. 51
5.2 Our control for HVAC. 52
5.3 PMV index scales to thermal sensations. 54
5.4 The illustration of the model predicted control during $[t_1, t_3]$. 57
5.5 Gradient-based estimation algorithm 65
5.6 Gradient-based optimal control algorithm 66
5.7 Floor plan for simulated apartment. 67
5.8 Results of the experiments in Section 5.3.1. 69

5.9 Statistic results of simulations in Section 5.3.1 with 12 target areas. Columns in figure 5.9a: (M) is MPC with doors configuration estimator, (F) is MPC whose fixed doors configurations are fixed to be closed. Each column shows the median (red line), mean (red box), and first-to-third quartiles (blue box). The average estimation errors of θ in figure 5.9b are calculated as $e_\theta = \frac{1}{n_d}\sum_{i=1}^{n_d} |\theta_i - \hat{\theta}_i|$, where $\hat{\theta}_i$ are the real door's state and θ_i are the estimation from our MPC's estimator. 70
5.10 Energy usage, in [kW · h], with different combination of metabolic rates, [W/m^2], and clothing index, in [m^2 °C/W], in Section 5.3.2. $T_a = 20.0$[°C], in figure 5.10a, $I_{cl} = 0.155$ [m^2 °C/W], in figure 5.10b, $M = 81.0$[w/m^2]. 72
5.11 Results of the experiments in Section 5.3.3. 74

6.1 Trajectory of states $x_{1,2,3}$ under optimal control in section 6.4.1. The states start from the origin (blue dot) to the end (blue triangle), which is (-0.29, -0.56, -0.06). 94
6.2 Results of the simulation in section 6.4.1, a contrained LQR problem. . . . 95
6.3 The helicopter's trajectory moves from the origin (blue dot) down to (-1.12, -1.12, -0.98) (blue triangle) under the optimal control. Blue arrows are perpendicular vectors to the helicopter's plane, which are used to represent body axes. 99
6.4 The helicopter's trajectory climbs from the origin up to (1.23, 1.23, 1.18) (blue triangle) under the optimal control. Blue arrows are perpendicular vectors to the helicopter's plane, which are used to represent body axes. 100

7.1 Simulation results for problem (7.35). 126
7.2 Simulation results for problem (7.36). 128

Acknowledgments

Firstly, I am sincerely grateful to my research advisor, Dr. Humberto Gonzalez, for his continuous guidance and support for my research at Washington University and my career after graduation. He has given me a lot of freedom to explore research topics that interest me the most, and supported my exploration with advice and encouragement.

Secondly, I wish to thank my dissertation defense and preliminary committee members, Dr. Ramesh Agarwal, Dr. ShiNung Ching, Dr. Zachary Feinstein, Dr. Jr-Shin Li, and Dr. Hiro Mukai for their valuable suggestions.

I further thank my girlfriend, Linyun He, all my achievements would not be possible without her continuous support. Also I am thankful to my friends here in the university for their helps.

I owe my deepest thanks to my beloved parents for their unselfish love.

Runxin He

Washington University in Saint Louis

August 2017

Dedicated to my parents.

ABSTRACT OF THE DISSERTATION

Numerical Methods for Nonlinear Optimal Control Problems and Their Applications in Indoor Climate Control

by

Runxin He

Doctor of Philosophy in Electrical Engineering

Washington University in St. Louis, August 2017

Research Advisor: Humberto Gonzalez

Efficiency, comfort, and convenience are three major aspects in the design of control systems for residential Heating, Ventilation, and Air Conditioning (HVAC) units. In this dissertation, we study optimization-based algorithms for HVAC control that minimizes energy consumption while main- taining a desired temperature, or even human comfort in a room. Our algorithm uses a Computer Fluid Dynamics (CFD) model, mathematically formulated using Partial Differential Equations (PDEs), to describe the interactions between temperature, pressure, and air flow. Our model allows us to naturally formulate problems such as controlling the temperature of a small region of interest within a room, or to control the speed of the air flow at the vents, which are hard to describe using finite-dimensional Ordinary Partial Differential (ODE) models. Our results show that our HVAC control algorithms produce significant energy savings without a decrease in comfort.

Also, we formulate a gradient-based estimation algorithm capable of reconstructing the states of doors in a building, as well as its temperature distribution, based on a floor plan and a set of

thermostats. The estimation algorithm solves in real time a convection-diffusion CFD model for the air flow in the building as a function of its geometric configuration. We formulate the estimation algorithm as an optimization problem, and we solve it by computing the adjoint equations of our CFD model, which we then use to obtain the gradients of the cost function with respect to the flow's temperature and door states. We evaluate the performance of our method using simulations of a real apartment in the St. Louis area. Our results show that the estimation method is both efficient and accurate, establishing its potential for the design of smarter control schemes in the operation of high-performance buildings.

The optimization problems we generate for HVAC system's control and estimation are large-scale optimal control problem. While some optimal control problems can be efficiently solved using algebraic or convex methods, most general forms of optimal control must be solved using memory-expensive numerical methods. In this dissertation we present theoretical formulations and corresponding numerical algorithms that can find optimal inputs for general dynamical systems by using direct methods. The results show these algorithms' performance and potentials to be applied to solve large-scale nonlinear optimal control problem in real time.

Chapter 1

Introduction

Heating, Ventilation, and Air Conditioning (HVAC) systems are complex mechanical devices that control the climate of all kinds of buildings, large and small, residential and commercial. In most situations, HVAC systems are used to maintain comfortable temperatures, while limiting both humidity and air speed away from undesirable levels, as described in standards such as ASHRAE 55 [7]. Yet, current HVAC systems are typically controlled in a centralized or static fashion, disregarding variations in building configuration (windows or doors opened or closed dynamically), human activity, or even human perception of environmental conditions [14]. While, on the other hand, buildings currently account for more than 40% of the total energy consumption in the U.S. [120], and they cost $130 billion in energy leakage and inefficiency [121]. For this reason many research groups are developing new control algorithms to improve the performance and efficiency of HVAC systems in buildings [116, 50, 2, 115].

In the dissertation, we present a control and estimation framework, based on a PDE-constrained optimal control problem, that takes into account localized conditions at the

room or even person scale. Also numerical methods to solve corresponding nonlinear optimal control problems are studied, which show the potential to make our PDE-constrained HVAC system control fast enough for real time applications.

1.1 Indoor computational fluid dynamic model

In the aspect of architecture engineering and computational physics, the dynamic behavior of the air flow is mathematically complex due to turbulent dynamical responses [14]. Nonetheless, even if the flow is turbulent inside air ducts at reasonable ventilation rates, its response is laminar in larger areas [117, 20], thus it can be analyzed using simpler non-turbulent Computer Fluid Dynamics (CFD) models. Many results can be found in the literature using different variations of CFD models to study heating and ventilation situations in buildings. Bathe and Zhang [20] studied Navier–Stokes incompressible and compressible fluid flows with structural interaction. Sinha, Arora and Roy [117] studied the velocity and temperature distribution inside a room heated by a warm air stream introduced at various positions with an incompressible laminar Navier-Stokes model. Schijndel [124] worked on building a full 3D indoor dynamic distribution of heat, air flow and moisture. Waring and Siegel [131] used CFD model to study the air quality inside a building with various HVAC filters, heat exchangers, and ducts.

There are quite a lot researches on CFD model with partial differential equations both theoretically and numerically. For example, from the theoretical aspects, the existence and smoothness of the solutions of the non-turbulent models has been proved under suitable conditions [47, 57], and they can be used together with gradient-based optimization algorithms. Ito [84] studied the theoretical optimal control of stationary Navier-Stokes equations coupled

with the heat transfer equation, finding necessary conditions for the existence of an optimal argument. For numerical computation, Finite Element Method [140] (FEM) is applied to simulate CFD models with complicated geometries. Many well-established numerical solvers are also implemented for researchers and engineers, such as COMSOL Multiphysics [124] and FEniCS [4]. However, most numerical solvers which are used by researchers to find solutions of CFD models, for example COMSOL Multiphysics [124] are not suitable for integration with gradient-based optimization algorithms, which require the explicit formulation of all the approximating equations and their gradients. It is for this reason that we formulated our own numerical discretization of the CFD model using the FEM method and mixed boundary conditions.

1.2 Optimal control for HVAC system

Standard HVAC systems in market these days typically use a small number of thermostats, together with simple temperature regularization loops [58], to follow a temperature set point in each area of interests.

State-of-the-art results in the area of HVAC control can be categorized within two main trends. The first corresponds to learning-based methods, such as artificial intelligence and neural networks [56, 136, 81]. However, learning-based methods depends on their training data and building plans too much and their after-trained models are not flexible to apply to other environment [98]. The second corresponds to model-based predictive methods, which describe the dynamic evolution of building climate variables using first-principle physical models, or approximations of these models.

Many results exist in the control of HVAC units using optimization-based methods. Among those model-based predictive methods, MPC stands out due to its flexible mathematical formulation and its robust performance in real-world implementations [80, 133, 97]. Indeed, MPC has become one of the standard methods for solving constrained multivariate control problems in process control applications [2]. MPC has been applied to zoned temperature control and temperature regularization in the past, showing significant improvements in energy efficiency compared to other classical control methods [106]. Goyal and Barooah [70] studied in detail the use of RC network circuits to model the temperature within buildings. Kalman and Borelli [89], as well as Hazyuk et al. [74, 75], used low-dimension ODE-based models to control a HVAC unit using Model Predictive Control (MPC). Aswani et al. [12] used a learning-based MPC algorithm [11] to account for unmodeled dynamics and disturbance in ODE models when controlling HVAC units. Domahidi et al. [49] and Fux et al. [59] also used a learning-based method and MPC, the first using ADABOOST to estimate uncertainties and the second using an Extended Kalman Filter. Ma et al. [95] used Stochastic MPC to handle disturbances in the control of HVAC units, also using ODE models. These results show that optimal control strategies increase the efficiency of HVAC systems, yet the use of ODE (i.e., concentrated parameter) models means that there is no detailed control of the air flow or of the temperature in arbitrary points in a room.

In order to get rid of the inaccurate predictions by concentrated models, previous studies in literature focused on PDE-constrained optimal control of HVAC system. In recent years, Burns et al. [29, 33, 34] studied the optimal control of HVAC systems with linearized Navier-Stokes models around an arbitrary steady-state solution, and then used a Linear Quadratic Regulator (LQR) controller to find the optimal solution. However, the papers [19] and [111]

showed that in order to apply LQR method to Navier-Stokes Equation with Dirichlet boundary control, an extra compatibility condition needs to be satisfied. Or alternatively, a penalized Neumann condition approximation control is introduced [79, 34] to approach the optimal Dirichlet control problem, which however have no physical or mechanical meaning in HVAC system. But their preliminary results show that PDE models, usually considered too complex for online numerical calculations, can be effectively used for building control. Yet the authors' use of linearized approximations mean that the optimal solution is accurate only if it is close to the original steady-state linearization point, which poses a serious limitation in practical applications. Moreover, most simulations about PDE-constrained optimal control for HVAC system in literature are modeled in simple geometry, instead of real building plans.

In my study, we use a nonlinear non-turbulent Navier-Stokes model together with a convection-diffusion heat equation to model the climate in a building directly. We discretize this model using a Finite Element Method (FEM), and we use it to find the optimal control for the HVAC system in a building. Furthermore, we show via simulations that it is possible to design control objectives that are functions of the residents' locations, which greatly increase the efficiency of the HVAC system.

As mentioned above, many HVAC control systems in literature deal with thermal comfort simply by controlling air temperature, such that occupants are assumed to be comfortable as long as the room temperature was within a certain range, instead of quantifying resident's thermal comfort or considering other variables [101, 10, 100]. However, since thermal comfort has a great influence on the productivity and satisfaction of indoor building occupants, the focus of HVAC system control is not on only the energy efficiency, but also the fulfillment of resident's comfort requirement. The thermal comfort is a complicated quantity, a

large number of thermal comfort quantification methods have been studied these days, and among them the Predicted Mean Vote (PMV) index [54] is the most popular and standard one according to ASHRAE 55 [7]. Direct incorporation of the PMV in a model predictive control for HVAC systems could raise several challenges and the control algorithms seldom directly optimize a PMV index (or use it in a constraint). One concern relates to the additional computational burden due to the iterative computation of PMV [37]. Past work tried to approximate the PMV with a neural network model [56, 136, 81] or with a linearized parameter model [37, 55]. A second concern relates to the additional cost of sensing [36], in most residential buildings, typically there are no extra sensors to continually measure mean radiant temperature, humidity, or door configurations [14]. However, with help of the development of wearable devices, it is possible to monitor every resident's personal information with their mobile phones or smart watches [87, 134].

In this dissertation, we develop a MPC to optimize the thermal comfort around indoor residents based on CFD model. The thermal comfort is measured by PMV index's approximation and the optimization control pairs the heater's power with fan's speed, not focuses only on temperature regularity. Also the MPC is able to identify indoor climate distribution and an apartment's doors configuration based only on thermostatic data. The optimization problem is PDE-constrained, we mathematically derive a first order gradient-based method to solve the optimization problem which has been shown to be memory-efficient [76].

1.3 Estimators for HVAC system

According to section 1.2, MPC for HVAC systems has been shown to outperform other techniques on certain performance metrics, such as robustness [80], response improvement [133],

and fluctuation reduction [97]. And, it has been widely used to control entire HVAC systems or their important subsystems. However, a real-time MPC algorithm must predict the future state of the system and optimize the relative control strategies based on the system's current state information, and sometimes also on the previous state [2]. A mismatch in the model and an inaccurate initial state will deteriorate the optimal control and may lead to state offsets or even system instability [110] [53]. Retrieving these states from measurements is generally referred to as state estimation [90], and one practical necessity in estimating a process's state variable is an accurate process model with initial conditions.

For linear and non-constraint systems, a Kalman filter [62] can powerfully handle the estimation task, and often it is the standard choice. However, a HVAC system model usually is nonlinear and has inequality state constraints [14], so a general recursive method, like the Kalman filter, is not available [109]. Other optimization-based estimation algorithms have been developed, such as the results by [83] in Partial Differential Equation (PDE) estimation. Banks et al. viewed the parameters for the inverse problem as random variables, and used probabilistic inference methods to estimate the desired parameters [17, 18]. [73] fully discretized a weak form of the Stokes Equations in time and space and identified the system's discontinuous parameters. Based on the success of receding horizon control [96], moving horizon estimation (MHE) has been suggested as a practical strategy to incorporate inequality constraints and nonlinear models in the estimation.

The basic idea of MHE is to reformulate the estimation problem as an optimization problem using a moving, fixed-size estimation window [96]. The fixed moving window bounds the size of the optimization programming. From the basic strategy above, MHE can be understood as similar to MPC, since they share the time horizon approach and the optimization problem needs to be solved repeatedly. Advantages of the MHE formulation are

its explicit consideration of state and parameter constraints and proven stability properties, as shown in [109] [96]. Many works have considered MHE. Valdes-Gonzales, Flaus, and Acuna [122] showed an algorithm for globally convergent MHE, and Jorgensen, Rawlings, and Jorgensen [88] focused on the connection between linear MPC and linear MHE. More recently, a convincing real-time algorithm based on collocation has been presented in Zavala, Laird, and Biegler [137].

Applying the ideas of MHE and PDE-constrained estimator together, my study shows the potential to estimate not only the in-door fluid dynamic distribution but also the building's in-door configurations, for example the the doors' on-off states, in real time.

1.4 Numerical algorithm to nonlinear optimal control

As mentioned in the sections 1.2 and 1.3, the estimation and control related to HVAC system are related to optimal control problem. Optimal control is a theoretical and practical framework that has been widely used to analyze the behavior of controlled dynamical systems [138, 25], and to synthesize actuation actions for dynamical systems in the face of safety, robustness, or uncertainty considerations [32, 22]. While some optimal control problems can be solved using purely analytical or algebraic tools [30], modern computers and dynamical systems embedded in changing environments have led to a surge in numerical methods for optimal control [108]. Numerical methods for optimal control are typically divided into indirect methods, where the optimal solution is found as the solution of a set of equations typically derived from necessary optimality conditions, and direct methods, where the solution is found by iteratively minimizing the cost function at hand.

It is worth noting that while most numerical optimal control methods are provably convergent, they do not necessarily converge to input signals satisfying the Minimum Principle. Indeed, as shown by Polak [103, Sec. 4.2.6] and Schwartz [114], direct numerical methods that rely on explicit time discretization schemes converge to inputs satisfying necessary optimality conditions based on directional derivatives, which are strictly weaker than those resulting from the Minimum Principle. On the other hand, direct methods that converge to inputs satisfying the Minimum Principle can be developed, but often result in impractical implementations that require solving sequences of nonlinear programming problems [69].

It is possible to develop indirect methods that converge to inputs satisfying the Minimum Principle which lead to multiple-point boundary-value problems [108]. For example, a common indirect method is the shooting method [28, 27], which only converges for suitably chosen initial guesses [26].

In this dissertation, we present a theoretical formulation and a corresponding numerical algorithm, capable of finding optimal control inputs that satisfy the Pontryagin Minimum Principle by using a direct method. Our result is founded on the theory of relaxed control, as defined by J. Warga [130, 129], which we use to derive a convergent sampling-based numerical method. Once a relaxed control has been numerically computed, we use a projection operation originally devised for switched dynamical systems by Vasudevan et al. [125, 126], originally inspired by the theoretical work of Berkovitz [24] and Bengea et al. [23], to synthesize arbitrarily accurate approximations of the trajectories generated by the relaxed inputs.

Our result in this dissertation bridges a significant gap between the formulation of conceptual algorithms, which have excellent theoretical properties but fail to provide practical implementations, and implementable algorithms, which converge to input signals that do not necessarily satisfy the Minimum Principle. Moreover, our following method achieves its

goals in a numerically efficient and scalable way, which is suitable for applications where accuracy can be traded for computational speed.

1.5 Contributions of this work

For decades, the design of HVAC systems has been focused on minimizing energy waste by increasing the efficiency in heaters and coolers, or improving insulation of air ducts and exchangers [14]. A recent trend in smart homes has introduced machine learning and Internet-of-Things sensors to the control of HVAC systems in residential homes [56, 136]. In my study we take a step beyond, focusing on efficiently utilizing existing HVAC system technologies to maximize user comfort, rather than simply trying to maintain a constant temperature. To achieve our goal we develop estimation and control algorithms that consider spatio-temporal distributions of temperature and air flow, which take into account changes in floor-plan geometry (such as doors being opened or closed), outdoor weather, and the position of fans and portable heaters. All this information is fed into a distributed-parameter model and a multi-dimensional human comfort index to generate, and optimize, short-term predictions.

In general, the contribution of my study in this dissertation could be divided into following aspects.

Improve the accuracy and efficiency of the HVAC system. We directly use a non-linear non-turbulent Navier-Stokes model together with a convection-diffusion heat equation to model the climate in a building. And due to the use of the distributed PDE-based CFD

model, our HVAC system is able to design control objectives that are functions of the residents' locations, which greatly increase the efficiency of the HVAC system.

Real-time estimation to building's fluid and configuration changes via thermometers. Based on the nonlinear PDE-based CFD model, we mathematically formulate a gradient-based estimation method to identify real-time indoor climate distribution and the apartment doors' states based on only thermostatic data at the same time. Also, we show the accuracy of our estimation method under a limited number of thermostats by simulating an apartment in the St. Louis area. Our results show that thermostatic information, when used together with CFD models, provide enough information to estimate most of the variables relevant for building climate control. In other words, a handful of thermostats can provide information, such as the configuration of doors, without the need to physically install extra sensors in a building.

Develop a MPC algorithm for HVAC to control resident's indoor thermal comfort. In the dissertation, we develop a MPC to optimize the thermal comfort around indoor residents based on PDE-based CFD model. The thermal comfort is measured by PMV index's approximation and the optimization control pairs the heater's power with fan's speed, not focuses only on temperature regularity. Also the MPC use the same estimation algorithm we developed in this dissertation to identify indoor climate distribution and an apartment's doors configuration based only on thermostatic data. We mathematically derive a first order gradient-based method to solve the optimization problem which has been shown to be memory-efficient [76].

Study and develop nonlinear optimal control algorithm to make the PDE-based HVAC system control work in real-time. In this dissertation, we study several different direct methods to solve nonlinear large-scale optimal control problems. Furthermore, we

develop a numerical direct method whose optimal solution is proved to satisfy Minimum Principle. Moreover, our method achieves its goals in a numerically efficient and salable way, which is suitable for applications where accuracy can be traded for computational speed and make our PDE-based HVAC control working in real-time.

1.6 Organization of the dissertation

The dissertation is organized as follows. Chapter 2 introduces our notations and the PDE-based CFD model we use through the dissertation. Chapter 3 shows how we improve the HVAC system's energy efficiency via zoned control, which thanks to the accurate CFD models that describe the dynamical and distributed behavior of the climate variables in a building. Chapter 4 develops a gradient-based optimization method to estimate the doors' state and temperature distribution in the apartment. Chapter 5 describes a MPC to optimize the thermal comfort around indoor residents based on PDE-based CFD model. Chapter 6 presents a theoretical formulation and a corresponding numerical algorithm, capable of finding optimal control inputs that satisfy the Pontryagin Minimum Principle by using a direct method. Chapter 7 extends the theoretical works in chapter 6 to optimal control problems with state constraints. The proofs of theoretical works in chapter 6 and 7 are in appendix D. Finally, chapter 8 concludes the works in the dissertation and points to some possible future works.

Chapter 2

Notations and CFD Model

In section 2.1, we are going to introduce the mathmetical notations we use through the dissertation. In section 2.2, the CFD model and corresponding PDE equations will be shown with the study on the existence and uniqueness of the model's solution.

2.1 Notations

All the notations through the dissertation follows [1].

Given $n \in \mathbb{N}$ and $p \geq 1$, we denote the standard finite-dimensional p-norm by $\|\cdot\|_p$, and the induced matrix p-norm by $\|\cdot\|_{i,p}$. We will denote by $\mathcal{M}(\mathbb{R}^n)$ the set of Radon measures defined over the Borel sets of $\mathbb{R}^n$. Moreover, given a $\mu \in \mathcal{M}(\mathbb{R}^m)$ for $m \in \mathbb{N}$, we say that a function $f\colon \mathbb{R}^m \to \mathbb{R}^n$ is L^2_μ-integrable, denoted $f \in L^2_\mu(\mathbb{R}^m, \mathbb{R}^n)$, if there exists $p \geq 1$ such that $\|f\|_\mu = \left(\int_{\mathbb{R}^m} \|f(x)\|_p^2 \, \mathrm{d}\mu(x)\right)^{\frac{1}{2}} < \infty$. To simplify, we will denote by $L^2(\mathbb{R}^m, \mathbb{R}^n)$ the space of Lebesgue square-integrable functions. Furthermore, we say that $\mu \in \mathcal{M}(\mathbb{R}^m)$ is a probability measure if $\mu(\mathbb{R}^m) = 1$. We denote the set of all probability measures by

$\mathcal{M}_p(\mathbb{R}^m)$. A stochastic process is a function $\mu\colon [0,T] \to \mathcal{M}_p(\mathbb{R}^m)$, and throughout the paper we will simply write μ_t instead of $\mu(t)$.

Let $\mu_1, \mu_2 \in \mathcal{M}(\mathbb{R}^m)$ be two Radon measures. Then the difference between μ_1 and μ_2, say $\nu = \mu_1 - \mu_2$, is a signed measure, and we define $L^2_\nu(\mathbb{R}^m, \mathbb{R}^n) = L^2_{\mu_1}(\mathbb{R}^m, \mathbb{R}^n) \cap L^2_{\mu_2}(\mathbb{R}^m, \mathbb{R}^n)$. Given $f \in L^2_\nu(\mathbb{R}^m, \mathbb{R}^n)$, its integral with respect to ν is defined by

$$\int_{\mathbb{R}^m} f(x)\,\mathrm{d}\nu(x) = \int_{\mathbb{R}^m} f(x)\,\mathrm{d}\mu_1(x) - \int_{\mathbb{R}^m} f(x)\,\mathrm{d}\mu_2(x). \tag{2.1}$$

Suppose $\Omega \subset \mathbb{R}^2$ is connected and bounded, the *Sobolev space*, $H^1(\Omega)$ is defined as $H^1(\Omega) = \{f\colon \mathbb{R}^2 \to \mathbb{R} \mid f \;\&\; \frac{\partial f}{\partial x_1} \;\&\; \frac{\partial f}{\partial x_2} \in L^2(\Omega)\}$. Let the subspace for $H^1(\Omega) \times H^1(\Omega)$ with trivial boundary condition as $H^1_0(\Omega) = \{v \in H^1(\Omega) \mid v(x) = 0,\ \forall x \in \partial\Omega\}$. Define space $L^2([t_0, t_0']; H^1(\Omega))$ as $\{f : [t_0, t_0'] \to H^1(\Omega) \mid f \text{ is measurable w.r.t. } t, f(t) \in H^1(\Omega), \text{ for } t \text{ a.e.}\}$.

In $\mathbb{R}^n$, a point is defined as $x = (x_1, x_2, \cdots, x_n)$; its norm is $|x| = (\sum_{i=1}^n x_i^2)^{1/2}$, the inner product of x and y is $x \cdot y = \sum_{i=1}^n x_i y_i$. In the Hilbert space of square integrable functions $L^2(S)$, a function is defined as $f_1 : S \to \mathbb{R}^n$, its norm is $\|f_1\|_S = \left(\int_s |f_1(z)|^2\,\mathrm{d}z\right)^{1/2}$, the inner product of f_1 and f_2 is $\langle f_1, f_2\rangle_S = \int_S f_1(z) \cdot f_2(z)\,\mathrm{d}z$. In the Hilbert space of functions $L^\infty(S)$, a function is defined as $f_1 : S \to \mathbb{R}^n$, its norm is $\|f_1\|_{\infty,S} = \operatorname{ess\,sup}_{z\in S} |f_1(z)|$.

2.2 PDE-based CFD model

A commonly missing key feature in many physical climate models used to control HVAC systems is the ability to capture the real-time spatial variability of the temperature and air flow, depending on the floor plan and configuration of the building (e.g., open or closed door

and windows). For this reason, we use a CFD model, which explicitly considers temporal and spacial variations, to describe the interactions between the temperature, air flow, and pressure. We then formulate an optimal control problem where our CFD model appears as a constraint, and whose objective function aims to minimize the energy consumption of the HVAC system while maintaining the temperature constant at a desired reference. In the remainder of this section we introduce the CFD model used through the dissertation in detail.

The foundation of our model is the Navier-Stokes equation, which couples temperature with free flow convection (as explained Section 8 in [14], among other references). As shown in the literature, atmospheric air can be modeled as an incompressible Newtonian fluid when the temperature is between $-20\,[^{\circ}\mathrm{C}]$ and $100\,[^{\circ}\mathrm{C}]$ [13, 46]. Hence, we can use the Navier-Stokes equation for incompressible laminar flows, together with the convection-diffusion temperature model for fluids.

Throughout the paper we make two major simplifications to the CFD model. First, we assume that the air flow behaves as a laminar fluid which reaches a steady-state behavior much faster than the temperature in the building. As mentioned in Section 1, both laminar and turbulent flows are present in general in a residential building, for example, in the area around HVAC vents [14]. However, Sun et al. [118] found only minor differences between laminar and turbulent models in a geometry similar to ours, while turbulent models are significantly more complex than laminar models [3, 39]. Hence, we consider a stationary Navier-Stokes equation to describe the fluid behavior, and a time-dependent equation to describe the temperature behavior. Second, we consider only two-dimensional air flows moving parallel to the ground. This assumption intuitively makes sense since the air flow in the top half of a room can be accurately estimated using a two-dimensional model, mostly

due to the lack of obstacles (such as furniture). These assumptions reduce the accuracy of our model to some extent, e.g., van der Poel et al. [123] compared 2D and 3D Rayleigh-Bénard convection simulations for a cylindrical geometry and showed that differences arise for Prandtl constants $Pr < 1$, while our model's Prandtl constant is $Pr = 1.2$. Yet, both assumptions allow us to significantly simplify the computational complexity of our CFD-based control design (measured by the number of variables and number of equality constraints of the model), which in turn allows us to compute results on the order of tens of minutes or even in real time.

Let $\Omega \subset \mathbb{R}^2$ be the area of interest, connected and bounded. We will denote the *boundary of* Ω by $\partial\Omega$. Let $u\colon \Omega \to \mathbb{R}^2$ be the *stationary air flow velocity*, and $p\colon \Omega \to \mathbb{R}$ be the *stationary air pressure* in Ω. Also, given $t_0' > t_0$, let $T_e\colon \Omega \times [t_0, t_0'] \to \mathbb{R}$ be the *temperature* in Ω. Then, using the formulation found in [92], the convection-diffusion of temperature in Ω can be described by the following PDE,

$$\frac{\partial T_e}{\partial t}(x,t) - \nabla_x \cdot (\kappa(x)\, \nabla_x T_e(x,t)) + u(x) \cdot \nabla_x T_e(x,t) = g_{T_e}(x,t). \tag{2.2}$$

Where $g_{T_e}\colon \Omega \times [t_0, t_0'] \to \mathbb{R}$ represents the heat sources in the room, $\kappa\colon \Omega \to \mathbb{R}$ is the *thermal diffusivity*, $\nabla_x \cdot = \frac{\partial}{\partial x_1} + \frac{\partial}{\partial x_2}$ is the *divergence operator*, and $\nabla_x = \left(\frac{\partial}{\partial x_1}, \frac{\partial}{\partial x_2}\right)^T$ is the *gradient operator*. The initial condition of the temperature is:

$$T_e(x, t_0) = \pi_0(x), \quad \text{for } x \in \Omega. \tag{2.3}$$

Similarly, the stationary air flow in Ω is governed by the following set of incompressible Navier-Stokes stationary PDEs,

$$-\frac{1}{Re}\,\Delta_x u(x) + \big(u(x)\cdot\nabla_x\big)\,u(x) + \frac{1}{\rho}\,\nabla_x p(x) + \alpha(x)\,u(x) = g_u(x);\ \text{and,} \tag{2.4}$$

$$\nabla_x \cdot u(x) = 0. \tag{2.5}$$

Where $g_u\colon \Omega \to \mathbb{R}^2$ represents all the external forces applied to the air (such as fans), *Re* is the *Reynolds number* (which is inversely proportional to the *kinematic viscosity*), ρ is the *density of the air*, $\alpha\colon \Omega \to \mathbb{R}$ is the *friction constant*, $u(x)\cdot\nabla_x = u_1(x)\,\frac{\partial}{\partial x_1} + u_2(x)\,\frac{\partial}{\partial x_2}$ is the *advection operator*, and $\Delta_x = \frac{\partial^2}{\partial x_1^2} + \frac{\partial^2}{\partial x_2^2}$ is the *Laplacian operator*. Since we do not model the vertical dimension of Ω, we omit the Boussinesq-approximation buoyancy term proportional to T_e, which is typically included on the right-hand side of (2.4).

We modify κ and α to model obstacles to heat and air flow in Ω, such as walls, doors, and windows, as described in [63, 102]. In particular, when the point x corresponds to a material that blocks air, we choose $\alpha(x) \gg u(x)$, which results in $u(x) \approx 0$, and when the point x corresponds to air then we choose $\alpha(x) = 0$.

We divide the boundary of Ω to two outlets of the HVAC system, denoted by Γ_o, one air return inlet, denoted by Γ_i, and the exterior walls, denoted by Γ_w. Thus $\Gamma_i \cup \Gamma_o \cup \Gamma_w = \partial\Omega$.

We use a mix of boundary conditions to model the effect of the HVAC system in the room, as explained below . Let $\hat{n}(x)$ be the inward-pointing unit vector perpendicular to the boundary at $x \in \partial\Omega$.

Hence, the air flow has the following boundary conditions:

- The airflow satisfies a no-transverse condition at the exterior walls, hence

$$u(x) \equiv 0, \quad \text{for } x \in \Gamma_w. \tag{2.6}$$

- If HVAC unit's fan is set the air flow at Γ_o,

$$u(x) = u_o \, \hat{n}(x), \quad \text{for } x \in \Gamma_o, \tag{2.7}$$

  where $u_o > 0$ is the HVAC fan speed.

- The airflow at the inlet is not constrained, hence $u(x)$ is free for each $x \in \Gamma_i$.

The boundary condition for the temperature is:

$$T_e(x) \equiv T_A, \quad \text{for } x \in \partial\Omega, \tag{2.8}$$

where T_A is the *atmospheric temperature*. We only apply a boundary condition for the pressure equation at the inlet, setting $p(x) \equiv p_A$ for each $x \in \Gamma_i$, where p_A is the *atmospheric pressure*.

The existence and uniqueness to the CFD model's weak solution containing equations (2.2), (2.3), (2.4), (2.5), (2.8), (2.6) and (2.7) are given as,

Theorem 2.1 (Existence of weak solution to the CFD model)**.** *Given* $\alpha, \kappa \in L^2(\Omega) \cap L^\infty(\Omega)$, $g_{T_e} \in L^2([t_0, t_0'] \times \Omega)$ *and* $g_u \in L^2(\Omega) \times L^2(\Omega)$. *Let* $\Omega \subset \mathbb{R}^2$ *be bounded and locally Lipschitz, there exists at least one tuple* $(T_e, u, p) \in \Big(L^2([t_0, t_0']; H^1\big(\Omega\big)) \cap C^0([t_0, t_0']; L^2(\Omega))\Big) \times \Big(H^1(\Omega) \times H^1\big(\Omega\big)\Big) \times L^2\big(\Omega\big)$, *such that*

- $\big(u, p\big)$ *satisfies the weak formulas,*

$$\begin{aligned} &\langle \alpha u, \varphi \rangle_\Omega + \frac{1}{Re} \langle \nabla_x u, \nabla_x \varphi \rangle_\Omega + \\ &+ \langle u \cdot \nabla_x u, \varphi \rangle_\Omega - \langle p, \nabla_x \varphi \rangle_\Omega = \langle g_u, \varphi \rangle_\Omega, \\ &\forall \varphi \in H_0^1\big(\Omega\big) \times H_0^1\big(\Omega\big), \ \textit{and} \end{aligned} \tag{2.9}$$

$$\langle \nabla_x \cdot u, \psi \rangle_\Omega, \quad \forall \varphi \in L^2(\Omega). \tag{2.10}$$

And u satisfies the boundary condition in equations (2.6) *and* (2.7)*.*

- T_e *satisfies the boundary and initial condition in equations* (2.8) *and* (2.3)*, also* T_e *satisfied the following weak formula,*

$$\begin{aligned} &\langle \frac{\partial T_e}{\partial t}, \xi \rangle_\Omega + \langle \kappa(x) \nabla_x Te, \nabla_x \xi \rangle + \langle u \cdot \nabla_x Te, \xi \rangle_\Omega = \\ &=< g_{Te}, \xi >_\Omega, \quad \forall \xi \in H_0^1\big(\Omega\big). \end{aligned} \tag{2.11}$$

Theorem 2.2 (The sufficient condition for unique weak solution to CFD model)**.** *Let* $\Omega \subset \mathbb{R}^2$ *be bounded and locally Lipschitz, define the area of* Ω *as* $|\Omega|$*. For the weak solution tuple* (T_e, u, p) *in the theorem 2.1, if* $\left(\int_\Omega |\nabla_x u|^2 dx \right)^{1/2} < \frac{1}{C \cdot Re}$*, where* $C = \frac{|\Omega|^{1/2}}{2}$*, Then* (T_e, u, p) *is the only weak solution to the CFD system.*

The proofs to the theorem 2.1 and 2.2 are studied in the appendix A, The theorem 2.2 is a sufficient condition we derived for our problem. For the corresponding building simulations in chapters 3, 4 5 and 6, the value $\frac{1}{Re\, C} \approx 10^{-3}$, while the under HVAC system's control, for the flow's velocity, $\left(\int_\Omega |\nabla_x u|^2 dx \right)^{1/2}$ is in the range $(1, 10)$. Further study about a more

general condition for the fluid dynamic model's unique solution in our problem is needed in the future.

Chapter 3

HVAC System's Efficiency Improvement via Zoned Control

In this chapter, we exam the energy efficiency of the HVAC control algorithm to maintain the indoor climate in a zoned area around the residents and our nonliear PDE-based prediction model's accuracy. [1]

3.1 Problem statement

The CFD model is given in chapter 2, which follows the dynamics in equations 2.2, (2.4) and (2.5) with boundary and initial conditions in equations (2.3), (2.6), (2.7), and (2.8).

[1] This chapter is based on R. He and H. Humberto, "Zoned HVAC Control via PDE-Constrained Optimization," in *2016 American Control Conference*, Boston, USA, July. 2016, pp. 587–592. © IEEE 2016

Suppose $\Omega_z \subset \Omega$ is a local zone area around residents, to control the temperature in Ω_z during the time period $[0, t_f]$, we aim to minimize the following cost function,

$$\int_0^{t_f} \left(\int_{\Omega_z} \left(T_e(x,t) - T_e^* \right)^2 \mathrm{d}x + \lambda_1 \, v^2(t) \right) \mathrm{d}t + \lambda_2 \, u_o^2. \tag{3.1}$$

Where $\lambda_{1,2} > 0$, T_e^* is the reference temperature set by the user, and t_f is the time horizon. The heater power $v(t)$ and the fan speed u_o are our controlled variables, the former appearing as $g_{T_e}(x,t) = v(t)$ for each $x \in \Theta_h \subset \Omega$, and the latter appearing as a boundary condition. We formulate a PDE-constrained optimal control problem using the cost in (3.1), together with the CFD model in (2.2)-(2.5) and its boundary conditions as constraints. We also add inequality box constraints for all the controlled variables, so they remain within safety limits.

As explained in section 3.3, our experiments introduce variations to the cost function in (3.1) depending on the number of available actuators. Regardless, the goal of regulating the temperature will remain the same throughout all our experiments.

3.2 Numerical implementation

Our numerical implementation of the PDE-constrained optimal control problem described in section 2.2 is obtained by first using FEM to transform the CFD model in (2.2)-(2.5) to a set of ODEs as described in [43, Chapters 3 and 4], and then using the consistent approximation technique described in [103, Chapter 4] which transforms optimal control problems (with ODE constraints) into nonlinear programming problems. After those two transformations, we use commercially available numerical solvers to find approximations of the desired optimal control, as described in section 3.3.

3.2.1 FEM Discretization

Among the many discretization techniques for PDEs, FEM stands out for being compatible with complex geometries of the domain Ω. Intuitively speaking, FEM approximates PDEs by dividing the domain into polygons, and then finding a set of ODEs for each vertex, and possibly each facet, of each polygon. The resulting set of ODEs has the property that each ODE is dependent only on its neighbors.

Before we can formally describe the FEM discretization, we need to introduce extra notation. Let $H^1(\Omega, \mathbb{R}^n)$ be the set of functions from Ω to $\mathbb{R}^n$ belonging to $L^2(\Omega, \mathbb{R}^n)$, whose weak derivative is also in $L^2(\Omega, \mathbb{R}^n)$ [139]. Note that $H^1(\Omega, \mathbb{R}^n)$, endowed with the dot product $\langle f, g \rangle = \int_\Omega f(x) \cdot g(x)\, \mathrm{d}x$, is a Hilbert space. Similarly, we denote $\langle f, g \rangle_S = \int_S f(x) \cdot g(x)\, \mathrm{d}x$.

Let $\{W_k\}_{k=1}^{N_{pl}}$ be a polygonal partition of Ω, i.e., $\bigcup_{k=1}^{N_{pl}} W_k = \Omega$, $\mathrm{int}(W_k) \cap \mathrm{int}(W_j) = \emptyset$ for each $k \neq j$, and each W_k is a polygon. If $\{x_k\}_{k=1}^{N_v}$ is the set of vertices in the polygonal partition and $\{y_j\}_{j=1}^{N_w}$ is the set of nodal points, then we define the *test functions* $\{\xi_k\}_{k=1}^{N_v}, \{\psi_k\}_{k=1}^{N_v} \subset H^1(\Omega, \mathbb{R})$, and $\{\varphi_k\}_{k=1}^{2N_w} \subset H^1(\Omega, \mathbb{R}^2)$, where $N_v, N_w \in \mathbb{N}$ and $N_v \leq N_w$, with the following properties in table 3.1 for each $k \in \{1, \ldots, N_v\}$ and each $j \in \{1, \ldots, N_w\}$.

Table 3.1: Properties for FEM basis.

ξ_k, φ_k, and ψ_k are continuous.
ξ_k, φ_k, and ψ_k are nonzero only in the polygons containing x_k.
$\xi_k(x_k) = \psi_k(x_k) = 1$, $\varphi_{2j-1}(y_j) = \left[\begin{smallmatrix} 1 \\ 0 \end{smallmatrix}\right]$, and $\varphi_{2j}(y_j) = \left[\begin{smallmatrix} 0 \\ 1 \end{smallmatrix}\right]$.

Then, from (2.2)-(2.5), and using Green's Formulas (see Appendix C.2 in [52]), we get the following Galerkin identities (as described in [43, Chapter 3.6]),

$$\left\langle \frac{\partial T_e}{\partial t}(\cdot,t), \xi_k \right\rangle - \left\langle \kappa(x)\, \nabla_x T_e(\cdot,t), \nabla_x \xi_k \right\rangle + \left\langle u \cdot \nabla_x T_e(\cdot,t), \xi_k \right\rangle = \left\langle g_{T_e}(\cdot,t), \xi_k \right\rangle; \quad (3.2)$$

$$- \frac{1}{Re} \langle \nabla_x u, \nabla_x \varphi_j \rangle + \left\langle \left(u \cdot \nabla_x\right) u, \varphi_j \right\rangle + \langle \nabla_x p, \varphi_j \rangle + \langle \alpha\, u, \varphi_j \rangle = \langle g_u, \varphi_j \rangle; \text{ and, } \quad (3.3)$$

$$\langle \nabla_x \cdot u, \psi_k \rangle = 0, \quad (3.4)$$

for each $k \in \{1, \ldots, N_v\}$, $j \in \{1, \ldots, 2\, N_w\}$, and almost every $t \in [0, t_f]$.

Now, given $N_{T_e}, N_u, N_p \in \mathbb{N}$, consider the linearly independent sets of *basis functions* $\left\{\widehat{\xi}_j\right\}_{j=1}^{N_{T_e}}, \left\{\widehat{\psi}_j\right\}_{j=1}^{N_u} \subset H^1(\Omega, \mathbb{R})$, and $\left\{\widehat{\varphi}_j\right\}_{j=1}^{N_p} \subset H^1(\Omega, \mathbb{R}^2)$. Using these basis functions we can project the variables of our CFD model into finite-dimensional subspaces, i.e.,

$$\begin{aligned} T_e(x,t) &= \sum_{j=1}^{N_{T_e}} \eta_{T_e,j}(t)\, \widehat{\xi}_j(x), \\ u(x) &= \sum_{j=1}^{N_u} \eta_{u,j}\, \widehat{\varphi}_j(x), \\ p(x) &= \sum_{j=1}^{N_p} \eta_{p,j}\, \widehat{\psi}_j(x). \end{aligned} \quad (3.5)$$

Applying the representations in (3.5) to the Galerkin identities in (3.2) results in a set of N_v ODEs with state variables $\{\eta_{T_e,j}\}_{j=1}^{N_{T_e}}$. Similarly, applying the representations to (3.3)-(3.4) results in a set of $2\, N_w$ nonlinear algebraic equations with parameters $\{\eta_{u,j}\}_{j=1}^{N_u}$ and N_v linear ones with parameters $\{\eta_{p,j}\}_{j=1}^{N_p}$. All these differential and algebraic equations are, in practice, parametrized by constants corresponding to the inner products between basis and

test functions, as well as their gradients. We omit the technical details of the final set of equations due to space constraints, and we refer the interested reader to [43, Chapter 3] for more information.

3.2.2 Optimal Control Discretization

After the FEM discretization, we effectively have an Differential Algebraic Equation (DAE) optimal control problem where (3.2) contributes N_v ODEs, (3.3) contributes $2\,N_w$ nonlinear equality constraints, and (3.4) contributes N_v linear constraints. Several extra equality constraints are added due to the boundary conditions of the air flow and the pressure, as described in section 2.2. The actual number of constraints due to boundary conditions depends on the number of vertices in the polygonal partition $\{W_k\}_{k=1}^{N_{pl}}$ over the boundary.

The consistent approximation of this type of optimal control problem is studied in [103, Chapter 4]. We follow the procedure described there, i.e., we first normalize the problem using the technique described in Chapter 4.1.2 of the same book, and then we use the Forward-Euler discretization method to transform the ODEs into a sequence of equality constraints. Again, we omit the technical details of the final equality-constrained nonlinear programming problem due to space constraints.

3.3 Simulations

We simulated a two-room apartment with a square area of interest Ω_z (e.g., the area were a resident is located). Our goal is to show that using zoned control over the area of interest produces a significant improvement over controlling the temperature over the whole room.

The HVAC system consists of two heaters and two forced-air outlets with variable-speed fans. Moreover, in order to show the efficiency and stability of our zoned control algorithm, we simulated 18 different scenarios with different areas of interest, distributed uniformly over the apartment.

A diagram of the apartment is shown in Figures 3.1 and 3.2. The apartment's dimensions are $5 \times 10[\mathrm{m}^2]$, the width of all outlets and inlet is 0.5[m], and each of the areas has dimensions $2 \times 2[\mathrm{m}^2]$. The two heaters are denoted by Θ_h (left) and Θ_h' (right), with dimensions $1 \times 1[\mathrm{m}^2]$.

The fluid mechanics are governed by the constants $Re = 0.05$ and $Pr = 1.2$, with $k(x) = 10^{-2}$ and $\alpha(x) = 0$ when $x \in \Omega$ is located in free air, while $k(x) = 10^{-4}$ and $\alpha(x) = 100$ when $x \in \Omega$ is located on or in a wall. The atmospheric pressure is $p_A = 101.3[\mathrm{kPa}]$, and the atmospheric temperature is $T_A = 23.83[^\circ\mathrm{C}]$. We set the desired temperature to $T_e^* = 24.83[^\circ\mathrm{C}]$, the time horizon to $t_f = 300[\mathrm{s}]$, and we assume the function g_u is identically zero (i.e., no fans are inside the room). As explained in section 2.2, $g_{T_e}(x,t) = v(t)$ for each $x \in \Theta_h$, $g_{T_e}(x,t) = v'(t)$ for each $x \in \Theta_h'$, and $g(x,t) = 0$ otherwise. The parameters in the cost function (3.1) are $\lambda_1 = 0.002$ and $\lambda_2 = 0.001$. The optimal control problem finds the fan speeds u_o and u_o' for Γ_o and Γ_o', respectively, and the heater powers $v(t)$ and $v'(t)$ for Θ_h and Θ_h', respectively. We set the fan speed box constraints to $\big[0.1, 1\big]\big[\frac{\mathrm{m}}{\mathrm{s}}\big]$, and the heater power box constraints to $\big[0, 5\big][\mathrm{kW}]$.

We discretized the area into $N_{pl} = 452$ elements, and the number of total nodes is $N_v = 227$. We used first-order Lagrangian elements to define the test and basis functions ξ_k, $\widehat{\xi}_k$, ψ_k, and $\widehat{\psi}_k$, thus $N_{T_e} = N_p = 227$. We used second-order Lagrange elements to define the test and basis functions φ_k and $\widehat{\varphi}_k$, thus $2\,N_w = N_u = 1696$. More details regarding our choice of test and basis functions can be found in [94, Chapter 3.3.1]. The ODE discretization time step was chosen as $\Delta t = 10[\mathrm{s}]$.

We calculated the total energy usage as the sum of the heater energy usage, i.e., $\int_0^{t_f} v(t) + v'(t)\,\mathrm{d}t$, and the fan energy usage as $\int_0^{t_f} \int_{\Gamma_o \cup \Gamma_o'} \|u(x)\|\, p(x)\,\mathrm{d}x\,\mathrm{d}t$. Our results were obtained using a 16-core *Xeon E5-2680* computer running at 2.7[GHz], with 128[GB] of RAM. We wrote our code using Python, the FEM discretization was computed using tools from the *FEniCS Project* [94], and the nonlinear programming problem was numerically solved using the *SNOPT* library [66] interfaced using the *OptWrapper* library [82]. The computation time ranged between 15[min] and 45[min] for each experiment.

3.3.1 Nonlinear Navier-Stokes Model

Using the nonlinear Navier-Stokes model described in (2.2)-(2.5) we simulated two major scenarios, the first where the objective function in (3.1) uses $\Omega_z = \Omega$, i.e., the target area is the whole apartment, and the second where we use a zoned approach with a smaller Ω_z which moves around the apartment to 18 different locations, as explained above. Figure 3.1a shows the temperature distribution for the first scenario, while Figures 3.1b and 3.1c show the temperature distribution for two of the 18 zoned simulations. Also, Figure 3.2 shows the stationary airflow for the first scenario.

In the first scenario, where $\Omega_z = \Omega$, the optimal average absolute temperature error in the apartment was 0.502[°C] at time t_f, and the ratio of energy usage over average temperature change within Ω was 1009.2[Wh/°C]. We calculated the same statistics for the 18 different zones Ω_z, which are summarized in Column (A) of Figures 3.3a and 3.3b. To make both scenarios comparable, we recalculated these statistics for the first scenario, this time considering the average temperature changes in Ω_z instead of Ω, which are summarized in Column (B) of Figures 3.3a and 3.3b. Those figures clearly show that using zoned control is significantly

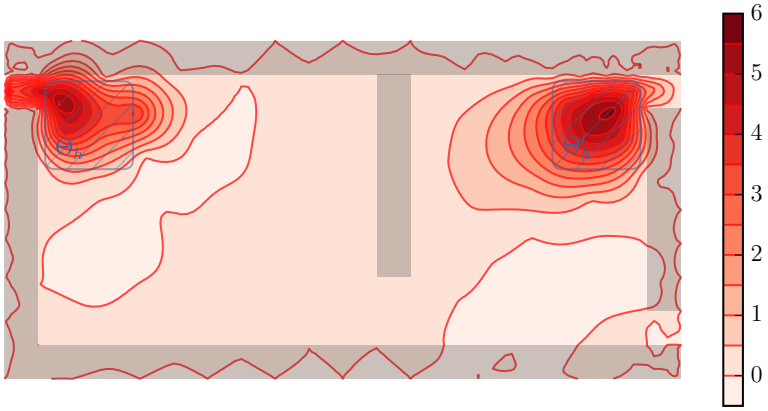

(a) Temperature distribution at time t_f with target area Ω, i.e., the whole apartment.

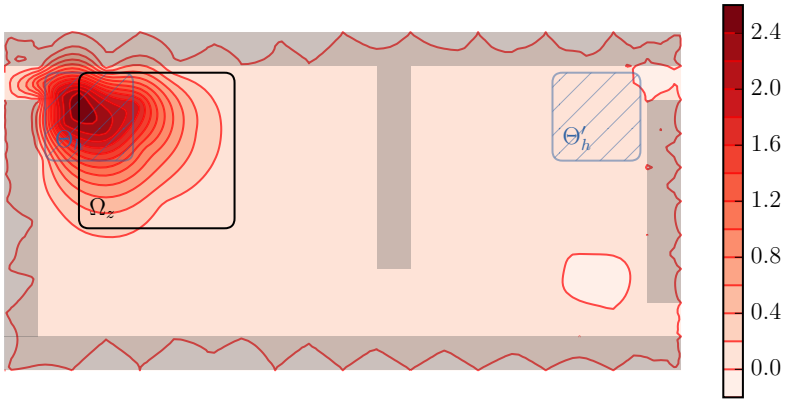

(b) Temperature distribution at time t_f with target area Ω_z.

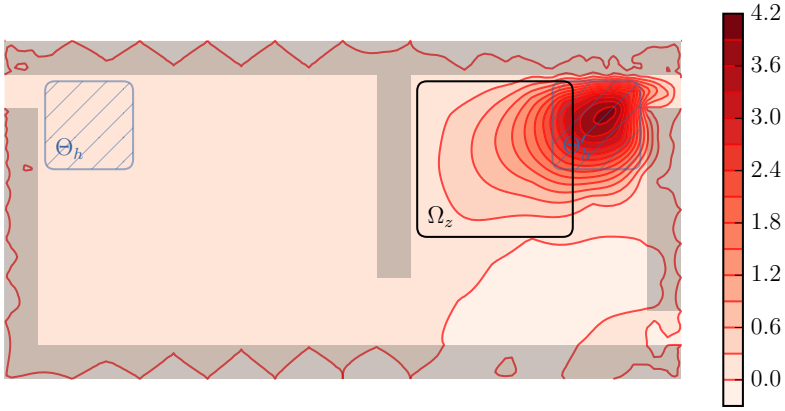

(c) Temperature distribution at time t_f with target area Ω_z.

Figure 3.1: Results of the experiments in section 3.3.1. Walls are shown in shaded black, and heaters are shown in shaded blue. Values are in [°C] with respect to T_A.

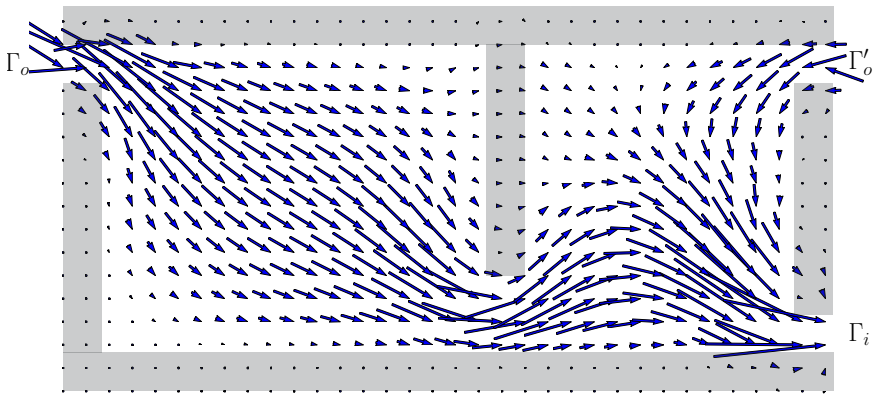

Figure 3.2: Air flow of the experiment in section 3.3.1 with target area Ω, i.e., the whole apartment. Average air speed in the apartment is 0.11[m/s]. Walls are shown in shaded black. Two outlets and one inlet of the HVAC system are marked as Γ_o, Γ'_o and Γ_i respectively.

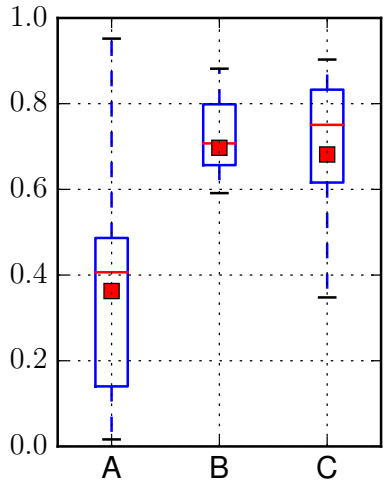

(a) Average absolute temperature error, in [°C], within Ω_z at time t_f with respect to T_e^*.

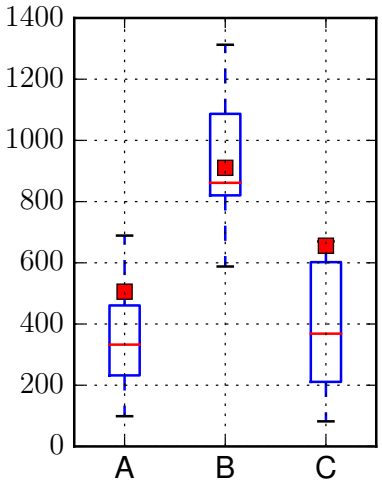

(b) Ratio of energy usage over average temperature change within Ω_z, in [Wh/°C].

Figure 3.3: Results of the experiments in section 3.3.1 and 3.3.2. Columns: (A) nonlinear model with zoned control, (B) nonlinear model without zoned control, (C) linearized model with zoned control. Each column shows the median (red line), mean (red box), and first-to-third quartiles (blue box).

more accurate and more efficient than heating the whole apartment. It is worth noting that the zoned approach requires roughly half the energy to change the average temperature by 1[°C] in Ω_z when compared to the first scenario.

The results in Figure 3.1 indicate that when the resident is near one heater, say Θ_h, our algorithm automatically shut down the other heater, say $\Theta_{h'}$, as intuitively expected. Therefore, if it is possible to localize a resident within an apartment, e.g., via Bluetooth beacons or using a sensor network, then we can increase the efficiency of the HVAC unit significantly without major modifications to the mechanical ventilation system.

3.3.2 Linearized Navier-Stokes model

We also computed the optimal control using the linearized Navier-Stokes model described in [33, 34]. The linearized model has clear advantages over our nonlinear model, including a larger set of theoretical results supporting it, and a faster computation time. On the other hand, linearized models perform well only when the values produced by the model are close to the stationary linearization point.

We ran the same experiments as in the second scenario of section 3.3.1, i.e., controlling the temperature in 18 different zones. The statistics for average absolute temperature error in Ω_z, and ratio of energy usage over average temperature in Ω_z, are shown in Column (C) of figures 3.3a and 3.3b. Even though the energy efficiency is comparable when we use linearized or nonlinear models, the accuracy is significantly different, with the nonlinear model consistently performing better than the linearized model. We believe the difference is due to the lack of accuracy of the linearized model. As exemplified in figure 3.4, there is a large error in temperature distribution between the linearized model and an accurate

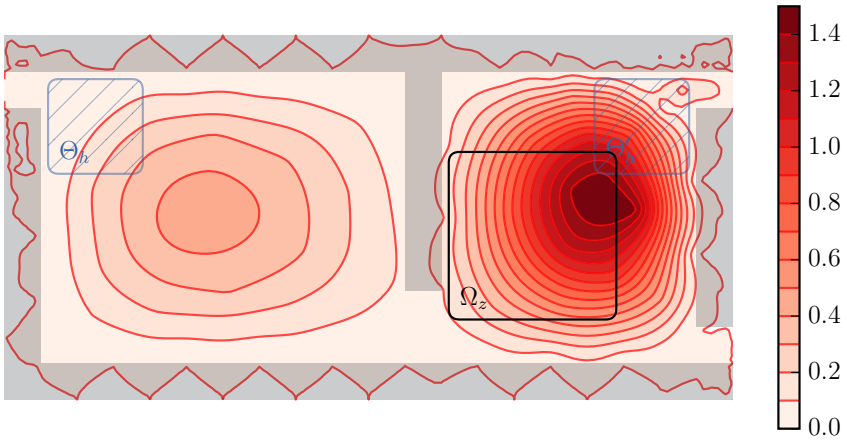

Figure 3.4: Absolute error in temperature distribution, with respect to *FEniCS* simulation, for the linearized model in section 3.3.2, at time t_f with target area Ω_z. Values are in [°C].

benchmark simulation using the *FEniCS* solver, which is consistent with the highly nonlinear behavior of the Navier-Stokes equation.

3.4 Chapter conclusion

Our results in this chapter open the door to a large number of exiting opportunities to improve the energy efficiency of buildings. The results validate the idea that an accurate distributed indoor climate model is able to improve the HVAC system's efficiency by focusing on local indoor target areas. Also, the comparasion results show the inaccuracy of a linearized model and related LQR method to predict and control indoor climates.

By making small improvements to existing HVAC units it is possible to dramatically increase the efficiency of HVAC units without a decrease in human comfort. It is worth noting that our results do not require, in principle, the use of expensive variable-speed fans or variable-power heaters, since those control signals can be implemented using switched strategies [125, 126].

More importantly, our simplifications have allowed us to obtain results in tens of minutes while still capturing the distributed behavior of the climate variables, which is much closer to real-time applications than previous results [46], achieving a good trade-off when compared to less accurate linearized Navier-Stokes models.

Chapter 4

Gradient-Based Estimation of Indoor Air Flow and Geometry Configurations via PDE-based CFD Model

In this chapter, we develop a gradient-based optimization method to estimate the doors' state and temperature distribution in the apartment. First, we mathematically formulate a gradient-based estimation method to identify real-time indoor climate distribution and the apartment doors' states based on only thermostatic data. Second, we show the accuracy of our estimation method under a limited number of thermostats by simulating an apartment in the St. Louis area. Our results show that thermostatic information, when used together with CFD models, provide enough information to estimate most of the variables relevant for building climate control. In other words, a handful of thermostats can provide information, such as the configuration of doors, without the need to physically install extra sensors in a building.

The chapter is organized as follows. The fluid dynamic model and finite element method are formulated in section 4.1. We present the theoretical basis for our gradient-based estimation algorithm in section 4.2. Finally, our simulation results are presented in Section 4.3. [2]

4.1 Optimization problem statement

Let $\Omega \subset \mathbb{R}^2$ be the area of interest, assumed to be bounded and connected, and let $\partial\Omega$ be its boundary. In this chapter, we assume the fans in the HVAC system is inside the building, thus for the indoor fluid dynamic climate in section 2.2, there is no boundary condition related to Γ_o, and the dynamic system follows the equation (2.2), (2.4) and (2.5) with initial condition in equation (2.3), temperature boundary conditions in equation (2.8) and velocity boundary condition only in equation (2.6).

We assume that there are n_t thermostats in the building. The i-th thermostat is located at $x_i \in \Omega$, and samples the temperature in a neighborhood averaged using the *bump weight function* $\Phi_i(x) = \sigma \exp\big(-(r^2 - \|x - x_i\|^2)^{-1}\big)$ for $\|x - x_i\| < r$, and $\Phi_i(x) = 0$ otherwise, where $\sigma > 0$ is a normalization factor such that $\int_\Omega \Phi_i(x)\,\mathrm{d}x = 1$.

We also assume that there are n_d doors in the building. We define $\theta_i \in \{0, 1\}$ as the configuration of the i-th door, i.e., $\theta_i = 1$ when the i-th door is open, and $\theta_i = 0$ when is closed. Let $\Omega_{\theta_i} \subset \Omega$ be the area occupied by the i-th door when it is closed, and let $\mathbb{I}_i$ be the indicator function of Ω_{θ_i}, i.e., $\mathbb{I}_i(x) = 1$ for $x \in \Omega_{\theta_i}$, and $\mathbb{I}_i(x) = 0$ otherwise.

[2] This chapter is based on R. He and H. Humberto, "Gradient-Based Estimation of Air Flow and Geometry Configurations in a Building Using Fluid Dynamic Adjoint Equations," in *2016 International High Performance Buildings Conference*, pp.3446.1–3446.10, Purdue University, USA, July. 2016,

As mentioned in section 2.2, in equation (2.2) $\kappa : \Omega \to \mathbb{R}$ is the *thermal diffusivity*, and in equation (2.4) $\alpha \colon \Omega \to \mathbb{R}$ is the *viscous friction coefficient*. When the door configuration changes, so does the prediction generated by our CFD model in equations (2.2) and (2.4). In particular, these two parameters α and κ change for each $x \in \Omega_{\theta_i}$ as a function of θ_i. We model this relation by defining $\alpha \colon \Omega \times \{0,1\}^{n_d} \to \mathbb{R}$ and $\kappa \colon \Omega \times \{0,1\}^{n_d} \to \mathbb{R}$ as follows,

$$\begin{aligned} \alpha(x,\theta) &= \alpha_0 + \sum_{i=0}^{n_d} (1-\theta_i)\,(\alpha_w - \alpha_0)\,\mathbb{I}_i(x), \quad \text{and} \\ \kappa(x,\theta) &= \kappa_0 + \sum_{i=0}^{n_d} (1-\theta_i)\,(\kappa_w - \kappa_0)\,\mathbb{I}_i(x), \end{aligned} \tag{4.1}$$

where α_0 and κ_0 are the parameters for open air, while α_w and κ_w are the parameters for solid walls. Note that both α and κ are affine functions of $\theta \in \mathbb{R}^{n_d}$.

Now, using binary values for each θ_i means that our estimation algorithm will have to use combinatorial methods, which tend to scale poorly in both computation time and computational resources. To avoid this problem we relax the binary parameters $\theta_i \in \{0,1\}$, instead allowing them to belong to the unit interval $[0,1]$. Although for each θ_i only the extreme values have meaningful physical interpretations, non-integer values can theoretically be interpreted as averaged observations over the optimization horizon, as explained in [125, 126]. For example, if throughout the optimization horizon a door is open half the time, and closed half the time, it is likely that we will observe $\theta_i \approx 0.5$. The relaxation of each θ_i is also important in our numerical calculations, since it transforms the optimization program from a mixed-integer program to a more convenient nonlinear format [64].

Now we can formulate our main estimation algorithm to compute the door configuration θ and the initial temperature π_0 using the information from the n_t thermostats in the building. Given an arbitrary estimation time horizon, say $[0,T]$, we write our optimal estimation

problem as follows:

$$\begin{aligned}\min_{\pi_0 \colon \Omega \to \mathbb{R},\, \theta \in \mathbb{R}^{n_d}} J(\pi_0, \theta) = \sum_{i=1}^{n_t} \int_0^T \left(\int_{\Omega_i} \Phi_i \, T_e(x, t; \pi_0, \theta) \, \mathrm{d}x - T^*_{e,i} \right)^2 \mathrm{d}t + \\ + \eta_0 \sum_{i=1}^{n_t} \left(\int_{\Omega_i} \Phi_i \, \pi_0 \, \mathrm{d}x - \pi^*_{0,i} \right)^2 + \eta_1 \, \|\pi_0\|^2_\Omega, \\ \text{subject to: partial differential equations (2.2), (2.4), and (2.5),} \\ \text{boundary and initial conditions (2.3), (2.8), and (2.6),} \\ 0 \le \theta_i \le 1, \quad \forall i \in \{1, \ldots, n_d\}.\end{aligned} \tag{4.2}$$

Where, $\eta_0, \eta_1 > 0$ are weight parameters, $T_e(x, t; \pi_0, \theta)$ is the unique solution of equation (2.2) with initial condition π_0 and configuration θ, $T^*_{e,i}(t)$ is the time signal obtained from the i-th thermostat over the horizon $[0, T]$, and $\pi^*_{0,i}$ is just notation for the initial thermostat temperature, i.e., $\pi^*_{0,i} = T^*_{e,i}(0)$.

4.2 Costate-based gradient computation

In this section we develop a numerical algorithm to solve the optimization problem defined in equation (4.2). We use a gradient-based optimization algorithm to find local minimizers of our optimization problem, where the gradients are computed using the adjoint equations of the CFD model, similar to the techniques in [71] and [135]. We then discretize the adjoint equations using the Finite Element Method (FEM), resulting in a practical algorithm which we test in Section 4.3.

4.2.1 Adjoint equations and Fréchet derivatives

In order to derive our CFD model's adjoint equations, first we need to write the *Lagrangian function* of the optimization problem [65, 71]. Let $\{\lambda_i\}_{i=1}^{6}$ be the set of *Lagrange multipliers*, or *adjoint variables*, each associated to one of the equations (2.2) to (2.6) and defined in its respective dual space. Then, the Lagrangian function of our optimal estimation problem is:

$$\begin{aligned} &L\big(T_e, u, p, \pi_0, \theta, \{\lambda_i\}_{i=1}^{6}\big) = J(\pi_0, \theta) + \\ &+ \Big\langle \lambda_1, \frac{\partial T_e}{\partial t} - \nabla_x \cdot (\kappa(x)\, \nabla_x T_e) + u \cdot \nabla_x T_e - g_{T_e} \Big\rangle_{\Omega \times [0,T]} + \\ &+ \Big\langle \lambda_2, -\frac{1}{Re} \Delta_x u + (u \cdot \nabla_x) u + \nabla_x p + \alpha\, u - g_u \Big\rangle_{\Omega} + \\ &+ \langle \lambda_3, \nabla_x \cdot u \rangle_{\Omega} + \langle \lambda_4, T_e \rangle_{\partial\Omega \times [0,T]} + \langle \lambda_5, u \rangle_{\Gamma_w} + \langle \lambda_6, T_e(0, \cdot) - \pi_0 \rangle_{\Omega}. \end{aligned} \tag{4.3}$$

Where $\langle f_1, f_2 \rangle_S = \int_S f_1(z)\, f_2(z)\, \mathrm{d}z$ is the inner product of the Hilbert space of square integrable functions $\mathcal{L}^2(S)$. We write the necessary conditions for optimality using Galerkin methods [67], i.e., by setting the inner product of the partial derivatives of L with respect to all the dual directions equal to zero. That is, we look for solutions such that $\big\langle \frac{\partial L}{\partial T_e}, w \big\rangle_{\Omega \times [0,T]} = 0$, $\big\langle \frac{\partial L}{\partial u}, v \big\rangle_{\Omega} = 0$, and $\big\langle \frac{\partial L}{\partial p}, q \big\rangle_{\Omega} = 0$ for each set of functions (w, v, q) in the respective dual spaces, and sufficiently weakly differentiable. As detailed in appendix B, the conditions above are satisfied when the dual variables satisfy,

$$\begin{aligned} &- 2 \sum_{i=1}^{n_t} \bigg(\int_{\Omega_i} \Phi_i(z)\, T_e(z,t)\, \mathrm{d}z - T^*_{e,i}(t) \bigg) + \frac{\partial \lambda_1}{\partial t}(x,t) + \\ &+ \nabla_x \cdot (\kappa(x)\, \nabla_x \lambda_1(x,t)) + u(x) \cdot \nabla_x \lambda_1(x,t) = 0, \end{aligned} \tag{4.4}$$

$$\lambda_6(x) = \lambda_1(x, 0), \tag{4.5}$$

$$\int_0^T \lambda_1(x,t)\,\nabla_x T_e(x,t)\,\mathrm{d}t + \alpha(x)\,\lambda_2(x) - \frac{1}{Re}\Delta_x\lambda_2(x) + \\ - u(x)\cdot\nabla_x\lambda_2(x) + \lambda_2(x)\cdot\nabla_x u(x) - \nabla_x\lambda_3(x) = 0, \quad \text{and,} \tag{4.6}$$

$$\nabla_x\cdot\lambda_2(x) = 0. \tag{4.7}$$

with boundary conditions $\lambda_1(x,t) = 0$ and $\lambda_2(x,t) = 0$ for each $x \in \partial\Omega$ and $t \in [0,T]$, together with final condition $\lambda_1(x,T) = 0$ for each $x \in \Omega$. The adjoint functions λ_4 and λ_5 are irrelevant to our Fréchet derivative calculation, therefore we omit them from this presentation.

Now we can compute the Fréchet derivatives of the cost function with respect to θ and π_0. Consider a parameter change from (θ, π_0) to $(\theta + \delta\theta, \pi_0 + \delta\pi_0)$. Since both α and κ are affine in θ, these variations will result in changes from (α, κ) to $(\alpha + \delta\alpha, \kappa + \delta\kappa)$, which will also imply changes from (T_e, u, p) to $(T_e + \delta T_e, u + \delta u, p + \delta p)$. As detailed in Appendix B, these variations allow us to compute a first-order approximation of the cost function J, which result in,

$$\begin{aligned} \left\langle \mathcal{D}_\alpha J, \delta\alpha \right\rangle_\Omega &= \langle \lambda_2 \cdot u, \delta\alpha \rangle_\Omega, \quad \text{and} \\ \left\langle \mathcal{D}_\kappa J, \delta\kappa \right\rangle_\Omega &= \int_0^T \left\langle \nabla_x\lambda_1 \cdot \nabla_x T_e, \delta\kappa \right\rangle_\Omega \mathrm{d}t, \end{aligned} \tag{4.8}$$

and using the chain rule and the formulas in equation (4.8) we get the desired directional derivatives for J,

$$\begin{aligned} \left\langle \mathcal{D}_{\pi_0} J, \delta\pi_0 \right\rangle_\Omega &= \langle \nabla_{\pi_0} J - \lambda_6, \delta\pi_0 \rangle_\Omega, \quad \text{and} \\ \mathcal{D}_\theta J \cdot \delta\theta &= \sum_{i=1}^{n_d} \left(\left\langle \mathcal{D}_\alpha J, \frac{\partial\alpha}{\partial\theta_i} \right\rangle_\Omega + \left\langle \mathcal{D}_\kappa J, \frac{\partial\kappa}{\partial\theta} \right\rangle \right) \delta\theta_i. \end{aligned} \tag{4.9}$$

Note that both directional derivatives are linear bounded operators, hence they are also Fréchet derivatives as desired.

4.2.2 Gradient-Based Optimization Algorithm

Using the closed-form formulas for the Fréchet derivatives of J with respect to π_0 and θ, we build a gradient-based optimization algorithm to solve the problem in equation (4.2) using a projected-gradient method [99, Chapter 18.6].

First, we find descent directions $\delta\pi_0$ and $\delta\theta$ as solutions of the following Quadratic Program (QP) with value V,

$$\begin{aligned} V = \min_{\delta\pi_0 \colon \Omega\to\mathbb{R},\, \delta\theta\in\mathbb{R}^{n_d}} & \langle \mathcal{D}_{\pi_0} J, \delta\pi_0 \rangle_\Omega + \mathcal{D}_\theta J \cdot \delta\theta + \frac{\gamma}{2} \left\|\delta\pi_0\right\|_\Omega^2 + \frac{\gamma}{2} \left\|\delta\theta\right\|^2, \\ \text{subject to: } & 0 \leq \theta_i + \delta\theta_i \leq 1,\ \forall i \in \{1, \ldots, n_d\}. \end{aligned} \tag{4.10}$$

Where $\gamma > 0$ is a parameter. The QP in equation (4.10) is derived using first-order approximations for the cost function using the derivatives in equation (4.9), together with a condition to guarantee the feasibility of the desired direction. Note that $V \leq 0$, since $\delta\pi_0 = 0$ and $\delta\theta = 0$ always belong to the feasible set. Hence, if $V = 0$ then our method cannot find further descent directions, and it thus terminates.

Second, a step size is computed using the following Armijo line search method:

$$\begin{aligned} \beta = & \arg\max_{j\in\mathbb{N}} \bar{\beta}^j, \\ & \text{subject to: } J\big(\pi_0 + \bar{\beta}^j\, \delta\pi_0, \theta + \bar{\beta}^j\, \delta\theta\big) - J(T_e, \pi_0, \theta) \leq \bar{\alpha}\, \bar{\beta}^j\, V. \end{aligned} \tag{4.11}$$

Where $\bar{\alpha}, \bar{\beta} \in (0, 1)$ are parameters.

Algorithm 1 Gradient-based estimation algorithm

Require: Initial values for θ and π_0.

1: **loop**
2: Compute T_e, u, and p by solving the CFD model in equations (2.2) to (2.6).
3: Compute λ_1, λ_2, λ_3, and λ_6 by solving the adjoint equations (4.4) to (4.7).
4: Compute the gradients $\mathcal{D}_{\pi_0}$ and $\mathcal{D}_\theta$ in equation (4.9).
5: Compute the projected-gradient descent directions $(\delta\pi_0, \delta\theta)$ by solving the QP in equation (4.10), with value V.
6: **if** $V = 0$ **then**
7: Stop.
8: Compute the step size β using the Armijo line search method in equation (4.11).
9: Update $\pi_0 \leftarrow \pi_0 + \delta\pi_0$ and $\theta \leftarrow \theta + \beta\,\delta\theta$.

Our gradient-based optimization method is detailed in Algorithm 1. Steps 2 and 3, are numerically solved using FEM discretizations, implemented using the FEniCS package [94].

4.3 Simulations

We applied our estimation algorithm to a simulated St. Louis area apartment with $n_d = 4$ doors, labeled $\{d_i\}_{i=1}^4$, and $n_t = 3$ thermostats, labeled $\{s_i\}_{i=1}^3$. The floor plan of the apartment is shown in figure 4.1, with dimensions $7.6 \times 16.8[\text{m}^2]$ (approx. 1375[sq ft]). The apartment is equipped with four HVAC vents, labeled $\{h_i\}_{i=1}^4$. We assume that each vent is endowed with a fan acting on a $1 \times 0.5[\text{m}^2]$ area, and oriented in a fixed direction. The four HVAC fan units work independently to control both the indoor temperature and air flows.

The CFD model is governed by the constants $Re = 10^2$, $\alpha_0 = 0$, and $\kappa_0 = 10^{-2}$ when $x \in \Omega$ corresponds to free air, while $\alpha_w = 10^3$ and $\kappa_w = 10^{-4}$ when $x \in \Omega$ corresponds to a wall. The atmospheric pressure is $p_A = 101.3[\text{kPa}]$, and the atmospheric temperature is $T_A = 23.83[^\circ\text{C}]$. We assume that h_1 and h_2 work at a low output setting, producing 0.1[kW] of heat and an air flow speed of 0.1[m/s]. On the other hand, h_3 and h_4 work at a normal

setting, producing 4[kW] of heat and and an air flow speed of 0.5[m/s]. The time horizon is 300[s], sampled uniformly at 10[s] steps. The sensors' observation radius is $r = 1.0$[m]. The parameters in (4.2) are set to $\eta_0 = 1.0$, $\eta_1 = 0.1$. The parameter in (4.10) is set to $\gamma = 1.0$. The parameters in (4.11) are set to $\bar{\alpha} = 0.01$ and $\bar{\beta} = 0.7$. We wrote our code in Python, the FEM discretization was computed using tools from the FEniCS Project [94], and the building plan was discretized into $n_{\text{elem}} = 6276$ elements.

4.3.1 Probabilistic estimation method

In our simulations below we compare our estimation method with a probabilistic-based estimation algorithm formulated by [17], and applied to problems involving parameter estimation of differential equations [18]. Under Banks and Bihari's framework, π_0 and θ are random variables with unknown probability distributions, thus the estimation problem is formulated to find the optimal distributions that would most likely produce the acquired sensor data in expectation. Due to space constraints we omit a detailed description of this method, and we refer interested readers to [17].

Let $\pi_{0,\Delta}$ be the FEM discretization of π_0, hence $\pi_{0,\Delta} \in \mathbb{R}^{n_{\text{elem}}}$. We assume that θ and $\pi_{0,\Delta}$ follow probability distributions $\mathbb{P}(\theta)$ and $\mathbb{P}(\pi_0)$. In the particular case of θ, since it is a vector of independent binary variables, its distribution is $\mathbb{P}(\theta) = \prod_{i=1}^{n_d} p_i^{\theta_i} (1 - p_i)^{1-\theta_i}$. We assume that θ and $\pi_{0,\Delta}$ are independent.

Banks and Bihari's estimation algorithm relies on closed-form formulas of the expected values of each of the random variables in the cost function. Using the cost function in equation (4.2), the only nontrivial expected value is that of $T_{e,\Delta}(x, t; \pi_{0,\Delta}, \theta)$, the FEM discretization of T_e. Note that given $x \in \Omega$, $t \in [0, T]$, and $\theta \in \{0, 1\}^{n_d}$, then $T_{e,\Delta}(x, t; \pi_{0,\Delta}, \theta)$ is a linear

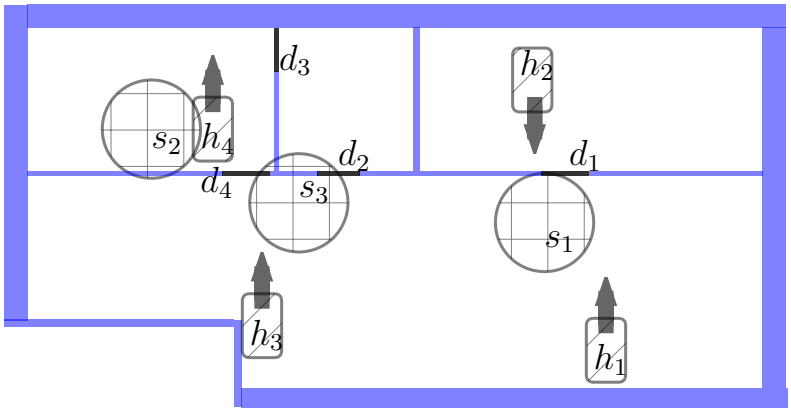

Figure 4.1: Floor plan of the apartment simulated in section 4.3.

function of $\pi_{0,\Delta}$; hence, as shown by [91, Chapter 3], the conditional expected value of $T_{e,\Delta}$ is $\mathbb{E}[T_e(x,t;\pi_{0,\Delta},\theta) \mid \theta] = T_{e,\Delta}(x,t;\mathbb{E}[\pi_{0,\Delta}],\theta)$ for each pair (x,t). Then, using Bayes' rule,

$$\begin{aligned} &\mathbb{E}[T_{e,\Delta}(x,t;\pi_{0,\Delta},\theta)] = \sum_{\theta\in\{0,1\}^{n_d}} T_{e,\Delta}(x,t;\mathbb{E}[\pi_{0,\Delta}],\theta)\ \mathbb{P}(\theta), \\ &\forall x \in \Omega,\ t \in [0,T]. \end{aligned} \tag{4.12}$$

It is worth noting that the cardinality of $\{0,1\}^{n_d}$ is 2^{n_d}, hence each evaluation of equation (4.12) involves solving a PDE an exponentially growing number of times as a function of n_d.

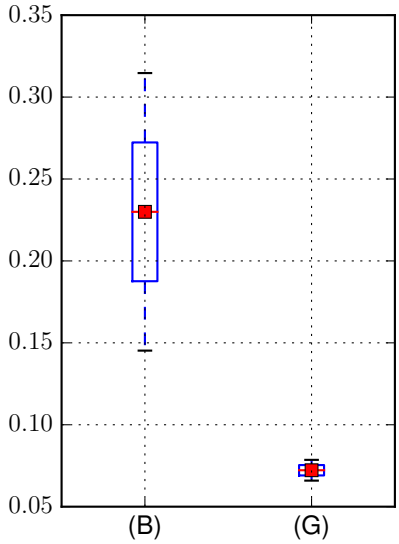

(a) Average estimation error of θ.

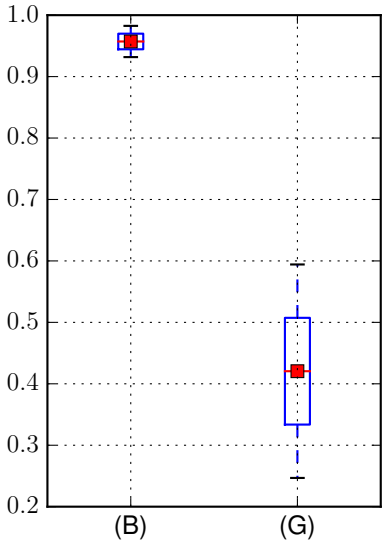

(b) Relative estimation error of π_0.

Figure 4.2: Results of the experiments in section 4.3.2. Columns: (B) Banks and Bihari's method, (G) Gradient-based method, algorithm 1.

4.3.2 Estimation using three thermostats

We run both estimation algorithms, Banks and Bihari's method and gradient-based method, algorithm 1, under six different combinations for

$$\theta \in \{(0,0,0,0),(0,0,1,1),(0,1,1,0),(0,1,1,1),(1,0,0,0),(1,1,1,1)\},$$

and two different initial temperatures π_0. Since algorithm 1 converges to local minimizers, we also run five estimations for each pair (π_0, θ) initializing the algorithm with different values.

Figure 4.2a is a bar plot of the average estimation errors of θ, calculated as

$$e_\theta = \frac{1}{n_d}\sum_{i=1}^{n_d}\left|\theta_i - \hat{\theta}_i\right|,$$

where $\hat{\theta}$ is either the estimated probability distribution from Banks and Bihari's method, or the estimated relaxed configuration from gradient-based method, algorithm 1.

Figure 4.2b shows a similar bar plot for the relative estimation error of π_0, calculated as $e_{\pi_0} = \frac{\|\pi_0 - \hat{\pi}_0\|_\Omega}{\|\pi_0\|_\Omega}$, where $\hat{\pi}_0$ is either the estimated expected value of π_0 from Banks and Bihari's method, or the estimated initial distribution from gradient-based, algorithm 1. From these results we can observe that algorithm 1 is significantly more accurate than the probabilistic method in estimating both doors' states and initial temperature distribution. It is worth noting that the average error of gradient-based method, algorithm 1, in figure 4.2a is small enough so that one can use a constant threshold to convert from relaxed values of θ to binary values. Also, the accuracy of our results enables further smart applications, such as the locating the residents in a building by using thermostat data and further behavioural assumptions.

In figures 4.3, 4.4 and 4.5 we show the actual initial temperature distribution for one configuration θ, and the estimation errors by both algorithms. These results show that even with the temperature of three points, the gradient-based method, algorithm 1, can accurately reconstruct the initial temperature distribution in the building, thus enabling advanced control methods such as MPC to significantly improve the energy efficiency of the HVAC system [77].

4.3.3 Estimation using only one thermostat

Now we only assume that only one thermostat, s_1, is functional. The motivation is to show the performance of both estimation algorithms in a realistic scenario, since most residential buildings' HVAC systems operate using a single thermostat. We simulated the same scenarios as in Section 4.3.2.

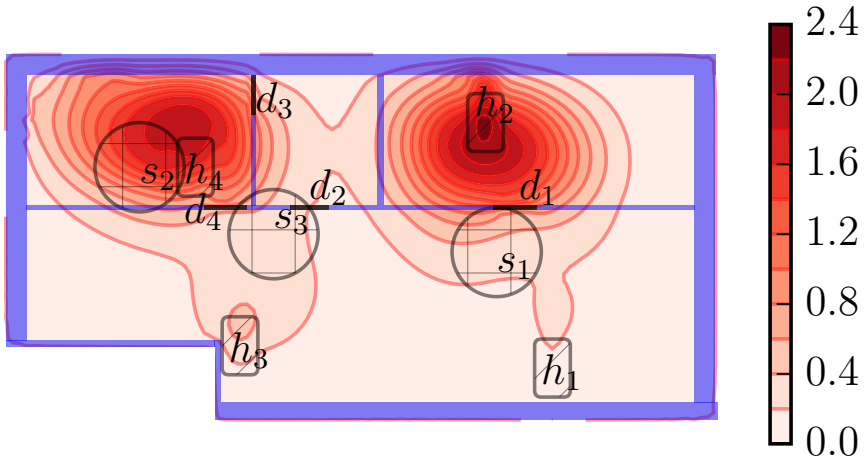

Figure 4.3: Initial temperature π_0 in [°C] with respect to T_A.

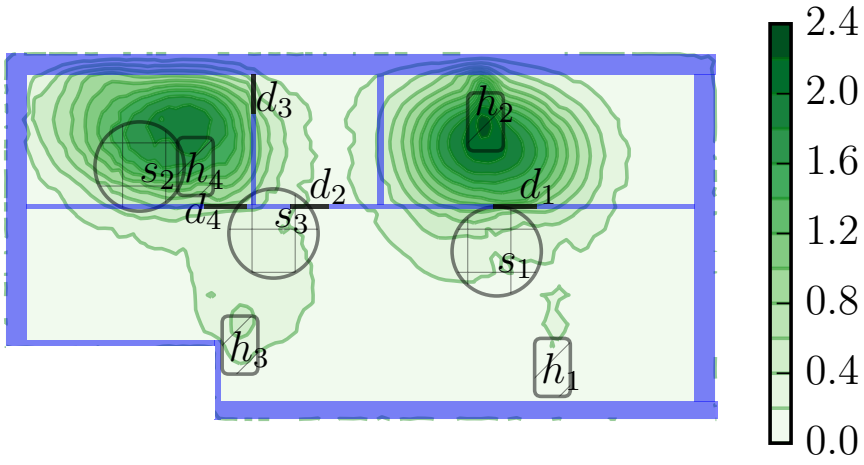

Figure 4.4: Estimation error of π_0 by Banks and Bihari's method, when all doors are closed.

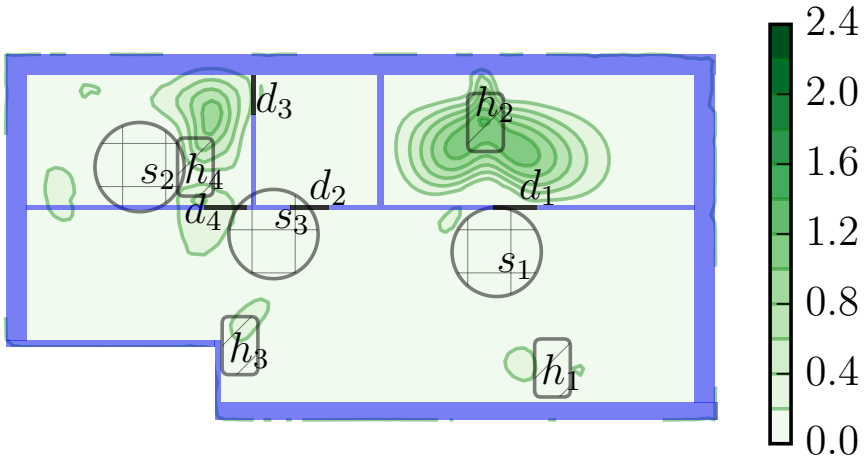

Figure 4.5: Estimation error of π_0 by gradient-based method, algorithm 1, when all doors are closed.

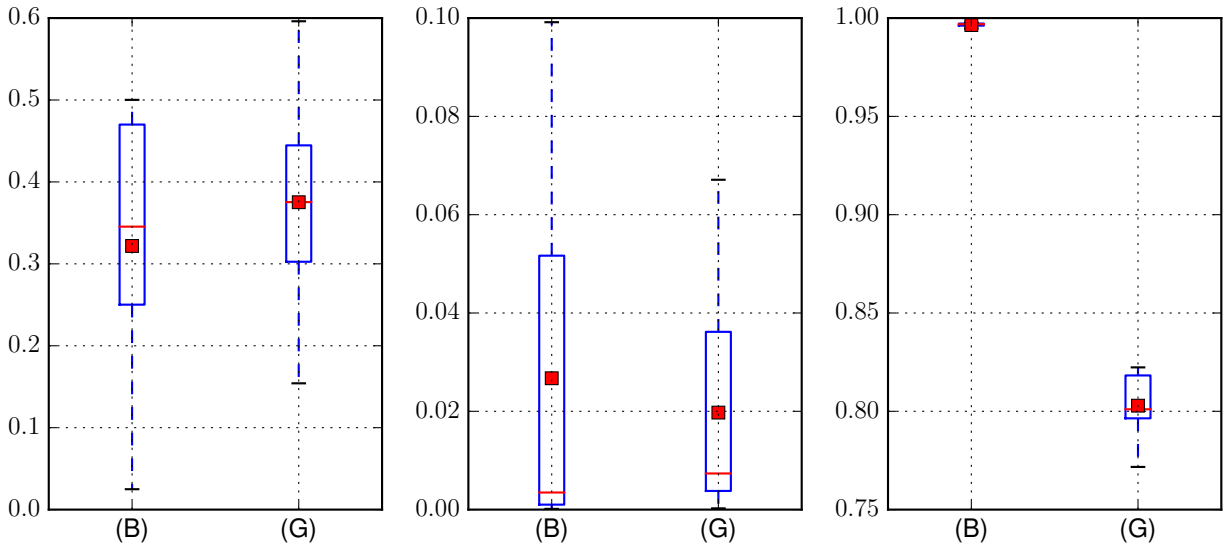

(a) Average estimation error of θ. (b) Estimation error of θ_1. (c) Relative estimation error of π_0.

Figure 4.6: Results of the experiments in section 4.3.3. Columns: (B) Banks and Bihari's method, (G) Gradient-based method, algorithm 1.

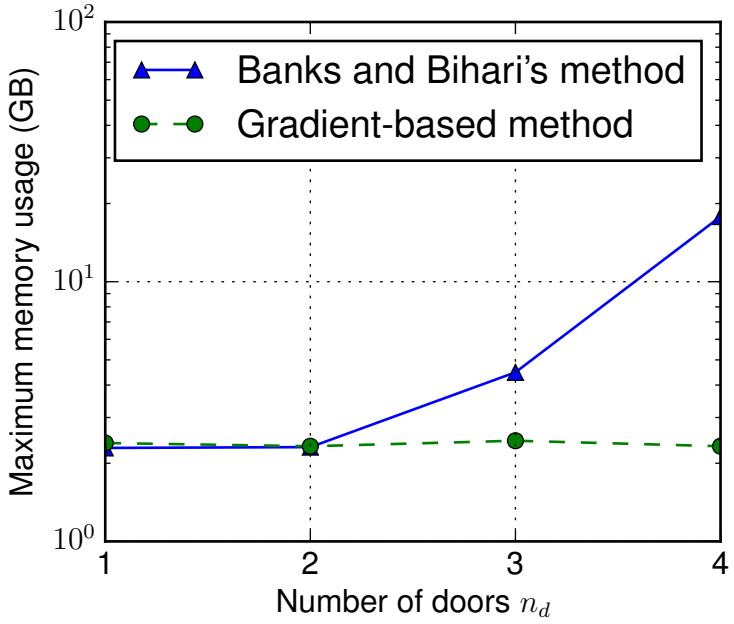

Figure 4.7: Memory usage in [GB] of the experiments in Sec. 4.3.4.

Figures 4.6a and 4.6c are analogous to those in figure 4.2, while Figure 4.6b shows the estimation error just for door d_1, which is located very close to thermostat s_1. As shown in these figures, both estimation algorithms do an almost equally poor job at estimating the doors' states, and the gradient-based method, algorithm 1, is marginally better at estimating the initial temperature distribution. Yet, both algorithms are capable of accurately estimating the configuration of the door closest to the thermostat.

4.3.4 Memory usage comparison

A significant advantage of the gradient-based method, algorithm 1, when compared to probabilistic estimation algorithms is that our method does not need to compute numerical solutions of the set of differential equations for each possible configuration $\theta \in \{0, 1\}^{n_d}$. Figure 4.7 shows the maximum memory usage of both algorithm implementations as the

number of doors to estimate increases from 1 to 4. Our results show that the probabilistic estimation method can be used only for small values of n_d, quickly outgrowing the amount of memory in standard computers (for $n_d = 4$ the usage was 16[GB] approx.), while algorithm 1 memory usage remains almost constant (at 2.4[GB] approx.).

4.4 Chapter conclusion

In this chapter, we introduce a gradient-based estimation method to estimate the fluid dynamic system's distribution and building's indoor congiguration at the same time. Our gradient-based estimation method and simulation results show the potential for reconstructing indoor climate and building configuration by using only thermostat sensor data, thus reducing the need for extra sensors to monitor a smart buildings. Also, since the method can accurately estimate the indoor climate and configuration with acceptable memory usage, it can be used in coordination to advanced MPC control strategies, significantly increasing the efficiency of HVAC units without a decrease in human comfort. Our method has the potential to enable interesting new applications. For example, since it is able to identify a building's configuration in real-time, it can potentially be applied to monitor an unexpected break-in.

Chapter 5

MPC for Indoor Thermal Comfort via PDE-based CFD Model

In this chapter, we apply the numerical algorithm in chapter 4 to develop a Model Predicted Control (MPC) to optimize the thermal comfort around indoor residents based on our PDE-based CFD model. The thermal comfort is measured by PMV index's approximation and the optimization control pairs the heater's power with fan's speed, not focuses only on temperature regularity. Optimizing the thermal comfort zoned area around indoor residents instead of the whole apartment is potential to make the HVAC system energy efficient [77]. Also the MPC is able to identify indoor climate distribution and an apartment's doors configuration based only on thermostatic data.

The chapter is organized as follows: section 5.1 describes the formulation of MPC which consists of an estimator and optimal controller; section 5.2 discusses the first order gradient-based algorithm to solve the PDE-constrained optimization problem, the introduction to the fluid dynamic system's adjoint equations and the finite element discretization of the PDEs; and section 5.3 gives the results of our simulated experiments which is based on the floor plan of a real apartment from our university's housing company. Our theoratical and numerical

results validate our MPC controller which can balance energy savings and occupants' thermal comfort at the same time, and the accurate CFD models enables the details of the climate variables inside apartment and the change of door's configuration.

5.1 Problem statement

5.1.1 Framework of the MPC for indoor comfort

In the aspect of framework of the HVAC system's control, figure 5.2 is the flow chart for our thermal comfort control for HVAC system, compared with single temperature loop control in figure 5.2, our thermal comfort control system has several improvements. We introduce a distributed-parameter model which will capture the real-time spatial variability of indoor flow's climate according to floor plan. Secondly, in order to control the thermal comfort directly, wearable devices are used to monitor occupant's personal variable [87, 40, 134] in order to make the thermal comfort's prediction accurately. Also the control strategy is different, we separately control each HVAC units in order to better control a local area's climate and make the HVAC system more energy-efficient [77].

5.1.2 CFD model and building configurations

The CFD model in this chapter follows equations (2.2), (2.4) and (2.5) in chapter (2). And we assume the fans are inside the building, thus $\Gamma_i = \emptyset$ and the fluid follows the eqautions (2.8) and (2.6) and the initial condition (2.3).

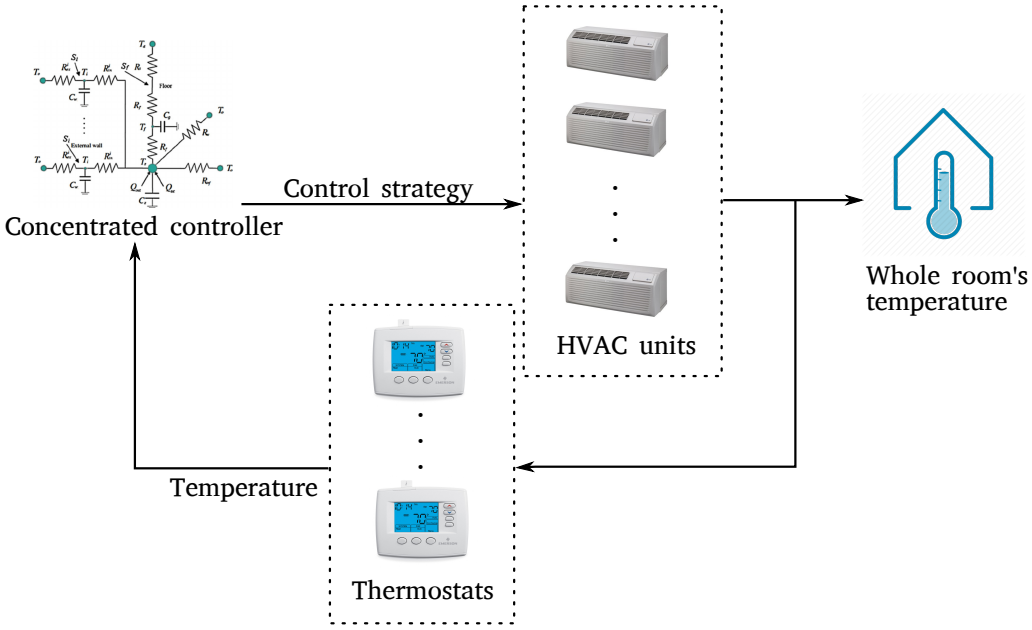

Figure 5.1: Single temperature loop control for HVAC.

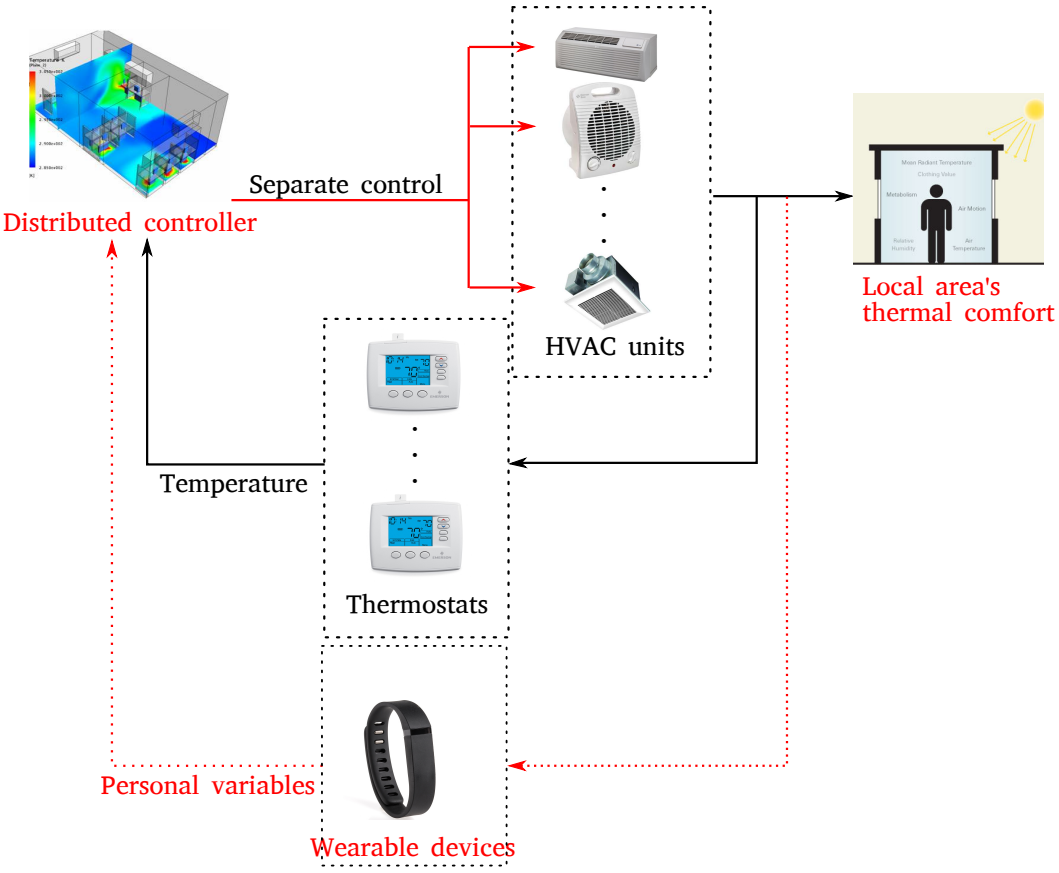

Figure 5.2: Our control for HVAC.

Based on the control framework in figure 5.2, we assume that there are n_t thermostats in the building. The i-th thermostat is located at $x_i \in \Omega$, and samples the temperature in a neighborhood averaged using the *bump weight function*

$$\Phi_i(x) = \sigma \, \exp\big(-\big(r^2 - \|x - x_i\|^2\big)^{-1}\big), \text{ for } \|x - x_i\| < r,$$

and $\Phi_i(x) = 0$ otherwise, where $\sigma > 0$ is a normalization factor such that $\int_\Omega \Phi_i(x)\,\mathrm{d}x = 1$.

We also assume that there are n_d doors in the building. We define $\theta_i \in \{0, 1\}$ as the configuration of the i-th door, i.e., $\theta_i = 1$ when the i-th door is open, and $\theta_i = 0$ when is closed. Let $\Omega_{\theta_i} \subset \Omega$ be the area occupied by the i-th door when it is closed, and let $\mathbb{I}_i$ be the indicator function of Ω_{θ_i}, i.e., $\mathbb{I}_i(x) = 1$ for $x \in \Omega_{\theta_i}$, and $\mathbb{I}_i(x) = 0$ otherwise. As mentioned in chapter 4, when the door configuration changes, so does the prediction generated by our CFD model in equations (2.2) and (2.4). In particular, the parameters α and κ change for each $x \in \Omega_{\theta_i}$ as a function of θ_i. We model this relation by defining $\alpha\colon \Omega \times \{0, 1\}^{n_d} \to \mathbb{R}$ and $\kappa\colon \Omega \times \{0, 1\}^{n_d} \to \mathbb{R}$ as follows,

$$\begin{aligned} \alpha(x, \theta) &= \alpha_0 + \sum_{i=0}^{n_d} (1 - \theta_i)\,(\alpha_w - \alpha_0)\,\mathbb{I}_i(x), \quad \text{and} \\ \kappa(x, \theta) &= \kappa_0 + \sum_{i=0}^{n_d} (1 - \theta_i)\,(\kappa_w - \kappa_0)\,\mathbb{I}_i(x), \end{aligned} \tag{5.1}$$

where α_0 and κ_0 are the parameters for open air, while α_w and κ_w are the parameters for solid walls. Note that both α and κ are affine functions of $\theta \in \mathbb{R}^{n_d}$.

Then we relax these binary parameters, $\theta_i \in \{0, 1\}$, to the unit interval, $[0, 1]$, because the binary estimation variables will generate mix-integered optimization problem which performance poorly in both computation time and computational resources [64]. Although for each

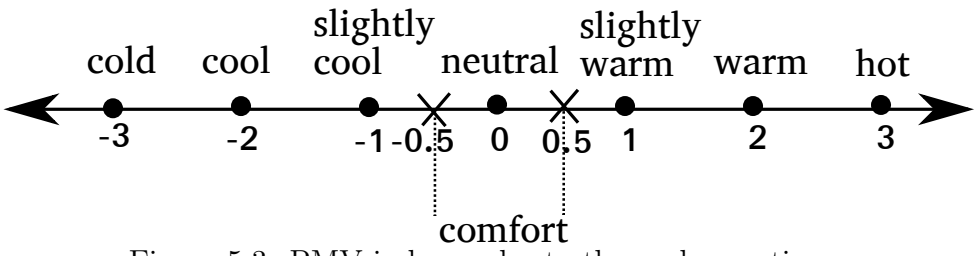

Figure 5.3: PMV index scales to thermal sensations.

θ_i only the extreme values have meaningful physical interpretations, non-integer values can theoretically be interpreted as averaged observations over the optimization horizon [125, 126]. For example, if throughout the optimization horizon a door is open half the time, and closed half the time, it is likely that we will observe $\theta_i \approx 0.5$.

5.1.3 Predicted Mean Vote Index and Its Approximation

The PMV index was proposed by Fanger [54] and recommended by the American Society of Heating Refrigerating and Air Conditioning Engineers (ASHRAE) [7] in order to predict the average vote of a large group of persons on the thermal sensation scale. It uses heat balance equation to relate six key factors to the average response of people on the thermal comfort. The PMV index will become inaccurate when facing high clothing insulation and high human activity cases, however, for occupant's daily activity levels and clothing insulation inside apartment, the index is accurate. As figure 5.3, the closer the PMV index to zero, the more comfortable the occupant feels. According to [7], the range of PMV index for an acceptable thermal environment of general comfort is from -0.5 to 0.5.

The PMV index depends on six factors: metabolic rate, clothing insulation, air temperature and humidity, air velocity, and the mean radiant temperature. Due to its iterative computation and in order to reduce the related computational burden, we approximate the PMV

index function for the optimization problem [37], [55]. The PMV index is computed by

$$\begin{aligned} pmv = &\left(0.303e^{-0.036M} + 0.028\right)\Big[(M-W)- \\ &- 3.05\cdot 10^{-3}[5733 - 6.99(M-W) - p_a] - 0.42[(M-W) - 58.15] - 1.7\cdot \\ &\cdot 10^{-5}M(5867 - p_a) - 0.0014M(34 - T_e) + \\ &- 3.96\cdot 10^{-8} f_{cl}\cdot\left[(T_{cl}+273)^4 - (T_r+273)^4\right] - f_{cl}h_c(T_{cl}-T_e)\Big]. \end{aligned} \tag{5.2}$$

In the Equation (5.2), M and W are the metabolic rate and external work, both in [W/m^2]. According to the references [14] and [7], the external work normally is around 0, and the average value of human's sedentary activity and standing activity is 70[W/m^2] and 93[W/m^2] respectively. The occupant's metabolic rate can be obtained either from their wearable devices or some posterior estimation [87, 40, 134].

p_a is the partial water vapor pressure in Pascal. According to [15], [113], the specific humidity inside house, w_i with unit [kg $\cdot$ kg^{-1}], can be expressed by,

$$w_i = \frac{\rho\sum_{j=1}^{n_f} Q_j w_{o,j} + m_g}{\rho\sum_{i=1}^{n_f} Q_i}. \tag{5.3}$$

where $w_{o,j}$ is the specific humidity comes out of the j-th HVAC, the total number of indoor HVAC units is n_f, ρ is the inside air's density. m_g is the rate of moisture generation within the building with unit [kg $\cdot$ s^{-1}], Q_j is the volume flow rate of air comes out of the j-th HVAC unit with unit [m^3 $\cdot$ s^{-1}], and we ignore the moisture diffusion through the fabric material [14]. In our model $Q_j = |g_{u,j}| = A_j v_j$, where A_j is the size of the j-th fan with unit [m^2], v_j is the working speed for the j-th fan with unit [m $\cdot$ s^{-1}]. Under ideal air condition, $p_a = p_o w_i/0.622$, where the mixed air's pressure p_o is the standard atmosphere, 1.013×10^5[Pa].

T_e and T_r are the air temperature and mean radiant temperature, both with unit [°C]. Experiments results [128] show that their indoor distributions are close. In order to simplify the PMV index for optimization computation and noting that most buildings typically do not have sensors to continually measure the mean radiant temperature, we set the T_r equal to the air temperature, T_e. Moreover, since the range of temperatures in the indoor environment is small, the difference of the fourth power terms can be adequately replaced by a lower-order difference [14],

$$\begin{aligned} &3.96 \cdot 10^{-8} f_{cl} \cdot \left[(T_{cl}+273)^4 - (T_r+273)^4\right] \approx \\ &\approx 4.6 f_{cl}(1+0.01T_r)(T_{cl}-T_r) \end{aligned} \tag{5.4}$$

The clothing surface temperature is approximated as [14] [54],

$$\begin{aligned} T_{cl} &= 35.7 - 0.028(M-W) + \\ &- 0.155 I_{cl} f_{cl}[4.6(1+0.01T_r)(T_{cl}-T_r) + h_c(T_{cl}-T_e)]. \end{aligned} \tag{5.5}$$

Where we approximate the radiation term with equation (5.4), then we can derive an explicit formula of T_{cl} and get rid of the iteration numerical solving process. h_c is the convective heat transfer coefficient [54] [41] and is approximated as the natural convective heat transfer coefficient, h_{cn} [37] [55]. The parameter f_{cl} is equal to $1.0{+}1.29I_{cl}$ when $I_{cl} \leq 0.078$, otherwise $1.05 + 0.645I_{cl}$, where I_{cl} is the clothing insulation index, in [m^2 °C/W].

Thus after the approximation, in our model, the PMV index is influenced by parameters T_e, g_u, M and I_{cl}, we denote it as $pmv(T_e, g_u, M, I_{cl})$.

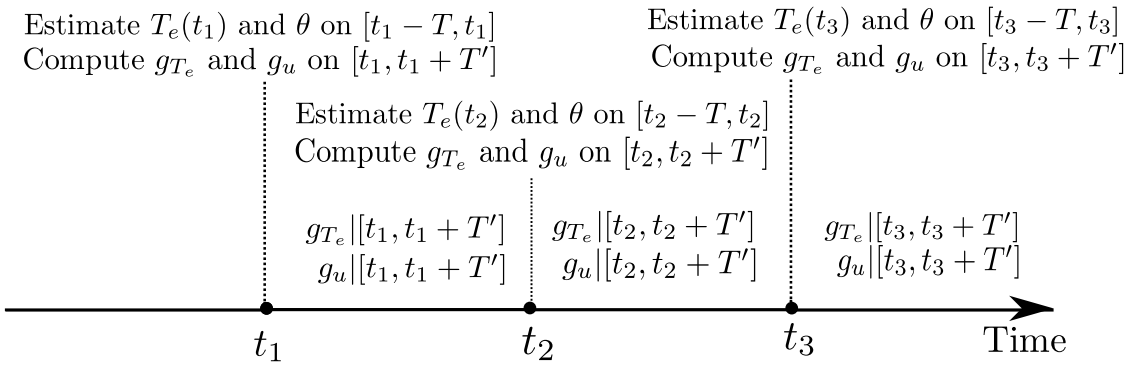

Figure 5.4: The illustration of the model predicted control during $[t_1, t_3]$.

5.1.4 Optimization Problem and Model Predicted Control

In this subsection, we are going to build an Model Predicted Control (MPC) in order to control the thermal comfort inside a target area. MPC is based on iterative, finite-horizon optimization. The illustration of the MPC process is shown in figure 5.4. At each time point, t_i, $i \in 1, 2, \cdots$, the MPC solves two optimization problems, the first is an estimation problem for indoor temperature distribution and doors configuration, and the other is to control the thermal comfort inside the target area.

First, we formulate the estimation algorithm to estimate the door configuration θ and the initial temperature π_0 using the information from the n_t thermostats in the building. Given the estimation time horizon as $[t_i - T, t_i]$, we write our optimal estimation problem as follows,

for $\pi_0 \colon \Omega \to \mathbb{R}$ and $\theta \in \mathbb{R}^{n_d}$,

$$\begin{aligned}
&\min_{\pi_0,\theta} J_e(\pi_0,\theta) = \\
&\quad = \sum_{i=1}^{n_t} \int_{t_i-T}^{t_i} \left(\int_{\Omega_i} \Phi_i \, T_e(x,t;\pi_0,\theta) \, \mathrm{d}x - T^*_{e,i} \right)^2 \\
&\quad \mathrm{d}t + \eta_0 \sum_{i=1}^{n_t} \left(\int_{\Omega_i} \Phi_i \, \pi_0 \, \mathrm{d}x - \pi^*_{0,i} \right)^2 + \eta_1 \left\| \pi_0 \right\|^2_{\Omega} \qquad (5.6) \\
&\text{subject to: partial differential equations (2.2), (2.4), and (2.5),} \\
&\qquad \text{boundary and initial conditions (2.3), (2.8), and (2.6),} \\
&\qquad 0 \le \theta_i \le 1, \quad \forall i \in \{1, \ldots, n_d\},
\end{aligned}$$

where, $\eta_0, \eta_1 > 0$ are weight parameters. Since during the estimation horizon, we know the HVAC system's outputs, g_{T_e} and g_u, $T_e(x,t;\pi_0,\theta)$ is the solution of equation (2.2) with certain initial condition $\pi_0(x)$ and configuration θ. $T^*_{e,i}(t)$ is the time signal obtained from the i-th thermostat over the horizon $[t_i - T, t_i]$, and $\pi^*_{0,i}$ is just notation for the initial thermostat temperature, i.e., $\pi^*_{0,i} = T^*_{e,i}(t_i - T)$.

For the optimal control problem, we use the previous estimation problem's results which are the door configuration, θ, and temperature estimation at time t_i, $T_e(x,t_i;\pi_0,\theta)$, to predict and control the approximated PMV index inside the target area, $\Omega_t \subset \Omega$. Since the door configuration, θ, and initial temperature distribution for the optimal control problem, $\pi_0 = T_e(x,t_i;\pi_0,\theta)$ are from the previous estimation results, the optimal control problem focuses on the HVAC system's outputs. Given the optimal control's horizon as $[t_i, t_i + T']$, where $T' > T$, the optimal control problem is written as, for $g_{T_e} \colon [t_i, t_i + T] \times \Omega \to \mathbb{R}$ and $g_u \colon \Omega \to$

$\mathbb{R}^2$,

$$
\begin{aligned}
&\min_{g_{T_e},\, g_u} J_c(g_{T_e}, g_u) = \\
&\qquad = \int_{t_i}^{t_i+T'} \int_{\Omega_t} pmv^2(T_e(x,t;\pi_0,\theta), g_u, M, I_{cl}) \\
&\qquad \mathrm{d}x\mathrm{d}t + \eta_0' \left\| g_{T_e} \right\|_{\Omega\times[t_i,t_i+T']} + \eta_1' \int_{t_i}^{t_i+T'} \left\| g_u \right\|_{\Omega}, \\
&\text{subject to: partial differential equations (2.2), (2.4), and (2.5),} \\
&\qquad \text{boundary and initial conditions (2.3), (2.8), and (2.6),} \\
&\qquad \underline{g_{T_e}} \le \left\| g_{T_e,i} \right\|_\infty \le \overline{g_{T_e}}, \quad \forall i \in \{1,\ldots,n_f\}, \\
&\qquad \underline{g_u} \le \left\| g_{u,i} \right\|_\infty \le \overline{g_u}, \quad \forall i \in \{1,\ldots,n_f\},
\end{aligned}
\tag{5.7}
$$

where, $\eta_0', \eta_1' > 0$ are weight parameters, n_f is the number of HVAC units inside the apartment, $\underline{g_{T_e}}$ and $\overline{g_{T_e}}$ are the maximum and minimum power for each heater unit respectively, $\underline{g_u}$ and $\overline{g_u}$ are the maximum and minimum power for each fan unit respectively.

After the MPC solves the optimal problems in equations 5.6 and 5.7, the HVAC system will apply the MPC's control strategy for a T time horizon until the next time point t_{i+1} and repeat the procedure.

5.2 Methods

In this section we develop a numerical algorithm to solve the optimization problems defined in Section 5.1. We use a gradient-based optimization algorithm to find local minimizers of our optimization problems, where the gradients are computed using the adjoint equations of the CFD model, the method is similar to [71] and [135], then we numerically solve the original CFD model and adjoint equations using the Finite Element Method (FEM).

5.2.1 Adjoint Equations of CFD model

In order to derive our CFD model's adjoint equations, first we need to write the *Lagrangian function* of the optimization problems [65, 71]. Since both estimation and control problems follow the same CFD model, we define a general cost function as $J(\pi_0, \theta, g_{T_e}, g_u)$.

Let $\{\lambda_i\}_{i=1}^{6}$ be the set of *Lagrange multipliers*, or *adjoint variables*, each associated to one of the equations (2.2) to (2.6) and defined in its respective dual space. Then, the Lagrangian function of our optimal estimation problem is:

$$
\begin{aligned}
L\big(T_e, u, p, \pi_0, \theta, \{\lambda_i\}_{i=1}^{6}\big) = \Big\langle \lambda_1, \frac{\partial T_e}{\partial t} + \\
- \nabla_x \cdot (\kappa(x)\, \nabla_x T_e) + u \cdot \nabla_x T_e - g_{T_e} \Big\rangle_{\Omega \times [t_0, t_0']} + \\
+ \Big\langle \lambda_2, -\frac{1}{Re} \Delta_x u + (u \cdot \nabla_x) u + \nabla_x p + \alpha\, u - g_u \Big\rangle_{\Omega} + \\
+ \langle \lambda_3, \nabla_x \cdot u \rangle_{\Omega} + \langle \lambda_4, T_e \rangle_{\partial\Omega \times [t_0, t_0']} + \langle \lambda_5, u \rangle_{\Gamma_w} + \\
+ \langle \lambda_6, T_e(0, \cdot) - \pi_0 \rangle_{\Omega} + J(\pi_0, \theta, g_{T_e}, g_u),
\end{aligned}
\tag{5.8}
$$

The necessary condition for optimality is that the inner product of the partial derivatives of L with respect to all directions are equal to zero [71]. The adjoint equations are derived from the optimality's necessary condition L w.r.t. fluid dynamic model's variables' directions. That is, we look for solutions such that for each set of functions (w, v, q) in the respective dual spaces, and sufficiently weakly differentiable, we have $\big\langle \frac{\partial L}{\partial T_e}, w \big\rangle_{\Omega \times [t_0, t_0']} = 0$, $\big\langle \frac{\partial L}{\partial u}, v \big\rangle_{\Omega} = 0$ and $\big\langle \frac{\partial L}{\partial p}, q \big\rangle_{\Omega} = 0$.

Theorem 5.1. *If* $(T_e^\star, u^\star, p^\star, \pi_0^\star, \theta^\star)$ *is the optimal point to the problem* (5.6)*, then there exist Lagrange multipliers,* $\{\lambda_i\}_{i=1}^{6}$*, which are corresponding to PDE-constraints, such that* $\forall (w, v, q) \in L^2\big([t_0, t_0']; H^1(\Omega)\big) \times \big(H^1(\Omega) \times H^1(\Omega)\big) \times L^2(\Omega)$*, the Lagrange function's variation*

w.r.t. (w, v, q) *is zero, and* $\lambda_{1,2,3,6}$ *satisfy,*

$$\begin{aligned} &-\frac{\partial J}{\partial T_e} + \frac{\partial \lambda_1}{\partial t}(x,t) + \nabla_x \cdot (\kappa(x)\, \nabla_x \lambda_1(x,t)) + \\ &+ u(x) \cdot \nabla_x \lambda_1(x,t) = 0, \end{aligned} \tag{5.9}$$

$$\lambda_6(x) = \lambda_1(x, 0), \tag{5.10}$$

$$\begin{aligned} &\int_{t_0}^{t_0'} \lambda_1(x,t)\, \nabla_x T_e(x,t)\, \mathrm{d}t + \alpha(x)\, \lambda_2(x) - \frac{1}{Re} \Delta_x \lambda_2(x) + \\ &- u(x) \cdot \nabla_x \lambda_2(x) + \lambda_2(x) \cdot \nabla_x u(x) - \nabla_x \lambda_3(x) = 0, \quad \textit{and,} \end{aligned} \tag{5.11}$$

$$\nabla_x \cdot \lambda_2(x) = 0, \tag{5.12}$$

with boundary conditions $\lambda_1(x,t) = 0$ *and* $\lambda_2(x) = 0$ *for each* $x \in \partial\Omega$ *and* $t \in [t_0, t_0']$*, together with final condition* $\lambda_1(x, t_0') = 0$ *for each* $x \in \Omega$*. The adjoint functions* λ_4 *and* λ_5 *are irrelevant to our Fréchet derivative calculation, therefore we omit them from this presentation.*

If $\left(T_e^\star, u^\star, p^\star, g_{T_e}^\star, g_u^\star\right)$ *is the optimal point to the problem* (5.7)*, its Lagrange multipliers,* $\lambda_{1,2,3,6}$*, also satisfy the above ajoint PDE system.*

The proof to theorem 5.1 is based on [86, Theorem 1.17] and shown in C.

5.2.2 Fréchet Derivatives of optimization problems

Firstly, we can compute the Fréchet derivatives of the cost function with respect to θ and π_0 for the estimation problem in the equation (5.6). Consider a parameter change from (θ, π_0) to $(\theta + \delta\theta, \pi_0 + \delta\pi_0)$. Since both α and κ are affine in θ, these variations will result

in changes from (α, κ) to $(\alpha + \delta\alpha, \kappa + \delta\kappa)$, which will also imply changes from (T_e, u, p) to $(T_e + \delta T_e, u + \delta u, p + \delta p)$.

Then, from equations (2.2), (2.4), and (2.5), it follows that the variations satisfy the following differential equations:

$$\begin{aligned} &\frac{\partial \delta T_e}{\partial t} - \nabla_x \cdot (\delta\kappa \, \nabla_x T_e) - \nabla_x \cdot (\kappa \, \nabla_x \delta T_e) + \\ &+ \delta u \cdot \nabla_x T_e + u \cdot \nabla_x \delta T_e = 0, \end{aligned} \tag{5.13}$$

$$\delta\alpha \, u + \alpha \, \delta u - \frac{1}{Re} \, \Delta_x \delta u + \delta u \cdot \nabla_x u + u \cdot \nabla_x \delta u + \nabla \delta p = 0, \tag{5.14}$$

$$\nabla_x \cdot \delta u = 0, \tag{5.15}$$

with the following boundary and initial conditions: $\delta T_e(x,t) = 0$ for each $x \in \partial\Omega$ and $t \in [t_0, t_0']$, $\delta T_e(x, t_0) = \delta\pi_0(x)$ for each $x \in \Omega$, and $\delta u(x) = 0$ for each $x \in \Gamma_w$.

Then with the help of dual variables, $\{\lambda_i\}_{i=1}^6$, from equations (5.13), (5.14), and (5.15), the difference between $J_e(\theta + \delta\theta, \pi_0 + \delta\pi_0)$ and $J_e(\theta, \pi_0)$ can be written as,

$$\begin{aligned} &J_e(\theta + \delta\theta, \pi_0 + \delta\pi_0) - J_e(\theta, \pi_0) = \\ &= \left\langle \nabla_{\pi_0} J_e - \lambda_6, \delta\pi_0 \right\rangle_\Omega + \left\langle \nabla_x \lambda_1 \cdot \nabla_x T_e, \delta\kappa \right\rangle_{\Omega \times [t_0, t_0']} + \left\langle \lambda_2 \cdot u, \delta\alpha \right\rangle_\Omega, \end{aligned} \tag{5.16}$$

The details about how to derive equation (5.16) are in chapter 4.

Thus the first-order approximation of the cost function J_e can be written as,

Theorem 5.2 (Fréchet derivatives of cost function J_e in Problem 5.6)**.** *Given variables $\pi_0 \in H^1(\Omega)$, $\theta \in \mathbb{R}^{n_d}$ and $\alpha, \kappa \in L^2(\Omega) \cap L^\infty(\Omega)$. The directional derivatives in equations* (5.17)

and (5.18) *are Fréchet derivatives of cost function* J_e *to corresponding variables.*

$$\begin{aligned} \left\langle \mathcal{D}_\alpha J_e, \delta\alpha \right\rangle_\Omega &= \langle \lambda_2 \cdot u, \delta\alpha \rangle_\Omega, \quad \textit{and} \\ \left\langle \mathcal{D}_\kappa J_e, \delta\kappa \right\rangle_\Omega &= \int_{t_0}^{t_0'} \left\langle \nabla_x \lambda_1 \cdot \nabla_x T_e, \delta\kappa \right\rangle_\Omega \mathrm{d}t, \end{aligned} \tag{5.17}$$

$$\begin{aligned} &\left\langle \mathcal{D}_{\pi_0} J_e, \delta\pi_0 \right\rangle_\Omega = \langle \nabla_{\pi_0} J_e - \lambda_6, \delta\pi_0 \rangle_\Omega, \quad \textit{and} \\ &\mathcal{D}_\theta J_e \cdot \delta\theta = \sum_{i=1}^{n_d} \left(\left\langle \mathcal{D}_\alpha J_e, \frac{\partial \alpha}{\partial \theta_i} \right\rangle_\Omega + \left\langle \mathcal{D}_\kappa J_e, \frac{\partial \kappa}{\partial \theta} \right\rangle \right) \delta\theta_i. \end{aligned} \tag{5.18}$$

For the optimal control problem in the equation (5.7), similarly, we can derive its cost function's derivatives w.r.t. related variables.

Theorem 5.3 (Fréchet derivatives of cost function J_c in Problem 5.7)**.** *Given variables,* $g_{T_e} \in L^2([t_0, t_0'] \times \Omega)$ *and* $g_u \in L^2(\Omega) \times L^2(\Omega)$*, the directional derivatives in equation* (5.19) *are Fréchet derivatives of cost function* J_c *to corresponding variables.*

$$\begin{aligned} &\left\langle \mathcal{D}_{g_{T_e}} J_c, \delta g_{T_e} \right\rangle_{\Omega \times [t_0, t_0']} = \left\langle \nabla_{g_{T_e}} J_c - \lambda_1, \delta g_{T_e} \right\rangle_{\Omega \times [t_0, t_0']}, \\ &\quad \textit{and} \quad \left\langle \mathcal{D}_{g_u} J_c, \delta g_u \right\rangle_\Omega = \langle \nabla_{g_u} J_c - \lambda_2, \delta g_u \rangle_\Omega. \end{aligned} \tag{5.19}$$

The proof to theorem 5.2 and 5.3 are in the appendix C.

5.2.3 Gradient-Based Optimization Algorithm

Using the closed-form formulas for the Fréchet derivatives of J_e w.r.t. π_0 and θ and J_c w.r.t. g_{T_e} and g_u in subsection 5.2.2, after the discretization by FEM method, we build a

gradient-based optimization algorithm to solve the problem in equation (5.6) and (5.7) using a projected-gradient method [99, Chapter 18.6] respectively.

First, we find descent directions $\delta\pi_0 : \Omega \to \mathbb{R}$ and $\delta\theta \in \mathbb{R}^{n_d}$ as solutions of the following Quadratic Program (QP) with value $V_e(\pi_0, \theta)$:

$$\begin{aligned} V_e(\pi_0, \theta) = \min_{\delta\pi_0,\, \delta\theta} & \langle \mathcal{D}_{\pi_0} J_e, \delta\pi_0 \rangle_\Omega + \mathcal{D}_\theta J_e \cdot \delta\theta + \\ & + \frac{1}{2}\, \mathcal{D}^2_{\pi_0} J_e(\delta\pi_0, \delta\pi_0) + \frac{1}{2}\, \mathcal{D}^2_\theta J_e(\delta\theta, \delta\theta), \\ \text{subject to: } & 0 \le \theta_i + \delta\theta_i \le 1,\ \forall i \in \{1, \dots, n_d\}, \end{aligned} \tag{5.20}$$

where $\mathcal{D}^2_{\pi_0} J_e$ and $\mathcal{D}^2_\theta J_c$ are the second derivatives of J_e w.r.t. π_0 and θ, when we solve the problem numerically, we use BFGS algorithm [99, Chapter 6.1] to approximate them.

Also we find descent directions $\delta g_{T_e} \colon \Omega \times [t_0, t_0'] \to \mathbb{R}$ and $\delta g_u \colon \Omega \to \mathbb{R}$ as solutions of the following Quadratic Program (QP) with value $V_c(g_{T_e}, g_u)$:

$$\begin{aligned} V_c(g_{T_e}, g_u) = \min_{\delta g_{T_e},\, \delta g_u} & \left\langle \mathcal{D}_{g_{T_e}} J_c, \delta g_{T_e} \right\rangle_{\Omega \times [t_0, t_0']} + \\ & + \langle \mathcal{D}_{g_u} J_u, \delta g_u \rangle_\Omega + \\ & + \frac{1}{2}\, \mathcal{D}_{g_{T_e}} J_c(\delta g_{T_e}, \delta g_{T_e}) + \\ & + \frac{1}{2}\, \mathcal{D}_{g_u} J_c(\delta g_u, \delta g_u), \\ \text{subject to: } & \underline{g_{T_e}} \le \left\| g_{T_e,i} + \delta g_{T_e,i} \right\|_\infty \le \overline{g_{T_e}}, \\ & \underline{g_u} \le \left\| g_{u,i} + \delta g_{u,i} \right\|_\infty \le \overline{g_u}, \\ & \forall i \in \{1, \dots, n_h\}, \end{aligned} \tag{5.21}$$

where $\mathcal{D}^2_{g_{T_e}} J_c$ and $\mathcal{D}^2_{g_u} J_c$ are the second derivatives of J_c w.r.t. g_{T_e} and g_u, when we solve the problem numerically, we use BFGS algorithm [99, Chapter 6.1] to approximate them.

Require: Initial values for θ and π_0.

1: **loop**
2: Numerically compute T_e, u, and p by solving the CFD model in equations (2.2) to (2.6).
3: Numerically compute λ_1, λ_2, λ_3, and λ_6 by solving the adjoint equations (4.4) to (4.7).
4: Compute the gradients $\mathcal{D}_{\pi_0} J_e$ and $\mathcal{D}_\theta J_e$ in equation (4.9).
5: Compute the projected-gradient descent directions $(\delta\pi_0, \delta\theta)$ by solving the QP in equation (5.20), with value $V_e(\pi_0, \theta)$.
6: **if** $V_e(\pi_0, \theta) = 0$ **then**
7: Stop.
8: Update $\pi_0 \leftarrow \pi_0 + \beta_e\, \delta\pi_0$ and $\theta \leftarrow \theta + \beta_e\, \delta\theta$.
9: Update Hessian matrix by BFGS algorithm.

Figure 5.5: Gradient-based estimation algorithm

The QP problems in equations (5.20) and (5.21) are derived using first-order approximations for the cost functions using the derivatives in equations (4.9) and (5.19), together with conditions to guarantee the feasibility of the desired directions.

Our gradient-based optimization method to solve the estimation problem in equation (5.20) and optimal control problem in equation (5.21) are detailed in figure 1 and 5.6 respectively. The PDE equations in the algorithms 1 and 5.6 are numerically solved using FEM discretizations, implemented using the FEniCS package [94]. In order to speed up the optimization algorithm, we used fixed heuristic step sizes, β_e and β_c, to update varaibles in the algorithms 1 and 5.6. If during the computation, β_e or β_c fail for the assumption in Theorem 5.4, we switch to Amijo method [8] to find feasible step sizes.

Theorem 5.4. *Suppose the cost functions in problem* (5.6) *and* (5.7) *are bounded from below, and* $\beta_e, \beta_c \in (0, 1)$ *in algorithm 1 and 5.6 satisfy respectively, when* $V_e(\theta, \pi_0), V_c(g_{T_e}, g_u) < 0$,

Require: Initial values for g_{T_e} and g_u.

1: **loop**
2: Numerically compute T_e, u, and p by solving the CFD model in equations (2.2) to (2.6).
3: Numerically compute λ_1, λ_2, λ_3, and λ_6 by solving the adjoint equations (4.4) to (4.7).
4: Compute the gradients $\mathcal{D}_{g_{T_e}} J_c$ and $\mathcal{D}_{g_u} J_c$ in equation (5.19).
5: Compute the projected-gradient descent directions $(\delta g_{T_e}, \delta g_u)$ by solving the QP in equation (5.20), with value $V_c(g_{T_e}, g_u)$.
6: **if** $V_c(g_{T_e}, g_u) = 0$ **then**
7: Stop.
8: Update $g_{T_e} \leftarrow g_{T_e} + \beta_c \, \delta g_{T_e}$ and $g_u \leftarrow g_u + \beta_c \, \delta g_u$.
9: Update Hessian matrix by BFGS algorithm.

Figure 5.6: Gradient-based optimal control algorithm

$a \in (0, 1)$

$$J_e(\theta + \beta_e \delta\theta, \pi_0 + \beta_e \delta\pi_0) - J_e(\theta, \pi_0) \leq a \, \beta_e V_e(\theta, \pi_0),$$

$$J_c(g_{T_e} + \beta_c \delta g_{T_e}, g_u + \beta_c \delta g_u) - J_c(g_{T_e}, g_u) \leq$$

$$\leq a \, \beta_c V_c(g_{T_e}, g_u).$$

where $(\delta\theta, \delta\pi_0)$ *are derived from problem* (5.20), $(\delta g_{T_e}, \delta g_u)$ *are derived from problem* (5.21). *Then for arbitrary sequence generated by the algorithm 1 or 5.6, its accumulate point satisfies* $V_e(\pi_0, \theta) = 0$ *or* $V_c(g_{T_e}, g_u) = 0$.

The proof of theorem 5.4 is in the appendix C.

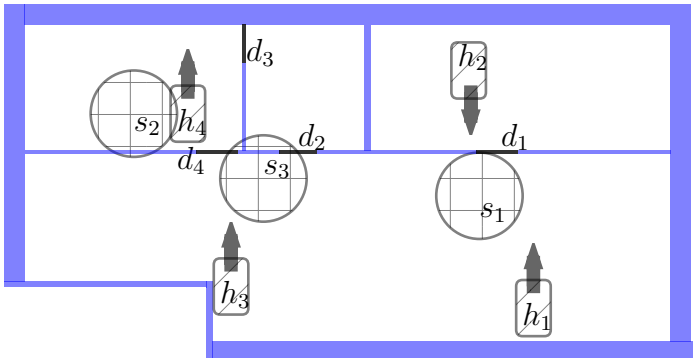

Figure 5.7: Floor plan for simulated apartment.

5.3 Simulations

We applied our MPC controller to a simulated St. Louis area apartment, whose floor plan is shown in figure 5.7, it has $n_d = 4$ doors, labeled as $\{d_i\}_{i=1}^{n_d}$, and $n_t = 3$ thermostats, labeled as $\{s_i\}_{i=1}^{3}$. The apartment is with dimensions $7.6 \times 16.8[\text{m}^2]$ (approx. 1375[sq ft]) and equipped with four HVAC vents, labeled $\{h_i\}_{i=1}^{4}$. We assume that each vent is endowed with a fan acting on a $1 \times 0.5[\text{m}^2]$ area, and oriented in a fixed direction. These HVAC fan units work independently to control the indoor flow's temperature, velocity and humidity.

The CFD model is governed by the constants $Re = 10^2$, $\alpha_0 = 0$, and $\kappa_0 = 10^{-2}$ when $x \in \Omega$ corresponds to free air, while $\alpha_w = 10^3$ and $\kappa_w = 10^{-4}$ when $x \in \Omega$ corresponds to a wall. The atmospheric pressure is $p_A = 101.3[\text{kPa}]$. The time horizon $T = 150[\text{s}]$ and $T' = 900[\text{s}]$, both sampled uniformly at 10[s]. The sensors' observation radius is $r = 1.0[\text{m}]$. The parameters in (5.6) are set to $\eta_0 = 1.0$, $\eta_1 = 0.1$, in (5.7) are set to $\eta_0' = 0.1$, $\eta_1' = 0.15$. The parameters in (5.20) and (5.21) are set to be 1.0. The specific humidity comes out of the HVAC system, $\{w_{o,j}\}_{j=1}^{4}$, are set to be 50% and the moisture generated inside the building is set to be $m_g = 0.5[\text{kg} \cdot \text{h}^{-1}]$. The natural convective heat transfer coefficient is set to $h_{cn} = 12.1[\text{W}/(\text{m}^2 \cdot^\circ \text{C})]$. The programs are implemented in Python, the FEM

discretization was computed using tools from the FEniCS Project [94], and the building plan was discretized into $n_{\text{elem}} = 6276$ elements.

5.3.1 Simulation with different door configurations and target locations

Since the performance of the estimator in our MPC has been tested in [76] with different temperature distributions and doors configurations. In this subsection, we valid the performance of our MPC system with controller and estimator together. We test its ability to adapt the changes of doors configuration and its spatial resolution to control local area's thermal comfort. Also, we compare the performance of the MPC whose estimation of doors configuration is always closed in order to show the importance of doors configuration's estimation to thermal comfort control. 12 test cases are simulated with different locations of target areas. The total time period we test is 900 [s] and the time horizon for MPC is 150 [s]. The atmospheric temperature is 5[°C], the clothing insulation is 0.155 [$\text{m}^2\,°\text{C/W}$], the metabolic rate is 64.0 [W/m^2], and the PMV index outside is around -4.10. During the simulation, we set all the four doors are closed at beginning, and at the time 50 [s], all the doors are changed to open.

Figures 5.8a and 5.8b show the spatial resolution of our MPC system, if the target area is close to one of the HVAC units, only this HVAC unit will operate to maintain the thermal comfort. Also these two figures indicate that if we are able to localize the resident inside an apartment, for example via wearable devices, then we can focus on the thermal comfort around the resident and improve the efficiency of the HVAC unit without major modifications to the mechanical ventilation system.

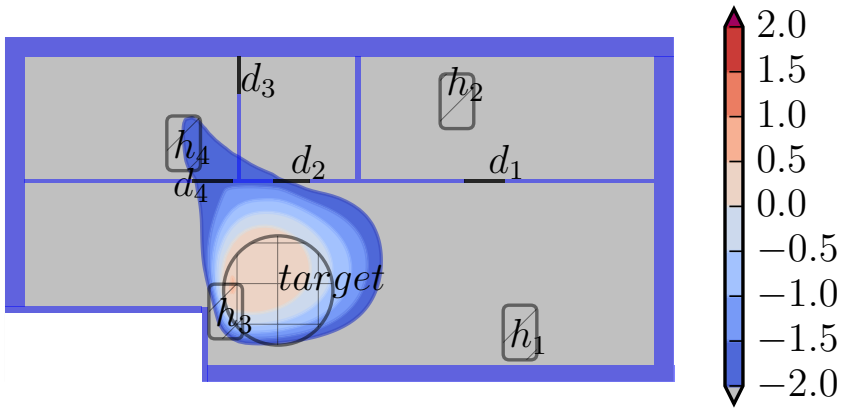

(a) The PMV distribution at final with target area *target*.

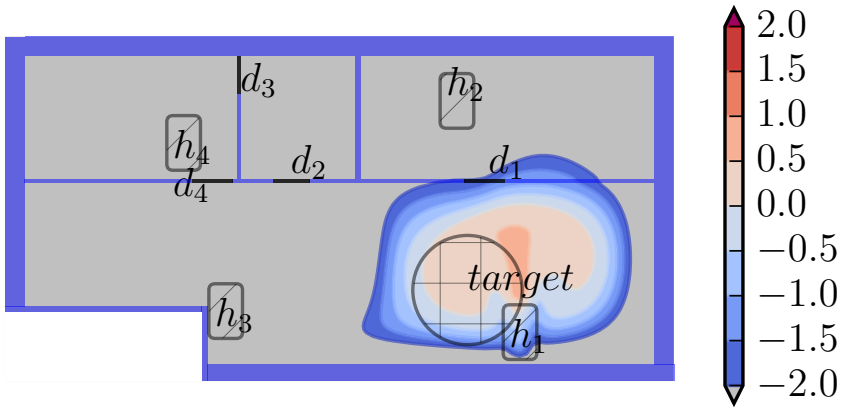

(b) The PMV distribution at final with target area *target*.

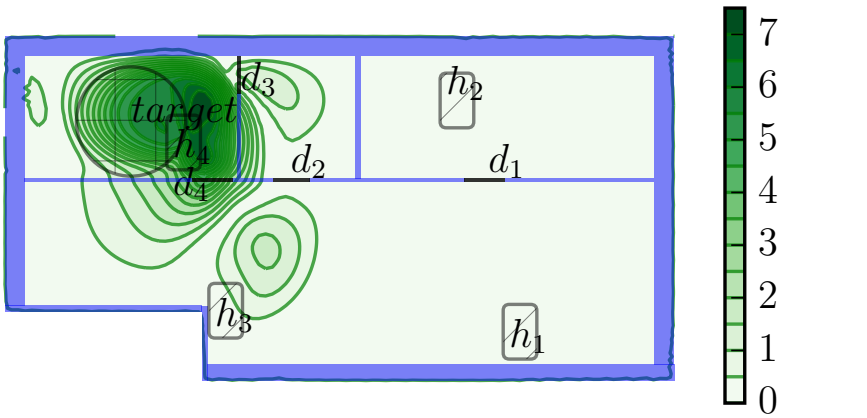

(c) The error distribution to temperature at final time for fixed model MPC in one test with target area *target*.

Figure 5.8: Results of the experiments in Section 5.3.1.

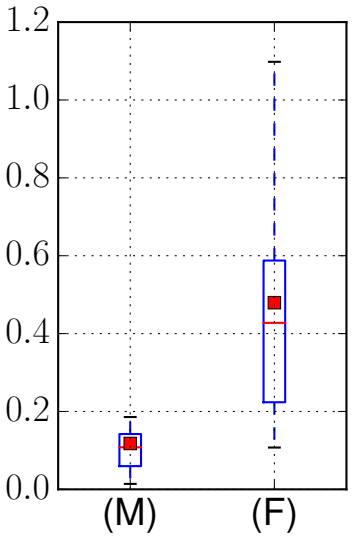

(a) The average absolute PMV value inside target area.

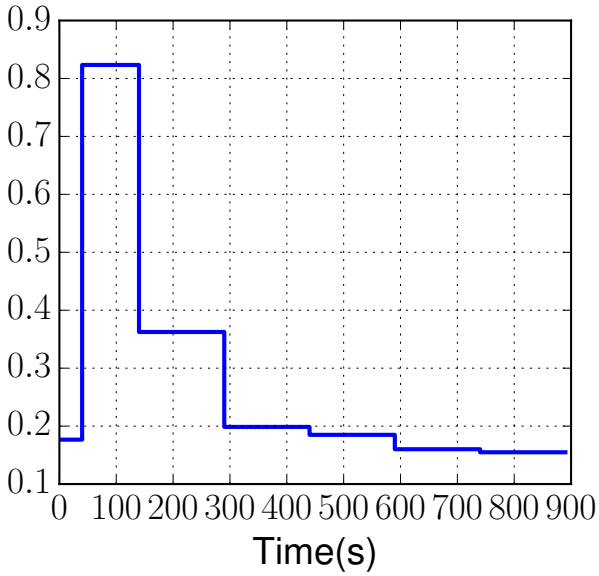

(b) The average estimation errors θ during 900[s].

Figure 5.9: Statistic results of simulations in Section 5.3.1 with 12 target areas. Columns in figure 5.9a: (M) is MPC with doors configuration estimator, (F) is MPC whose fixed doors configurations are fixed to be closed. Each column shows the median (red line), mean (red box), and first-to-third quartiles (blue box). The average estimation errors of θ in figure 5.9b are calculated as $e_\theta = \frac{1}{n_d}\sum_{i=1}^{n_d} |\theta_i - \hat{\theta}_i|$, where $\hat{\theta}_i$ are the real door's state and θ_i are the estimation from our MPC's estimator.

Figure 5.9a shows the range of average PMV value inside target areas under two MPC systems at the final time. First, the data validates the performance of our MPC system, since our system controls the average final PMV value inside the target area inside the range $[-0.5, 0.5]$, which is the range for thermal comfort. Also figures 5.9a and 5.8c show the importance of door configurations to control the thermal comfort inside target locations. If the MPC fails to track the doors configurations, for example like the comparison MPC which ignores the doors configuration changes in Column (F) of figure 5.9a, the final time's PMV value inside target area is further from the comfort point and the index's variance is also larger than when doors configuration is accurately estimated.

The average estimation errors of θ are shown in the figure 5.9b. After $t = 300$ [s] the average estimation is lower than 0.25 which means estimation of all the doors' configuration is correct. During the time $[0, 300$ [s]], the error of doors configuration is high and it is due to two reasons. First, the doors configuration changes at $t = 50$ [s], which is between two time steps when MPC's estimator wakes up. Thus the error during $[0, 150$ [s]] is high. Secondly, during the time $[150$ [s], 300 [s]] the doors configuration result is based on the thermostats data from $[0, 150$ [s]] and an assumption that the doors' states are fixed during this time period. However, the doors configuration changes at time $t = 50$ [s], thus the doors configuration estimation result is influenced during for the next time loop, $[150$ [s], 300 [s]]. The figure 5.9b shows the MPC needs at least one time step to track the doors configuration changes, in order to decrease the time length of inaccurate estimation to doors configuration, we can shorten the MPC's time horizon, which, at the same time, will also shorten the time MPC uses to stabilize the target area's thermal comfort based on the simulation in section 5.3.3.

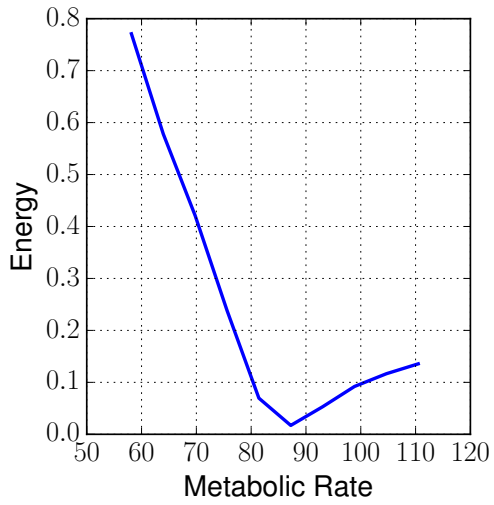

(a) The total energy usage under different metabolic rates.

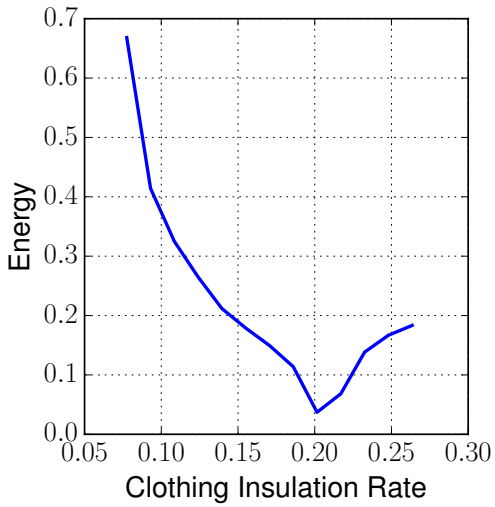

(b) The total energy usage under different clothing insulation.

Figure 5.10: Energy usage, in [kW · h], with different combination of metabolic rates, [W/m^2], and clothing index, in [m^2 °C/W], in Section 5.3.2. $T_a = 20.0$[°C], in figure 5.10a, $I_{cl} = 0.155$ [m^2 °C/W], in figure 5.10b, $M = 81.0$[w/m^2].

5.3.2 Simulation with different personal variables related to PMV

In this simulation, we study the influences of metabolic rate and clothing insulation to MPC's energy usage in a period of 600 [s]. The outside temperature is 20 [°C], around this temperature point the PMV value is negative when occupant has low metabolic rate and clothing index and becomes positive when the occupant has high metabolic rate and clothing index. Thus in figures 5.10a and 5.10b as the occupant's metabolic rate and clothing index increase, the HVAC system switches from heating mode into cooling mode.

The figures 5.10a and 5.10b validates our MPC system and show its several advantages. First, the MPC's energy usages change with different metabolic rates and clothing index and this change corresponds to the fact that when heating the area to make it comfortable, the more the occupant wears and the more active the occupant is, the less energy HVAC

units need. Second, the results show the importance of personal parameters, metabolic rate and clothing insulation, to thermal comfort and HVAC system's control strategy. As shown in figures 5.10a and 5.10b, around some temperature points, the occupant's thermal feeling, whether hot or cold, and HVAC system's corresponding control strategy, whether cooling or heating mode, are dependent on the occupant's personal variables. However, for a single-loop temperature control HVAC system, since it lacks efficient method to receive information from occupant, it is hard to adjust control strategy with different personal variables.

Studies about using wearable devices such as mobile phone and smart watch to monitor these personal variables have been shown in publications [87, 40, 134]. It is possible for our HVAC system to track the personal variables' changes and make corresponding thermal comfort control strategies. Finally, the results in figures 5.10a and 5.10b show the potential for our controller to give thermal comfort strategy in a different way. Instead of only giving control strategies to HVAC system, when the occupant has a strict energy budget limit, our MPC thermal controller may give occupant suggestions to change his or her clothing or metabolic habits at the same time.

5.3.3 Memory and time usage analysis

In this section, we study our algorithm's memory and time usage with different number of element, n_{elem}, then we study the time response of our system with different time horizons.

The figure 5.11a shows the average memory usage with different number of elements, n_{elem}, and both axis are in logarithmic scale. From this log-log plot, we can see a linear relationship between memory usage and n_{elem} where the line's slope is 1.14, thus the memory complexity is around $\mathcal{O}(n_{elem}^{1.14})$. The figure 5.11b shows the average time usage of each iteration loop

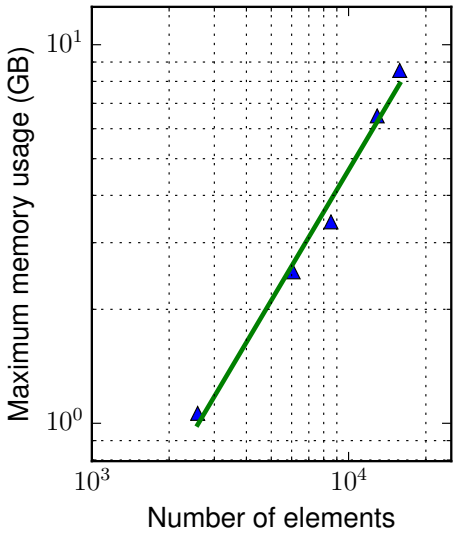

(a) Memory usage with different number of elements, in log-log scale.

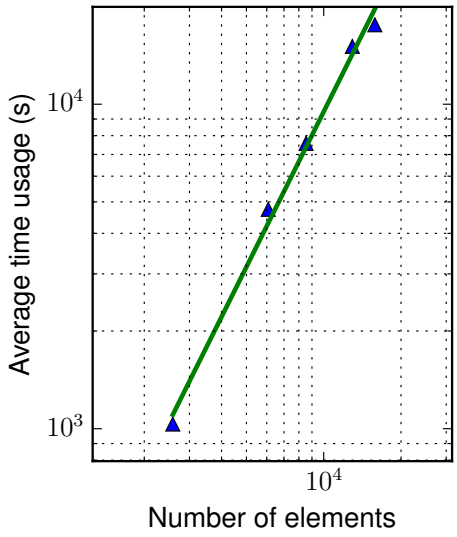

(b) Time usage with different number of elements, in log-log scale.

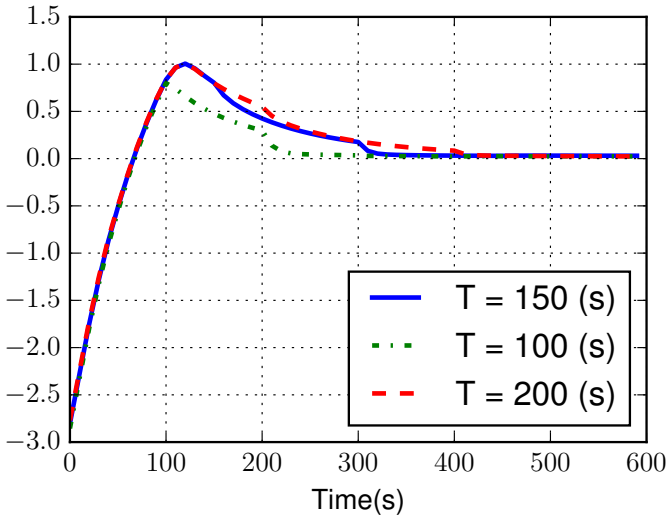

(c) The average PMV value inside target location with different time horizons. $T_a = 5$ [°C], $I_{cl} = 0.155$ $\left[\text{m}^2\,^\circ\text{C/W}\right]$, each line consists 5 different metabolic rates.

Figure 5.11: Results of the experiments in Section 5.3.3.

with different number of elements, also both axes are in logarithmic scale. Similarly, and the slope is 1.59, thus the time complexity is about $\mathcal{O}(n_{elem}^{1.59})$. The memory and time complexity show the potential to apply our MPC system into bigger and more complicated buildings.

Figure 5.11c shows the time response of our MPC system to control target area's PMV index. In this simulation, five cases of different combinations of metabolic rate and clothing index are tested with three different time horizons to our MPC. For all three time horizons, the average PMV index goes to zero after two time loops, which shows that if the occupant's PC's computation capacity is strong, the occupant can choose a shorter time step for the MPC in order to make the indoor target area comfortable in a shorter period of time. However, currently, our MPC is not able to work in real-time. The bottleneck for real-time is the time used to solve the original and adjoint PDE systems. There are several ways to fast our algorithm, first, we use the FEniCS [94] in Python as the numerical PDE solver, if we implement our algorithm in a more efficient language, for example C++, and extend our PDE solver into parallel [16]. Second, model reduction method related to FEM method should be studied in the future.

5.4 Chapter conclusion

In this chapter, we develop a MPC system to control the thermal comfort around indoor residents based on distributed CFD model. In order to fulfill this task, we develop a projected gradient-based optimization method to solve related PDE-constrained optimization problems. The simulation section validate the performance of our MPC to estimate state changes and adapt its control strategy. Also we studied the influence of personal variables to thermal comfort and MPC system's energy usage, which points out that in order to make

the HVAC system energy efficient to thermal comfort control, it is necessary to use some devices to measure occupant's personal variable data. In the future, based on the memory and time usage studies, in order to speed up our MPC and make it work in real-time, model reduction method will be studied for related PDE-constraint optimization problems.

Chapter 6

Numerical Synthesis of Pontryagin Optimal Control Minimizers Using Sampling-Based Method

In this chpater, we present a theoretical formulation and a corresponding numerical algorithm, capable of finding optimal control inputs that satisfy the Pontryagin Minimum Principle by using a direct method. Our paper is organized as follows. Section 6.1 introduces our notation and the optimal control problem we aim to solve. A conceptual algorithm is presented in section 6.2, and section 6.3 describes an implementable sampling-based numerical algorithm. Finally, simulation results are shown in section 6.4. [3]

[3]This chapter is based on R. He and H. Humberto, "Numerical Synthesis of Pontryagin Optimal Control Minimizers Using Sampling-Based Methods," in *56th IEEE Conference on Decision and Control*, Melbourne, Australia, December, 2017.

6.1 Problem statement

In this section, we formulate the conceptual optimal control problem we will address throughout this paper. In my study, we are interested in solving a control-constrained optimal control problem, formulated as follows,

$$\begin{aligned} &\min_{\substack{x\in L^2([0,T],\mathbb{R}^n)\\ u\in L^2([0,T],\mathbb{R}^m)}} \Psi\big(x(T)\big), \\ \text{subject to:}\quad &x(0)=\xi, \\ &\dot{x}(t)=f\big(t,x(t),u(t)\big), \\ &u(t)\in U, \text{ for a. e. } t\in[0,T], \end{aligned} \tag{6.1}$$

where U is a connected and compact subset of $\mathbb{R}^m$, $\xi \in \mathbb{R}^n$, and the functions f and Ψ are well-defined, each with an appropriate domain and range. We will say that f is the vector field, and Ψ the final cost, of the problem in equation (6.1). Note that the optimal control problem in equation (6.1) is quite general, since other standard formulations, such as those including running cost functions or minimum-time cost functions, can be easily converted to it (see section 4.1.2 in [103] for a thorough exposition of this topic).

First we give the following assumption to guarantee the uniqueness of the trajectories, as well as the convergence of our numerical method, in this paper.

Assumption 6.1. *The functions f and Ψ are Lipschitz continuously differentiable. That is, there exists $L>0$ such that, for each $t_1,t_2\in[0,T]$, $x_1,x_2\in\mathbb{R}^n$, and $u_1,u_2\in U$:*

$$|\Psi(x_1)-\Psi(x_2)| \le L\,\|x_1-x_2\|_2, \tag{6.2}$$

$$\left\|\frac{\partial\Psi}{\partial x}(x_1)-\frac{\partial\Psi}{\partial x}(x_2)\right\|_2 \le L\,\|x_1-x_2\|_2, \tag{6.3}$$

$$
\begin{aligned}
&\|f(t_1,x_1,u_1)-f(t_2,x_2,u_2)\|_2 \leq \\
&\qquad \leq L\left(|t_1-t_2|+\|x_1-x_2\|_2+\|u_1-u_2\|_2\right), &(6.4)\\
&\left\|\frac{\partial f}{\partial x}(t_1,x_1,u_1)-\frac{\partial f}{\partial x}(t_2,x_2,u_2)\right\|_{i,2} \leq \\
&\qquad \leq L\left(|t_1-t_2|+\|x_1-x_2\|_2+\|u_1-u_2\|_2\right), &(6.5)\\
&\left\|\frac{\partial f}{\partial u}(t_1,x_1,u_1)-\frac{\partial f}{\partial u}(t_2,x_2,u_2)\right\|_{i,2} \leq \\
&\qquad \leq L\left(|t_1-t_2|+\|x_1-x_2\|_2+\|u_1-u_2\|_2\right). &(6.6)
\end{aligned}
$$

Then we relax the problem in equation (6.1) using the concept of relaxed inputs, as defined by J. Warga [129, 130]. Consider the following relaxed optimal control problem:

$$
\begin{aligned}
&\min_{\substack{x\in L^2([0,T],\mathbb{R}^n)\\ \mu\colon [0,T]\to\mathcal{M}_p(\mathbb{R}^m)}} \quad \Psi\big(x(T)\big),\\
&\text{subject to:}\quad x(0)=\xi,\\
&\qquad\qquad\quad \dot{x}(t)=\int_{\mathbb{R}^m} f\big(t,x(t),u\big)\,\mathrm{d}\mu_t(u),\\
&\qquad\qquad\quad \operatorname{supp}(\mu_t)\subset U,\ \text{for a. e. } t\in[0,T],
\end{aligned}
\tag{6.7}
$$

where $\operatorname{supp}(\mu_t)$ is the support of μ_t, i.e., the smallest set S such that $\mu_t(S)=1$. In other words, instead of optimizing over the space of L^2 functions, we optimize over the space of stochastic processes defined on U.

According to [130, Theorem II.6.5], if the vector field $f(t,x,u)$ satisfies assumption 7.1, the relaxed system in problem (6.7) always has a solution. Given a fixed initial condition $x(0)=\xi$, we will denote the unique trajectory resulting from the stochastic process μ by

$x^{(\mu)}$. For simplicity, we will also denote the unique trajectory resulting from an input u by $x^{(u)}$.

Note that the problem in equation (6.1) is a particular case of the problem in equation (6.7). Indeed, given an arbitrary input $\hat{u} \in L^2([0,T],\mathbb{R}^m)$, the stochastic process defined by $\mu_t(S) = 1$ whenever $\hat{u}(t) \in S$, and $\mu_t(S) = 0$ otherwise, produces exactly the same trajectory as $\hat{u}$. Colloquially this particular stochastic process is written using Dirac Delta functions, i.e., $\mathrm{d}\mu_t(u) = \mathbf{1}\big(u - \hat{u}(t)\big)\,\mathrm{d}u$. This case implies that the feasible set of the relaxed problem is strictly larger than that of the original problem, thus resulting in lower optimal values for the relaxed problem. Yet, perhaps surprisingly, this is not the case, since both problems, original and relaxed, result in the same optimal values. The equivalence between original and relaxed problems follows since every point in the feasible set of the relaxed problem can be arbitrarily approximated using points in the feasible set of the original problem.

Theorem 6.1. *Let f be a vector field satisfying assumption 7.1, and let $\mu\colon [0,T] \to \mathcal{M}_p(\mathbb{R}^m)$ be a stochastic process. Then, for each $\varepsilon > 0$ there exists a control signal $\tilde{u}(t)$ such that for each $t \in [0,T]$, $\big\|x^{(\mu)}(t) - x^{(\tilde{u})}(t)\big\|_2 < \varepsilon$.*

This theorem is an extension of the Chattering Lemma [24, Theorem 4.1], taking advantage of the fact that, for each time t, the relaxed trajectory defined in equation (6.7) can be arbitrarily approximated using a finite number of vectors in U.

6.2 Optimal conditions for optimal control

As shown by Pontryagin et al. [104] in their Minimum Principle, it is possible to find a necessary condition for optimal points that cannot be formulated using directional derivatives. On the other hand, KKT [132] necessary conditions, widely used in finite dimensional optimization problem, can be fully described using directional derivatives. As we show below, necessary conditions for the problem in equation (6.1) based on directional derivatives are strictly weaker than those based on the Minimum Principle. On the other hand, necessary conditions based on directional derivatives and the Minimum Principle are completely equivalent for the problem in equation (6.7).

Polak et al. [103, 114] have shown that numerical methods for optimal control that rely on common explicit time discretization methods converge to optimal points satisfying directional derivative-based necessary conditions. Moreover, to the best of our knowledge there exists no general direct numerical method for optimal control that is provably convergent to optimal inputs satisfying Minimum Principle optimality conditions.

6.2.1 Optimality Functions

Definition 6.2 (Section 1.2 in [103])**.** *Consider an optimization problem with feasible set $\mathcal{X}$. We say that $\theta\colon \mathcal{X} \to (-\infty, 0]$ is an optimality function iff whenever $x \in \mathcal{X}$ is a minimizer, then $\theta(x) = 0$.*

Optimality functions are useful in practice since $\theta(x) < 0$ implies x is *not* a minimizer. Hence, they can be used as numerical tests to check whether a minimizer has been reached.

Now, consider the following optimality functions for the original problem (6.1) with input u_0 and trajectory $x^{(u_0)}$:

$$\begin{aligned}
&\theta_{o,l}\big(x^{(u_0)}, u_0\big) = \\
&\quad = \min_{\substack{\delta x \in L^2([0,T],\mathbb{R}^n) \\ \delta u \in L^2([0,T],\mathbb{R}^m)}} \frac{\partial \Psi}{\partial x}\big(x^{(u_0)}(T)\big)' \delta x(T) \\
&\qquad \text{subject to:} \quad \delta x(0) = 0, \\
&\qquad\qquad \delta \dot{x}(t) = \frac{\partial f}{\partial x}\big(t, x^{(u_0)}(t), u_0(t)\big)\delta x(t) + \\
&\qquad\qquad\qquad + \frac{\partial f}{\partial u}\big(t, x^{(u_0)}(t), u_0(t)\big)\delta u(t), \\
&\qquad\qquad u_0(t) + \delta u(t) \in U, \text{ for a. e. } t \in [0,T],
\end{aligned} \tag{6.8}$$

and

$$\begin{aligned}
&\theta_{o,h}\big(x^{(u_0)}, u_0\big) = \\
&\quad = \min_{u \in L^2([0,T],\mathbb{R}^m)} \int_0^T p_0(t)'\Big(f\big(t, x^{(u_0)}(t), u(t)\big) + \\
&\qquad\qquad - f\big(t, x^{(u_0)}(t), u_0(t)\big)\Big)\,\mathrm{d}t, \\
&\qquad \text{subject to:} \quad u(t) \in U, \text{ for a. e. } t \in [0,T],
\end{aligned} \tag{6.9}$$

where $p_0(t)$ is the costate of the problem in equation (6.1), defined by:

$$\begin{aligned}
p_0(T) &= \frac{\partial \Psi}{\partial x}\big(x^{(u_0)}(T)\big), \\
\dot{p}_0(t) &= -\frac{\partial f}{\partial x}\big(t, x^{(u_0)}(t), u_0(t)\big)' p_0(t).
\end{aligned} \tag{6.10}$$

Proposition 6.1. *The functions $\theta_{o,l}\big(x^{(u_0)}, u_0\big)$ and $\theta_{o,h}\big(x^{(u_0)}, u_0\big)$, defined in equations* (6.8) *and* (6.9)*, are optimality functions of the problem* (6.1)*.*

$\theta_{o,l}$ is has been proved as an optimality function by Polak [103, Theorem 5.6.8 and 5.6.9]. For $\theta_{o,h}$, it can be proved by constructing a contradiction to Pontryagin's Minimum Principle.

Proposition 6.2. *For the original problem* (6.1) *with input* u_0 *and trajectory* $x^{(u_0)}$*, if* $\theta_{o,h}\big(x^{(u_0)}, u_0\big)$ *in equation* (6.9) *equals zero, then* $\theta_{o,l}\big(x^{(u_0)}, u_0\big)$ *in equation* (6.8) *equals zero.*

Given $\theta_{o,l}\big(x^{(u_0)}, u_0\big) = 0$, we show that u_0 satisfies the Pontryagin Minimum Principle. Then, using the result in [103, Theorem 5.6.8 and 5.6.9], $\theta_{o,l}\big(x^{(u_0)}, u_0\big) = 0$ as well.

Note that the other direction of proposition 6.2 is not true in general [103, Section 4.2.6]. Thus for the deterministic original problem (6.1), it is hard to connect the directional and Pontryagin optimality functions. However, for the corresponding relaxed problem (6.7), we are going to show the connection between its directional and Pontryagin optimality functions and derive a related descent direction.

First we define an optimality function for the relaxed problem in equation (6.7). Given control's stochastic process as μ_0, and its trajectory $x^{(\mu_0)}$, at time t, the Hamiltonian to the optimal control problem (6.7) is:

$$H\big(t, x^{(\mu)}(t), \mu_t, p(t)\big) = p(t)' \int_{\mathbb{R}^m} f\big(t, x^{(\mu)}(t), u\big)\, \mathrm{d}\mu_t(u), \tag{6.11}$$

where $p(t)$ is the corresponding adjoint variable to the problem (6.7), such that

$$\begin{aligned} p(T) &= \frac{\partial \Psi}{\partial x}\big(x^{(\mu)}\big)(T), \\ \dot{p}(t) &= -\int_{\mathbb{R}^m} \frac{\partial f}{\partial x}\big(t, x^{(\mu)}(t), u\big)'\, \mathrm{d}\mu_t(u)\, p(t). \end{aligned} \tag{6.12}$$

Then, the optimality function is defined as:

$$
\begin{aligned}
&\theta_h\big(x^{(\mu_0)}, \mu_0\big) = \\
&= \min_{\nu\colon [0,T]\to\mathcal{M}_p(\mathbb{R}^m)} \int_0^T H\big(t, x^{(\mu_0)}(t), \nu_t, p_0(t)\big) + \\
&\qquad\qquad - H\big(t, x^{(\mu_0)}(t), \mu_{0,t}, p_0(t)\big)\,\mathrm{d}t \\
&= \min_{\delta\mu\colon [0,T]\to\mathcal{M}(\mathbb{R}^m)} \int_0^T p_0(t)' \int_{\mathbb{R}^m} f\big(t, x^{(\mu_0)}(t), u\big)\mathrm{d}\delta\mu_t(u)\mathrm{d}t, \qquad (6.13)\\
&\quad \text{subject to:} \quad \operatorname{supp}(\delta\mu_t + \mu_{0,t}) \subset U, \\
&\qquad\qquad \delta\mu_t + \mu_{0,t} \geq 0, \\
&\qquad\qquad \int_{\mathbb{R}^m} \mathrm{d}\delta\mu_t(u) = 0 \text{ for a. e. } t \in [0,T].
\end{aligned}
$$

Note that in the definition above, $\delta\mu_t$ is a signed measure in $\mathbb{R}^m$.

Proposition 6.3. *Let a stochastic process μ_0, and its trajectory as $x^{(\mu_0)}(t)$ in problem* (6.7)*. Then, the function $\theta_h\big(x^{(\mu_0)}, \mu_0\big)$, defined in equation* (6.13)*, is an optimality function of problem* (6.7)*.*

The result is similar to Proposition 6.1.

In the next subsection we are going to argue that this new optimality function in proposition 6.3 captures both directional derivatives and the Minimum Principle; hence, it is the correct framework to use in numerical algorithms.

6.2.2 Gradient descent methods for relaxed problems

First, we show the directional optimality function for problem (6.7). For the original problem (6.7), given the control's stochastic process as μ_0 and the system's trajectory as $x^{(\mu_0)}$,

the directional optimality function is

$$
\begin{aligned}
&\theta_l\big(x^{(\mu_0)},\mu_0\big) = \\
&= \min_{\substack{\delta x\in L^2([0,T],\mathbb{R}^n)\\ \delta\mu\colon [0,T]\to\mathcal{M}(\mathbb{R}^m)}} \frac{\partial\Psi}{\partial x}\big(x^{(\mu_0)}(T)\big)'\delta x(T) \\
&\text{subject to: } \dot{\delta x}(t) = \int_{\mathbb{R}^m}\frac{\partial f}{\partial x}\big(t,x^{(\mu_0)}(t),u\big)\mathrm{d}\mu_{0,t}(u)\delta x(t) + \\
&\qquad\qquad + \int_{\mathbb{R}^m} f\big(t,x^{(\mu_0)}(t),u\big)\mathrm{d}\delta\mu_t(u), \qquad (6.14)\\
&\qquad \delta x(0) = 0, \\
&\qquad \operatorname{supp}(\delta\mu_t + \mu_{0,t}) \subset U, \\
&\qquad \delta\mu_t + \mu_{0,t} \geq 0, \\
&\qquad \int_{\mathbb{R}^m}\mathrm{d}\delta\mu_t(u) = 0 \text{ for a. e. } t\in[0,T].
\end{aligned}
$$

Proposition 6.4. *For the original problem* (6.7)*, the function defined in equation* (6.14) *is an optimality function.*

The proof is similar to [103, Theorem 5.6.8 and 5.6.9].

Now we can show the connection between the directional and Pontryagin optimality functions.

Theorem 6.3. *The optimality functions for the relaxed control problem* (6.7)*,* $\theta_h\big(x^{(\mu_0)},\mu_0\big)$ *in equation* (6.13)*, and* $\theta_l\big(x^{(\mu_0)},\mu_0\big)$ *in equation* (6.14)*, are equivalent.*

The proof follows using the costate of the optimal control problem (6.7) to derive the Fréchet derivative of the cost function. Then rewrite θ_l in equation (6.14) with the costate of problem (6.7).

Since the optimality function $\theta_l\big(x^{(\mu_0)}, \mu_0\big)$ in equation (6.14) is also the first order Taylor extension of problem (6.7), after relaxing the problem, we are able to find a descent direction to the optimization problem (6.1) based on the Pontryagin principle. Before we show the optimization algorithm and its convergence, first we show that the optimality functions in equations (6.14) and (6.13) find a descent direction. Then we introduce a line search algorithm here in the infinite-dimensional space which is similar to Armijo [8].

Proposition 6.5. *Let μ_0 be a stochastic process of the control in problem* (6.7) *and its corresponding trajectory $x^{(\mu_0)}$ to the nonlinear dynamic system in problem* (6.7). *Suppose $\big(\delta x^{(\delta\mu_0)}, \delta\mu_0\big)$ is the argument to the optimality function* (6.14), *such that*

$$\theta_l\big(x^{(\mu_0)}, \mu_0\big) = \frac{\partial \Psi}{\partial x}\big(x^{(\mu_0)}(T)\big)' \delta x^{(\delta\mu_0)}(T), \tag{6.15}$$

where $\theta_l\big(x^{(\mu_0)}, \mu_0\big)$ is the optimality function in equation (6.14), *and $x^{(\mu_0)}$ is the trajectory of the linear system under the optimal stochastic variance $\delta\mu_0$ in the problem* (6.14). *Then there exists $\lambda \in (0, 1)$ such that $\mu_0 + \lambda\delta\mu_0$ is a new control's stochastic process with its corresponding trajectory, $x^{(\mu_0+\lambda\delta\mu_0)}$, in the nonlinear optimization problem* (6.7). *Moreover, for the cost function in problem* (6.7)

$$\Psi\big(x^{(\mu_0+\lambda\delta\mu_0)}(T)\big) \leq \Psi\big(x^{(\mu_0)}(T)\big).$$

The proof is based on the linearization of problem (6.7) and the property that θ_l is always negative when it is at a non-optimal point.

According to theorem 7.3, the argument of the Banach optimality function in equation (6.14) is also the argument of the Hamiltonian optimality function in equation (6.13). Thus the Hamiltonian optimality function finds the same descent direction.

With a descent direction, we now introduce a line search algorithm to find a step size which is similar to the method of Armijo [8]. Suppose trajectory $x^{(\mu_0)}$ is based on control process μ_0 in problem (6.7), and further suppose that $\delta\mu_0$ is the argument to $\theta_h\big(x^{(\mu_0)}, \mu_0\big)$ and $\delta x^{(\delta\mu_0)}$ is its linearized system's trajectory in problem (6.14). Let $\alpha, \beta \in (0,1)$, and then the step size for μ_0 is chosen as $\beta^{\eta(\mu_0)}$ such that

$$\begin{aligned}\eta(\mu_0) = \min\{k \in \mathbb{N} \,|\, \Psi\big(x^{\left(\mu_0+\beta^k\delta\mu_0\right)}(T)\big) - \\ - \Psi\big(x^{(\mu_0)}(T)\big) \leq \alpha\beta^k\theta_h\big(x^{(\mu_0)}, \mu_0\big)\},\end{aligned} \tag{6.16}$$

where $x^{\left(\mu_0+\beta^k\delta\mu_0\right)}$ is the trajectory of the dynamics in the problem (6.7) with $\mu_0 + \beta^k\delta\mu_0$.

Now we can show the numerical algorithm in the infinite dimensional continuous space as algorithm 2 and its convergence.

Theorem 6.4. *Let $\{\mu_i\}_{i\in\mathbb{N}}$ be a sequence of control processes generated by algorithm 2, and let $\{x^{(\mu_i)}\}_{i\in\mathbb{N}}$ be its corresponding sequence of trajectories in the dynamical system in problem* (6.7)*. Then*

$$lim_{i\to\infty}\, \theta_h\Big(x^{(\mu_i)}, \mu_i\Big) \to 0.$$

Algorithm 2 Optimization algorithm to problem (6.7) in the infinite dimensional space

Require: $\big(x^{(\mu_0)}, \mu_0\big)$, $\alpha, \beta \in (0,1)$.

1: $k \leftarrow 0$.
2: **loop**:
3: Compute $\theta_h\big(x^{(\mu_k)}, \mu_k\big)$ and $\delta\mu_k$ based on problem (6.13).
4: Compute $\eta(\mu_k)$ based on problem (6.16).
5: **if** $\theta_h\big(x^{(\mu_k)}, \mu_k\big) = 0$ **then return** $\big(x^{(\mu_k)}, \mu_k\big)$.
6: $\mu_{k+1} \leftarrow \mu_k + \beta^{\eta(\mu_k)}\delta\mu_k$.
7: Update $x^{(\mu_{k+1})}$ based on μ_{k+1} and dynamic system in problem (6.7).
8: $k \leftarrow k + 1$.
End loop.

The proof is similar to [125, Theorem 5.12].

6.3 Synthesis of relaxed optimal inputs

Now that we have established a theoretical foundation for the equivalence between computing relaxed optimal control inputs and the Pontryagin Minimum Principle, we focus our attention on the development of numerical algorithms to synthesize approximated optimal control inputs. As we show in this section, the use of relaxed inputs is beneficial not only from a theoretical point of view, but also in our numerical algorithms, since the optimal control problem becomes equivalent to solving a sequence of convex optimization problems, even when the dynamical system is nonlinear.

6.3.1 Vector field representation

As we show in section 6.2.2, it is possible to formulate an iterative gradient descent method using relaxed inputs that converges to Pontryagin-optimal points. This theoretical iterative method revolves around computing the value of θ_h, as defined in equation (6.13), which aims to find a new stochastic process that locally reduces the cost function of the problem in equation (6.7).

Proposition 6.6. *The optimization problem in equation* (6.13) *is convex.*

We omit a detailed proof, but it can be shown that the feasible set and cost function of problem (6.13) are both convex.

We now focus our attention on methods to numerically represent the feasible set of the problem in equation (6.13).

Proposition 6.7. *Let $x \in \mathbb{R}^n$. Then*

$$\left\{ \int_{\mathbb{R}^m} f(x,u)\, \mathrm{d}\mu(u) \mid \mu \in \mathcal{M}(\mathbb{R}^m),\ \mathrm{supp}(\mu) \subset U \right\} = \\ = \mathrm{co}\{f(x,u) \mid u \in U\}, \tag{6.17}$$

where $\mathrm{co}(S)$ *is the convex hull of a set* $S \subset \mathbb{R}^n$.

We omit a detailed proof, but the result follows since the convex hull is clearly contained in the left-hand side set of all possible expected values, and every expected value can be written as the limit of a sequence of points in the convex hull since all Lebesgue-Stieltjes integrals can be approximated using finite Riemann integrals [44].

The result in Proposition 7.5 suggests that to synthesize optimal inputs, we need only to be able to compute the convex hull of the vector field at any given state $x \in \mathbb{R}^n$. Now, some points in the convex hull of the vector field have a particular input vector $u \in U$ associated with them, but others cannot be directly realized.

On the other hand, every point in the convex hull is, by definition, a convex combination of a finite set of vectors in the vector field. Hence, we can approximate the convex hull of the vector field at each $x \in \mathbb{R}^n$ with the convex hull of a finite collection of samples of the vector field for a set $\{\hat{u}_i\}_{i=1}^{N_s}$. Moreover, as shown in [125] and [126], we can arbitrarily approximate the trajectories resulting from any convex combination of vectors in a finite vector field by using a projection operation that results in switching between those vectors. In the next section we overview the main results of this method.

6.3.2 Sampled-Based Synthesis

First we are going to show that by using samples we can obtain approximations of the convex hull and the stochastic process. Given a control's stochastic process, μ, and its trajectory $x^{(\mu)}$ for the system in problem (6.7) at time $t \in [0, T]$, the sampling points for the vector field are $\left\{ f\big(t, x^{(\mu)}(t), u_i\big) \right\}_{i=1}^{N_s}$, where $\{u_i\}_{i=1}^{N_s} \subset U$. Each sampling point has a corresponding weight, and the sequence of $\{w_i(t)\}_{i=1}^{N_s}$ satisfies

$$\sum_{i}^{N_s} w_i(t) = 1. \tag{6.18}$$

$$w_i(t) \geq 0, \ \forall i \in \{1, \cdots, N_s\}. \tag{6.19}$$

We use these sampling points and their weights to represent the stochastic process. Asymptotically, the sampling and approximation converge to μ.

Proposition 6.8.

$$\sum_{i=1}^{N_s} w_i(t) f\big(t, x^{(\mu)}(t), u_i\big) \to \int_{\mathbb{R}^m} f\big(t, x^{(\mu)}(t), u\big)\, d\mu_t(u),$$

asymptotically as $N_s \to \infty$, *for a. e.* $t \in [0, T]$.

We omit a detailed proof, but the result is based on the Monte Carlo principle and particle filtering [5, 9].

A similar result holds for approximating the stochastic process's variance, $\delta\mu$, with sampling points in the vector field.

Since numerically the number of sampling points is finite and, at each time step, the only difference between each samples is the control value in the vector field, we get a relaxed switched system. At time t, the chance to perform control under value u_i is its weight $w_i(t) \in [0,1]$. In order to reconstruct a deterministic control, we need to project the weights $\{w_i(t)\}_{i=1}^{N_s}$ from $[0,1]^{N_s}$ into $\{0,1\}^{N_s}$, and at the same time, preserve the trajectory, $x^{(\mu)}$, and the sum of $w_i(t)$ to be 1. We use wavelet transformation and pulse-width modulation (PWM) to perform the projection. After wavelet transformation, the weight, $w_i(t)$, becomes a piecewise constant in energy spectrum space, and by using the PWM operator, we project the weight back into time space with only 0/1 values. Details about reconstructing a deterministic control from a relaxed switch system can be found in section 4.4 [125].

Now we present the numerical version of algorithm 2. In the algorithm, the sampling values for the control are fixed as $\{u_i\}_{i=1}^{N_s} \subset U$. At each iteration, the control's stochastic process, μ_k, and its vector field at time t are approximated by the samples' weights, $\{w_{k,i}(t)\}_{i=1}^{N_s}$. Also, we define the approximated weights to $\delta\mu_k$ from equation (6.13) as $\{\hat{w}_{k,j}(t)\}_{j=1}^{N_k}$. $\{\hat{w}_{k,j}(t)\}_{j=1}^{N_k}$ are derived from the discrete version of equation (6.13) with a regularity term formulated by taking the l_1 norm of the weights,

$$
\begin{aligned}
&\theta_h\big(x^{(\mu_k)}, \{w_{k,i}\}_{i=1}^{N_s}\big) = \\
&= \min_{\hat{w}_{k,i}(t)\in\mathbb{R}} \quad \int_{t=0}^{T} p_0(t)'\Big(\sum_{i=1}^{N_s} f\big(t, x^{(\mu_k)}(t), u_i\big)\, \hat{w}_{k,i}(t)\Big)\, dt + \\
&\qquad\qquad + \eta_w \int_{t=0}^{T} \|\hat{w}_{k,i}(t)\|_1\, dt, \\
&\qquad \text{subject to:} \quad \text{for a. e. } t \in [0,T], \\
&\qquad\qquad w_{k,i}(t) + \hat{w}_{k,i}(t) \geq 0,\ \forall i \in \{1, \cdots, N_s\}, \\
&\qquad\qquad \text{and } \sum_{i=1}^{N_s} \hat{w}_{k,i}(t) = 0.
\end{aligned}
\tag{6.20}
$$

We add a regularity term $\|\hat{w}_{k,j}(t)\|_1$ in equation (6.20) and $\eta_w > 0$ is the weight. The addition of the regularity term is due to numerical computation and the following proposition

Proposition 6.9. *For a signed measure $\nu \in \mathcal{M}(\mathbb{R}^m)$, if we define its norm as $\|\nu\|$, then the θ_h in equation* (6.13) *with a regularity term is still an optimality function of problem* (6.7)*, and it does not lose its convergence property. We write this new optimality function as*

$$\begin{aligned}
&\theta_n\big(x^{(\mu_0)}, \mu_0\big) = \\
&= \min_{\delta\mu\colon [0,T]\to\mathcal{M}(\mathbb{R}^m)} \int_0^T p_0(t)' \Big(\int_{\mathbb{R}^m} f\big(t, x^{(\mu_0)}(t), u\big) \mathrm{d}\delta\mu_t(u) + \\
&\qquad + \|\delta\mu_t\| \Big) \mathrm{d}t, \\
&\qquad \textit{subject to:} \quad \mathrm{supp}(\delta\mu_t + \mu_{0,t}) \subset U, \\
&\qquad\qquad \int_{\mathbb{R}^m} \mathrm{d}\delta\mu_t(u) = 0 \textit{ for a. e. } t \in [0,T].
\end{aligned} \tag{6.21}$$

We give a sketch of proposition 6.9 here. First, by construction we can show θ_n in equation (6.21) is always non-positive. Second, when θ_h reaches zero, θ_n is also zero. Hence, θ_n is an optimality function as well, and adding a regularity term does not change the critical points indicated by the optimality function, and therefore the convergence holds.

Now we can show the numerical implementation of algorithm 2 as follows:

6.4 Simulation results

In this section, we show two preliminary simulations to validate the performance of our numerical algorithm 3.

Algorithm 3 Numerical implementation to the optimization algorithm of problem (6.7)

Require: $\{u_i\}_{i=1}^{N_s}$, $\{w_{0,i}(t)\}_{i=1}^{N_s}$, $x^{(\mu_0)}$, and $\alpha, \beta \in (0,1)$.

1: $k \leftarrow 0$.
2: **loop**:
3: Compute θ_h and $\{\hat{w}_{k,i}(t)\}_{i=1}^{N_s}$ based on problem (6.20).
4: **if** $\theta_h = 0$ **then** Follow the section 4.4 [125] to use wavelet and PWM to reconstruct the optimal $u_o(t)$ from $\{w_{k,i}(t)\}_{i=1}^{N_s}$. **return** $x^{(\mu_k)}$, μ_k and $u_o(t)$.
5: Compute $\eta(\mu_{k,t})$ based on problem (6.16).
6: $w_{k+1,i}(t) \leftarrow w_{k,i}(t) + \beta^{\eta(\mu_{k,t})}\hat{w}_{k,i}(t)$, $\forall i \in \{1, \cdots, N_s\}$.
7: Update $x^{(\mu_{k+1})}$ based on $\{u_i\}_{i=1}^{N_s}$ and $\{w_{k+1,i}(t)\}_{i=1}^{N_s}$ and dynamic system in problem (6.7).
8: $k \leftarrow k+1$.
End loop.

6.4.1 Constrained LQR

The first simulation is a constrained LQR problem and can be transformed into a form like problem (6.1). The time horizen is $T = 2$, and the system has seven states as $x \in L^2([0,2], \mathbb{R}^7)$, two controls as $u \in L^2([0,2], \mathbb{R}^2)$, the initial states are $\xi = 0$ and the problems' final cost function is $\Psi\big(x(T)\big) = x_7(2)$. The dynamic of the problem $\dot{x} = f(t, x(t), u(t))$ is

$$
\begin{aligned}
\dot{x}_1(t) &= x_4(t),\\
\dot{x}_2(t) &= x_5(t),\\
\dot{x}_3(t) &= x_6(t),\\
\dot{x}_4(t) &= -\gamma x_3(t) - \frac{d}{m}x_4(t) + \frac{1}{m}u_1(t),\\
\dot{x}_5(t) &= -\frac{d}{m}x_5(t) + \frac{1}{m}u_2(t),\\
\dot{x}_6(t) &= -\frac{m\,g\,l}{J}x_3(t) + \frac{r}{J}u_1(t),\\
\dot{x}_7(t) &= (x_1(t) - c_1)^2 + (x_2(t) - c_2)^2 + x_3^2(t) +\\
&+ \eta\, u'(t)u(t).
\end{aligned}
$$

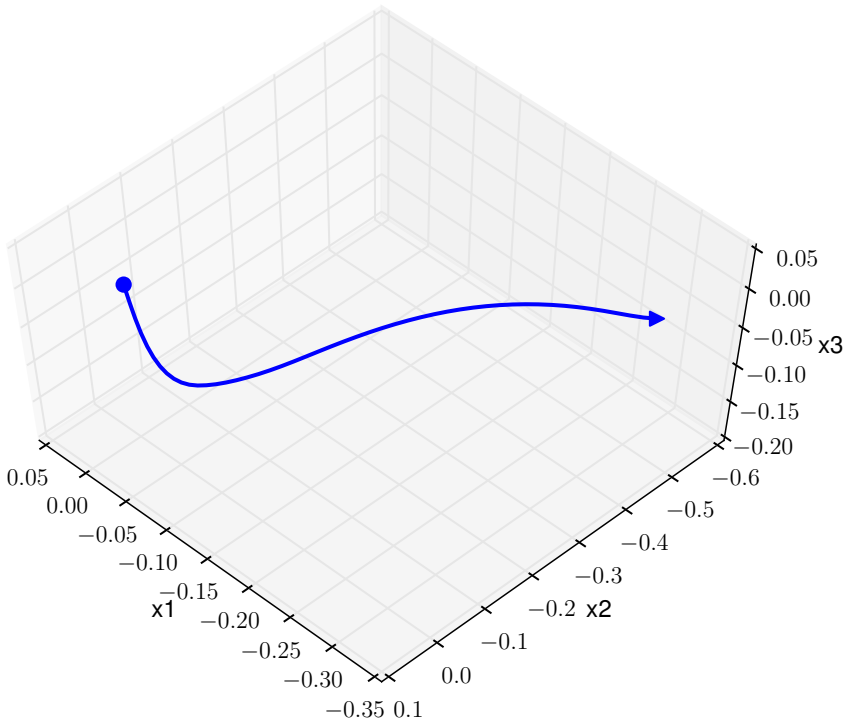

Figure 6.1: Trajectory of states $x_{1,2,3}$ under optimal control in section 6.4.1. The states start from the origin (blue dot) to the end (blue triangle), which is (-0.29, -0.56, -0.06).

Here $x_{4,5,6}$, are the time derivatives of $x_{1,2,3}$ respectively. The controls, $u_{1,2}$, are applied to $x_{4,5,6}$. The last state, x_7, is related to the optimal control problem's cost. It measures the difference between the current states of $x_{1,2,3}$ and the target, $(c_1, c_2, 0)$, and balances the total energy applied to the system. The parameters are given as $J = 0.0475$, $m = 1.5$, $r = 0.25$, $g = 9.8$, $\gamma = 0.51$, $d = 0.2$, $l = 0.05$, $\eta = 0.05$, and $c_1 = -0.3$, $c_2 = -0.5$. We use 81 points to sample the vector field, whose $\{u_i\}_{i=1}^{81}$ are evenly distributed in the control's space $U = [-1, 1]^2$.

The result validates our algorithm's performance and convergence. Figure 7.1a shows the trajectory of the first three states of the system as they move from the origin to the target. Figure 6.2b shows the corresponding controls after wavelet and PWM reconstruction. Since

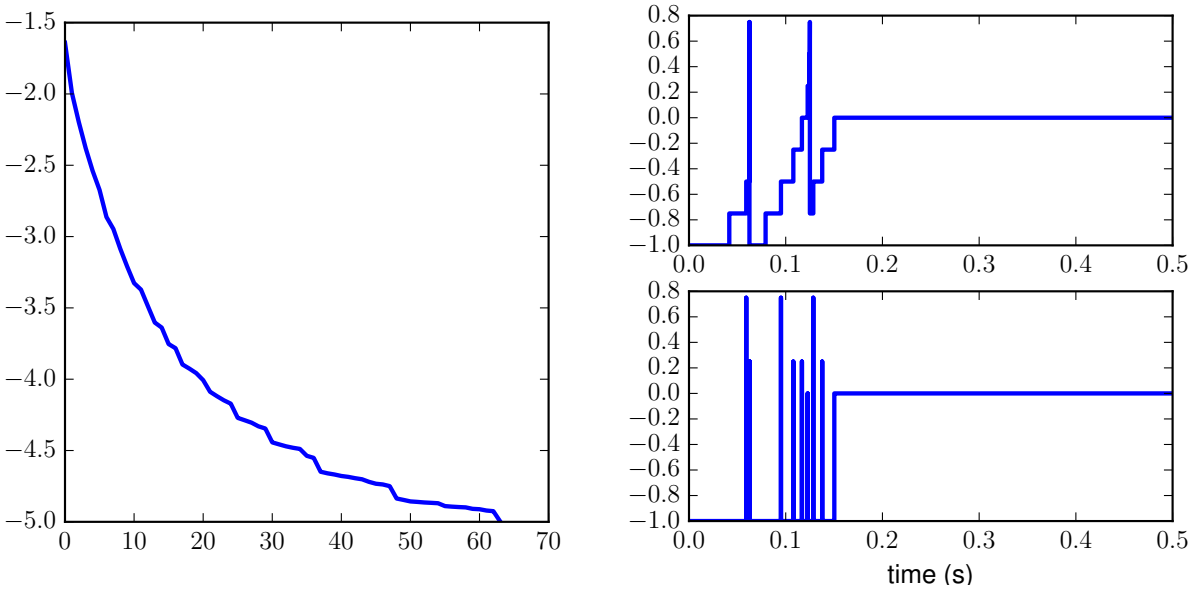

(a) The absolute value of optimality function, θ_h, at each iteration, in log_{10} scale.

(b) The optimal controls reconstructed by PWM, top is u_1 and bottom is u_2. When time $t \geq 0.5$, the controls, $u_{1,2}$, are zero.

Figure 6.2: Results of the simulation in section 6.4.1, a contrained LQR problem.

the problem's cost accounts for the difference between the target and current states during the whole time horizon, the algorithm prefers to add huge energy at the very beginning to modify $x_{1,2,3}$. Figure 6.2a shows the optimality function's absolute value at each iteration, and we can see the absolute value of θ_h decreases to lower than 10^{-5} after 62 iterations, which shows the convergence of our algorithm.

6.4.2 Quadrotor helicopter

Now, we consider an application to control a quadrotor helicopter in 3-dimensional space using a nonlinear model described in [105].

The optimal control problem also can be rewritten in to the form of the problem in equation (6.7). The problem's time horizen is $T = 2$[s], it has 13 states, $x \in L^2([0, 2], \mathbb{R}^{13})$, 4 controls, $u \in L^2([0, 2], \mathbb{R}^4)$, which are inside $U = [0, 2]^4$, and the cost function $\Psi(x(T)) = x_{13}(2)$.

The helicopter's initial states are $\xi = 0$, and its dynamic system $\dot{x}(t) = f\big(t, x(t), u(t)\big)$ is

$$
\begin{aligned}
\dot{x}_1(t) &= x_4(t),\\
\dot{x}_2(t) &= x_5(t),\\
\dot{x}_3(t) &= x_6(t),\\
\dot{x}_4(t) &= \frac{-b}{m}x_1(t) + \frac{1}{m}\sin x_8(t) K\vec{1}' u(t),\\
\dot{x}_5(t) &= \frac{-b}{m}x_2(t) + \frac{1}{m}\sin x_7(t)\cos x_8(t) K\vec{1}' u(t),\\
\dot{x}_6(t) &= \frac{-b}{m}x_3(t) - g + \frac{1}{m}\cos x_7(t)\cos x_8(t) K\vec{1}' u(t),\\
\dot{x}_7(t) &= x_{10}(t),\\
\dot{x}_8(t) &= x_{11}(t),\\
\dot{x}_9(t) &= x_{12}(t),\\
\dot{x}_{10}(t) &= -x_{11}(t)x_{12}(t) + \frac{L}{I_x}K(u_2(t) - u_4(t)),\\
\dot{x}_{11}(t) &= x_{10}(t)x_{12}(t) + \frac{L}{I_y}K(u_3(t) - u_1(t)),\\
\dot{x}_{12}(t) &= \frac{K}{I_x + I_y}\Big(u_1(t) - u_2(t) + u_3(t) - u_4(t)\Big),\\
\dot{x}_{13}(t) &= \big(x_1(t) - c_1\big)^2 + \big(x_2(t) - c_2\big)^2 + \big(x_3(t) - c_3\big)^2 +\\
&+ \sin^2(x_7(t)) + \sin^2(x_8(t)) + \sin^2(x_9(t)) + \eta\, u'(t)u(t).
\end{aligned}
$$

The first three states, $x_{1,2,3}$, represent the helicopter's position in x, y, z coordinations respectively, and $x_{4,5,6}$ are their related time derivatives. The states, $x_{7,8,9}$, represent the angular displacement of the quadrotor body axes, and $x_{10,11,12}$ are their time derivatives. The final state, x_{13}, is related to the problem's cost, and it measures the difference between helicopter's current and target position, $c_{1,2,3}$, and balances the energy usage be the four motors, $u_{1,2,3,4}$.

Here, we have simulate the helicopter moving down to $(-1.2, -1.0, -1.0)$ and up to $(1.2, 1.0, 1.0)$. At the same time, we also keep the helicopter's axes displacement as tiny as possible and balance the energy usage. The parameters for the helicopter are $m = 1.3$ [kg], $I_{x,y} = 0.0605$ [kg $\cdot$ m^2], $g = 9.8$[m/s^2], $b = 0.1$ and $K = 1.0$, $\eta = 0.05$.

We use 625 sampling points and the convergence threshold is $\theta_h \leq 10^{-4}$. The trajectories of the positions, $x_{1,2,3}$, and the body axes displacement, $x_{7,8,9}$, under optimal controls are shown in figures 6.3 and 6.4. Simulation results show our algorithm gives the optimal solutions to move the helicopter to the target positions and maintain a small body axes displacement at the same time.

6.5 Chapter conclusion

In this paper we present a theoretical formulation, and a corresponding numerical algorithm that can find Pontryagin-optimal inputs for general dynamical systems by using a direct method. The numerical implementation is based on a relaxed-control system and PWM reconstruction. Preliminary results validate the algorithm's performance. However, the current sampling method is to fix the sampling controls in the vector field, so it does not fully use the fact that the sampling points consist a convex hull in vector field space. When the dimension of the control is high, in order to make the algorithm perform well, chances are a large number of sampling points will be needed, which influence the memory usage and computation efficiency. In the future, the algorithm's improvement will focus on updating the relaxed control process by using only the vertices of the convex hull, which are constructed by the sampling points.

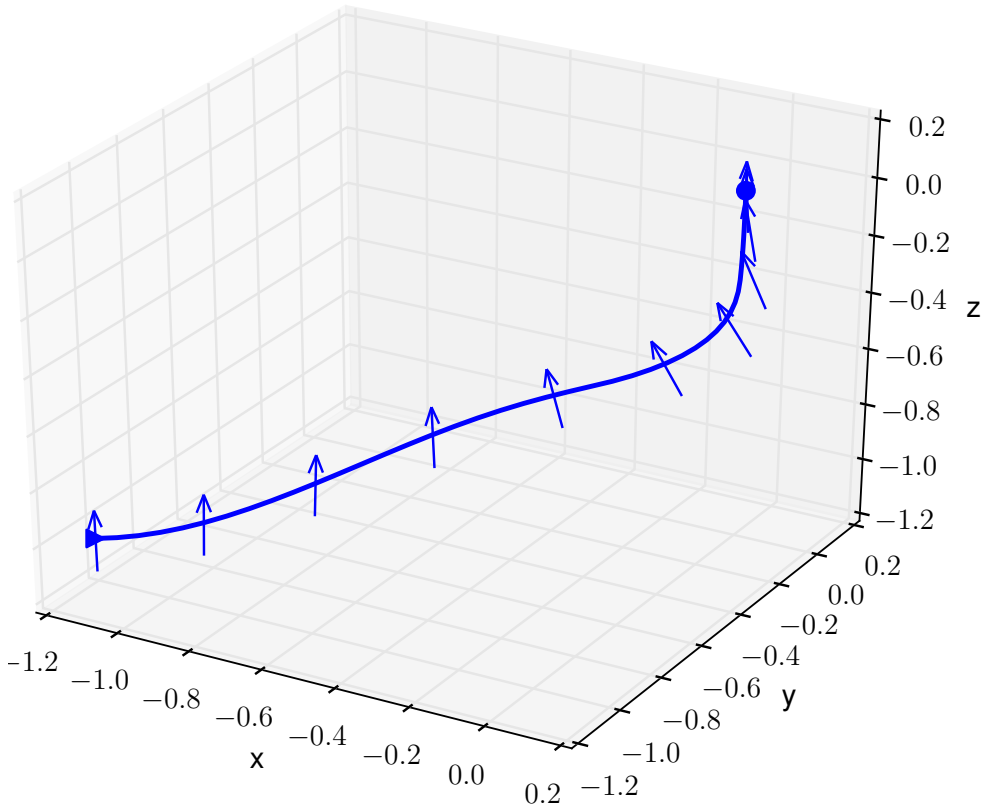

Figure 6.3: The helicopter's trajectory moves from the origin (blue dot) down to (-1.12, -1.12, -0.98) (blue triangle) under the optimal control. Blue arrows are perpendicular vectors to the helicopter's plane, which are used to represent body axes.

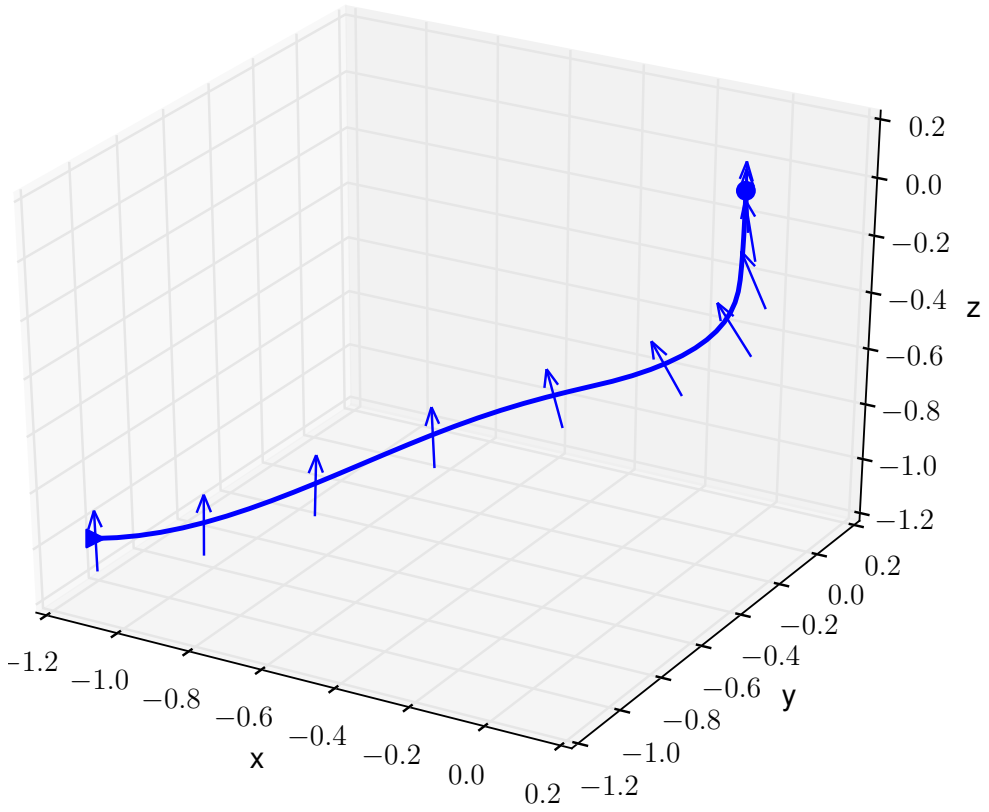

Figure 6.4: The helicopter's trajectory climbs from the origin up to (1.23, 1.23, 1.18) (blue triangle) under the optimal control. Blue arrows are perpendicular vectors to the helicopter's plane, which are used to represent body axes.

Chapter 7

Numerical Sampling-based Method to Pontryagin Optimal Control Minimizers in State-constrained Problems

7.1 Problem statement

In section 7.1.1, we are going to show the necessary mathematical notations and assumptions. Then in subsection 7.1.2, we formulate the original nonlinear problem with state constraints used in this paper and its corresponding relaxed problem.

7.1.1 Preliminaries

Given $n \in \mathbb{N}$ and $p \geq 1$, we denote the standard finite-dimensional p-norm by $\|\cdot\|_p$, and the induced matrix p-norm by $\|\cdot\|_{i,p}$. We will denote by $\mathcal{M}(\mathbb{R}^n)$ the set of Radon measures defined over the Borel sets of $\mathbb{R}^n$. Moreover, given a $\mu \in \mathcal{M}(\mathbb{R}^m)$ for $m \in \mathbb{N}$, we say that a function $f\colon \mathbb{R}^m \to \mathbb{R}^n$ is L^2_μ-integrable, denoted $f \in L^2_\mu(\mathbb{R}^m, \mathbb{R}^n)$, if there exists $p \geq 1$ such that $\|f\|_\mu = \left(\int_{\mathbb{R}^m} \|f(x)\|_p^2 \,\mathrm{d}\mu(x)\right)^{\frac{1}{2}} < \infty$. To simplify, we will denote by $L^2(\mathbb{R}^m, \mathbb{R}^n)$ the space of Lebesgue square-integrable functions. Furthermore, we say that $\mu \in \mathcal{M}(\mathbb{R}^m)$ is a probability measure if $\mu(\mathbb{R}^m) = 1$. We denote the set of all probability measures by $\mathcal{M}_p(\mathbb{R}^m)$. A stochastic process is a function $\mu\colon [0, T] \to \mathcal{M}_p(\mathbb{R}^m)$, and throughout the paper we will simply write μ_t instead of $\mu(t)$.

Let $\mu_1, \mu_2 \in \mathcal{M}(\mathbb{R}^m)$ be two Radon measures. Then the difference between μ_1 and μ_2, say $\nu = \mu_1 - \mu_2$, is a signed measure, and we define $L^2_\nu(\mathbb{R}^m, \mathbb{R}^n) = L^2_{\mu_1}(\mathbb{R}^m, \mathbb{R}^n) \cap L^2_{\mu_2}(\mathbb{R}^m, \mathbb{R}^n)$. Given $f \in L^2_\nu(\mathbb{R}^m, \mathbb{R}^n)$, its integral with respect to ν is defined by

$$\int_{\mathbb{R}^m} f(x) \,\mathrm{d}\nu(x) = \int_{\mathbb{R}^m} f(x) \,\mathrm{d}\mu_1(x) - \int_{\mathbb{R}^m} f(x) \,\mathrm{d}\mu_2(x). \tag{7.1}$$

For any function $G\colon \mathcal{X} \to \mathbb{R}^m$, for $\zeta \in \mathcal{X}$ in G's domain, the *directional derivative* of G at ζ, denoted as $DG(\zeta; \dot{)}$,is computed as

$$DG\big(\zeta; \zeta'\big) = \lim_{\lambda \to 0} \frac{G(\zeta + \lambda\zeta') - G(\zeta)}{\lambda},$$

when the limitation exists.

7.1.2 Conceptual optimal control problem

We are interested in solving a mixed-constrained optimal control problem, formulated as follows

$$\begin{aligned} &\min_{\substack{x\in L^2([0,T],\mathbb{R}^n)\\ u\in L^2([0,T],\mathbb{R}^m)}} \Psi\big(x(T)\big), \\ &\text{subject to:} \quad x(0) = \xi, \\ &\qquad \dot{x}(t) = f\big(t, x(t), u(t)\big), \\ &\qquad h_i\big(t, x(t)\big) \leq 0, \ \forall i \in \mathcal{I}, \text{for a. e. } t \in [0,T], \\ &\qquad u(t) \in U, \ \text{for a. e. } t \in [0,T]. \end{aligned} \tag{7.2}$$

Where constraints $h_i \colon [0,T]\times\mathbb{R}^n \to \mathbb{R}$ are a number of state constraints and $\mathcal{I} = \{1, 2, \cdots, n_s\}$, U is a connected and compact subset of $\mathbb{R}^m$, $\xi \in \mathbb{R}^n$, and the functions f and Ψ are well-defined, each with an appropriate domain and range. We will say that f is the vector field, and Ψ the final cost, of the problem in equation (7.2). The optimal control problem in equation (7.2) is quite general, it contains constraints to both control inputs and states. Also other standard formulations, such as those including running cost functions or minimum-time cost functions, can be easily converted to the form in problem (7.2) (see Sec. 4.1.2 in [103] for a thorough exposition of this topic).

First we give the following assumption to guarantee the uniqueness of the trajectories, as well as the convergence of our numerical method, in this paper.

Assumption 7.1. *The functions f and Ψ are Lipschitz continuously differentiable. That is, there exists $L > 0$ such that, for each $t_1, t_2 \in [0,T]$, $x_1, x_2 \in \mathbb{R}^n$, $u_1, u_2 \in U$, and $i \in \mathcal{I}$,*

$$|\Psi(x_1) - \Psi(x_2)| \leq L \left\|x_1 - x_2\right\|_2, \tag{7.3}$$

$$\left\| \frac{\partial \Psi}{\partial x}(x_1) - \frac{\partial \Psi}{\partial x}(x_2) \right\|_2 \leq L \left\| x_1 - x_2 \right\|_2, \tag{7.4}$$

$$\begin{aligned} &\left\| f(t_1, x_1, u_1) - f(t_2, x_2, u_2) \right\|_2 \leq \\ &\qquad \leq L \left(|t_1 - t_2| + \left\| x_1 - x_2 \right\|_2 + \left\| u_1 - u_2 \right\|_2 \right), \end{aligned} \tag{7.5}$$

$$\begin{aligned} &\left\| \frac{\partial f}{\partial x}(t_1, x_1, u_1) - \frac{\partial f}{\partial x}(t_2, x_2, u_2) \right\|_{i,2} \leq \\ &\qquad \leq L \left(|t_1 - t_2| + \left\| x_1 - x_2 \right\|_2 + \left\| u_1 - u_2 \right\|_2 \right), \end{aligned} \tag{7.6}$$

$$\begin{aligned} &\left\| \frac{\partial f}{\partial u}(t_1, x_1, u_1) - \frac{\partial f}{\partial u}(t_2, x_2, u_2) \right\|_{i,2} \leq \\ &\qquad \leq L \left(|t_1 - t_2| + \left\| x_1 - x_2 \right\|_2 + \left\| u_1 - u_2 \right\|_2 \right), \end{aligned} \tag{7.7}$$

$$\left| h_i(t_1, x_1) - h_i(t_2, x_2) \right| \leq L \left(|t_1 - t_2| + \left\| x_1 - x_2 \right\| \right), \tag{7.8}$$

$$\begin{aligned} &\left\| \frac{\partial h_i}{\partial x}(t_1, x_1) - \frac{\partial h_i}{\partial x}(t_2, x_2) \right\|_{i,2} \leq \\ &\qquad \leq L \left(|t_1 - t_2| + \left\| x_1 - x_2 \right\|_2 \right). \end{aligned} \tag{7.9}$$

Then we relax the problem in equation (7.2) using the concept of relaxed inputs, as defined by J. Warga [129, 130]. Consider the following relaxed optimal control problem

$$\begin{aligned} &\min_{\substack{x \in L^2([0,T], \mathbb{R}^n) \\ \mu \colon [0,T] \to \mathcal{M}_p(\mathbb{R}^m)}} \quad \Psi\big(x(T)\big), \\ &\text{subject to:} \quad x(0) = \xi, \\ &\qquad \dot{x}(t) = \int_{\mathbb{R}^m} f\big(t, x(t), u\big) \, \mathrm{d}\mu_t(u), \\ &\qquad h_i\big(t, x(t)\big) \leq 0, \ \forall i \in \mathcal{I}, \text{for a. e. } t \in [0, T] \\ &\qquad \operatorname{supp}(\mu_t) \subset U, \ \text{for a. e. } t \in [0, T]. \end{aligned} \tag{7.10}$$

Where $\text{supp}(\mu_t)$ is the support of μ_t, i.e., the smallest set S such that $\mu_t(S) = 1$. In other words, instead of optimizing over the space of L^2 functions, we optimize over the space of stochastic processes defined on U.

According to [130, Theorem II.6.5], if the vector field $f(t, x, u)$ satisfies assumption 7.1, the relaxed system in problem (7.10) always has a solution. Given a fixed initial condition $x(0) = \xi$, we will denote the unique trajectory resulting from the stochastic process μ by $x^{(\mu)}$. And for $i \in \mathcal{I}$, we define the state constraint function, $h_i\big(t, x^{\mu}(t)\big)$, governed by control process μ as

$$\varphi_{i,t}(\mu) = h_i\big(t, x^{\mu}(t)\big),$$

and at time $t \in [0, T]$, we define the maximum value of $\{\varphi_i\}_{i=1}^{N_s}$ as

$$\Phi(\mu) = \max_{(i,t) \in \mathcal{I} \times [0,T]} \varphi_{i,t}(\mu).$$

For simplicity, we will also denote the unique trajectory resulting from an input u by $x^{(u)}$ and corresponding state constraints as $\varphi_i(t, u)$ and the max value as $\Phi(u)$.

Note that the problem in equation (7.2) is a particular case of the problem in equation (7.10). Indeed, given an arbitrary input $\hat{u} \in L^2([0, T], \mathbb{R}^m)$, the stochastic process defined by $\mu_t(S) = 1$ whenever $\hat{u}(t) \in S$, and $\mu_t(S) = 0$ otherwise, produces exactly the same trajectory as $\hat{u}$. Colloquially this particular stochastic process is written using Dirac Delta functions, i.e., $\mathrm{d}\mu_t(u) = \delta\big(u - \hat{u}(t)\big)\,\mathrm{d}u$. This case implies that the feasible set of the relaxed problem is strictly larger than that of the original problem, thus resulting in lower optimal values for the relaxed problem. Yet, perhaps surprisingly, this is not the case, since both problems, original and relaxed, result in the same optimal values. The equivalence between original

and relaxed problems follows since every point in the feasible set of the relaxed problem can be arbitrarily approximated using points in the feasible set of the original problem.

Theorem 7.1. *Let f be a vector field satisfying assumption 7.1, and let $\mu\colon [0,T] \to \mathcal{M}_p(\mathbb{R}^m)$ be a stochastic process. Then, for each $\varepsilon > 0$ there exists a control signal $\tilde{u}(t)$ such that for each $t \in [0,T]$, $\left\|x^{(\mu)}(t) - x^{(\tilde{u})}(t)\right\|_2 < \varepsilon$.*

Nonetheless, this theorem is an extension of the Chattering Lemma [24, Theorem 4.1], taking advantage of the fact that, for each time t, the relaxed trajectory defined in equation (7.10) can be arbitrarily approximated using a finite number of vectors in U.

7.2 Optimality conditions for optimal control

As shown by Pontryagin et al. [104] in their Minimum Principle, it is possible to find a necessary condition for optimal points that cannot be formulated using directional derivatives. On the other hand, KKT [132] necessary conditions, widely used in finite dimensional optimization problem, can be fully described using directional derivatives. Polak et al. [103, 114] have shown that numerical methods for optimal control that rely on common explicit time discretization methods converge to optimal points satisfying directional derivative-based necessary conditions. While for the deterministic original problem (7.2), derivative-based optimality functions are weaker than Pontryagin optimal functions, and lead to solutions which have higher cost values [103, 78].

In this section, under the relaxed problem (7.10), we are going to show the equivalent connection between its directional and Pontryagin optimality functions and derive a related descent direction.

7.2.1 Optimality functions

Definition 7.2 (Section 1.2 in [103]). *Consider an optimization problem with feasible set $\mathcal{X}$. We say that $\theta\colon \mathcal{X} \to (-\infty, 0]$ is an optimality function iff whenever $x \in \mathcal{X}$ is a minimizer, then $\theta(x) = 0$.*

Optimality functions are useful in practice since $\theta(x) < 0$ implies x is *not* a minimizer. Hence, they can be used as numerical tests to check whether a minimizer has been reached.

First we define an optimality function for the relaxed problem in equation (7.10). Given control's stochastic process as μ_0, and its trajectory $x^{(\mu_0)}$, at time t, the Hamiltonian to the optimal control problem (7.10) is,

$$H\big(t, x^{(\mu)}(t), \mu_t, p(t)\big) = \\ = p(t)' \int_{\mathbb{R}^m} f\big(t, x^{(\mu)}(t), u\big)\, \mathrm{d}\mu_t(u). \quad (7.11)$$

Where $p(t)$ is the corresponding adjoint variable to the problem (7.10), such that

$$\begin{aligned} p(T) &= \frac{\partial \Psi}{\partial x}\big(x^{(\mu)}\big)(T), \\ \dot{p}(t) &= -\int_{\mathbb{R}^m} \frac{\partial f}{\partial x}\big(t, x^{(\mu)}(t), u\big)'\, \mathrm{d}\mu_t(u)\, p(t). \end{aligned} \quad (7.12)$$

Then, the optimality function is defined as

$$\theta_h\big(\mu_0\big) = \min_{\delta\mu\colon [0,T]\to\mathcal{M}(\mathbb{R}^m)} \zeta_h(\mu_0, \delta\mu). \quad (7.13)$$

Where $\zeta_h(\mu_0, \delta\mu)$ is

$$\begin{aligned}
&\zeta_h(\mu_0, \delta\mu) = \\
&\max\{\max_{(i,t)\in\mathcal{I}\times[0,T]} D\psi_{i,t}(\mu_0; \delta\mu) + \\
&\qquad + \mathbf{1}(\Phi(\mu_0) \leq 0)\gamma_0\Phi(\mu_0) + \gamma_1\|\delta\mu\|, \\
&\quad \Delta H(\mu_0; \delta\mu) - \mathbf{1}(\Phi(\mu_0) > 0)\Phi(\mu_0) + \gamma_1\|\delta\mu\|\}.
\end{aligned} \tag{7.14}$$

Where, $\mathbf{1}(\Phi(u_0) \leq 0)$ and $\mathbf{1}(\Phi(u_0) < 0)$ are judgment functions, for example

$$\mathbf{1}(\Phi(u_0) \leq 0) = \begin{cases} 1, \text{ if } \Phi(u_0) \leq 0, \\ 0, \text{ otherwise.} \end{cases}$$

Note that in the definition above, $\delta\mu_t$ is a signed measure in $\mathbb{R}^m$. $\Delta H(\mu_0; \delta\mu)$ follows

$$\begin{aligned}
\Delta H(\mu_0; \delta\mu) = \quad & \int_0^T p_0(t)' \int_{\mathbb{R}^m} f\big(t, x^{(\mu_0)}(t), u\big) \mathrm{d}\delta\mu_t(u)\mathrm{d}t, \\
\text{subject to:} \quad & \operatorname{supp}(\delta\mu_t + \mu_{0,t}) \subset U, \\
& \delta\mu_t + \mu_{0,t} \geq 0, \\
& \int_{\mathbb{R}^m} \mathrm{d}\delta\mu_t(u) = 0 \text{ for a. e. } t \in [0, T].
\end{aligned} \tag{7.15}$$

Where costate $p_0(t)$ follows the dynamic in equation (7.12) under control stochastic μ_0. $D\psi_{i,t}(\mu_0;\delta\mu)$ follows

$$\begin{aligned} D\psi_{i,t}(\mu_0;\delta\mu) = & \int_0^t p_{i,t}(s)' \int_{\mathbb{R}^m} f\big(s, x^{(\mu_0)}(s), u\big) \mathrm{d}\delta\mu_s(u)\mathrm{d}s, \\ \text{subject to:} \quad & \operatorname{supp}(\delta\mu_s + \mu_{0,s}) \subset U, \\ & \delta\mu_s + \mu_{0,s} \geq 0, \\ & \int_{\mathbb{R}^m} \mathrm{d}\delta\mu_s(u) = 0 \text{ for a. e. } s \in [0,T]. \end{aligned} \tag{7.16}$$

Where $p_{i,t}(s)$ is the costate to constraint $\psi_{i,t}(s)$ under μ_0 at time t and it follows,

$$\begin{aligned} p_{i,t}(t) &= \frac{\partial \psi_{i,t}}{\partial x}\big(x^{(\mu)}\big)(t), \\ \dot{p}_{i,t}(s) &= -\int_{\mathbb{R}^m} \frac{\partial f}{\partial x}\big(s, x^{(\mu)}(s), u\big)' \, \mathrm{d}\mu_s(u)\, p(s). \end{aligned} \tag{7.17}$$

Similar to optimality functions for deterministic problem (7.2) [103, Theorem 5.6.8 and 5.6.9], we have

Proposition 7.1. *Let a stochastic process μ_0, and its trajectory as $x^{(\mu_0)}(t)$ in problem* (7.10)*. Then, the function $\theta_h\big(x^{(\mu_0)}, \mu_0\big)$, defined in equation* (7.13)*, is an optimality function of problem* (7.10)*.*

In the next subsection we are going to argue that this new optimality function in proposition 7.1 captures both directional derivatives and the Minimum Principle; hence, it is the correct framework to use in numerical algorithms.

7.2.2 Gradient descent methods for relaxed problems

First, we show the directional optimality function for problem (7.10). For the original problem (7.10), given the control's stochastic process as μ_0 and the system's trajectory as $x^{(\mu_0)}$, the directional optimality function is

$$\theta_l\big(\mu_0\big) = \min_{\delta\mu\colon\, [0,T]\to\mathcal{M}(\mathbb{R}^m)} \zeta_l(\mu_0, \delta\mu), \tag{7.18}$$

where $\zeta_l(\mu_0, \delta\mu)$ follows,

$$\begin{aligned}
&\zeta_l(\mu_0, \delta\mu) = \\
&\max\{\max_{(i,t)\in\mathcal{I}\times[0,T]} D\psi_{i,t}(\mu_0; \delta\mu) + \\
&\qquad + \mathbf{1}(\Phi(\mu_0) \le 0)\gamma_0\Phi(\mu_0) + \gamma_1\|\delta\mu\|, \\
&\quad D\Psi(\mu_0; \delta\mu) - \mathbf{1}(\Phi(\mu_0) > 0)\Phi(\mu_0) + \gamma_1\|\delta\mu\|\},
\end{aligned} \tag{7.19}$$

$D\psi_{i,t}(\mu_0; \delta\mu)$ follows equation (7.16), $D\Psi(\mu_0; \delta\mu)$ is the directional derivative of $\Psi(\mu_0)$ at μ_0,

$$\begin{aligned}
&D\Psi(\mu_0; \delta\mu) = \frac{\partial\Psi}{\partial x}\big(x^{(\mu_0)}(T)\big)'\delta x(T) \\
&\text{subject to: } \dot{\delta x}(t) = \int_{\mathbb{R}^m}\frac{\partial f}{\partial x}\big(t, x^{(\mu_0)}(t), u\big)\mathrm{d}\mu_{0,t}(u)\delta x(t) + \\
&\qquad\qquad + \int_{\mathbb{R}^m} f\big(t, x^{(\mu_0)}(t), u\big)\mathrm{d}\delta\mu_t(u), \\
&\qquad \delta x(0) = 0, \\
&\qquad \mathrm{supp}(\delta\mu_t + \mu_{0,t}) \subset U, \\
&\qquad \delta\mu_t + \mu_{0,t} \ge 0, \\
&\qquad \int_{\mathbb{R}^m}\mathrm{d}\delta\mu_t(u) = 0 \text{ for a. e. } t \in [0,T].
\end{aligned} \tag{7.20}$$

Similar to [103, Theorem 5.6.8 and 5.6.9], we have

Proposition 7.2. *For the relaxed problem* (7.10)*, the function defined in equation* (7.18) *is an optimality function.*

Now we can show the connection between the directional and Pontryagin optimality functions.

Theorem 7.3. *The optimality functions for the relaxed control problem* (7.10)*, $\theta_h(\mu_0)$ in equation* (7.13)*, and $\theta_l(\mu_0)$ in equation* (7.18)*, are equivalent.*

The proof of theorem 7.3 is in appendix D.

Since the optimality function $\theta_l(\mu_0)$ in equation (7.18) is also the first order Taylor extension of problem (7.10), after relaxing the problem, we are able to find a descent direction to the optimization problem (7.2) based on the Pontryagin principle. Before we show the optimization algorithm and its convergence, first we show that the optimality functions in equations (7.18) and (7.13) find a descent direction. Then we introduce a line search algorithm here in the infinite-dimensional space which is similar to Armijo [8].

Proposition 7.3. *Let μ_0 be a stochastic process of the control in problem* (7.10) *and its corresponding trajectory $x^{(\mu_0)}$ to the nonlinear dynamic system in problem* (7.10)*. Suppose $\left(\delta x^{(\delta\mu_0)}, \delta\mu_0\right)$ is the argument to the optimality function* (7.18)*, such that*

$$\delta\mu_0 = \arg \min_{\delta\mu:\, [0,T]\to\mathcal{M}(\mathbb{R}^m)} \theta_l(\mu_0), \tag{7.21}$$

where $\theta_l(\mu_0)$ is the optimality function in equation (7.18)*.*

Then when $\Phi(\mu_0) \leq 0$*, there exists* $\lambda \in (0,1)$ *such that* $\mu_0 + \lambda\delta\mu_0$ *is a new control's stochastic process with its corresponding trajectory,* $x^{(\mu_0+\lambda\delta\mu_0)}$*, in the nonlinear optimization problem* (7.10)*. Moreover, for the cost function in problem* (7.10)

$$\Psi\big(x^{(\mu_0+\lambda\delta\mu_0)}(T)\big) \leq \Psi\big(x^{(\mu_0)}(T)\big).$$

The proof is in appendix D.

According to theorem 7.3, the argument of the Banach optimality function in equation (7.18) is also the argument of the Hamiltonian optimality function in equation (7.13). Thus the Hamiltonian optimality function finds the same descent direction.

With a descent direction, we now introduce a line search algorithm to find a step size which is similar to the method of Armijo [8]. Suppose trajectory $x^{(\mu_0)}$ is based on control process μ_0 in problem (7.10), and further suppose that $\delta\mu_0$ is the argument to $\theta_h(\mu_0)$ and $\delta x^{(\delta\mu_0)}$ is its linearized system's trajectory in problem (7.18). Let $\alpha, \beta \in (0,1)$, and then the step size for μ_0 is chosen as $\beta^{\eta(\mu_0)}$ such that

$$\eta(\mu_0) = \begin{cases} \min\{k \in \mathbb{N} \,|\, \Psi\big(x^{(\mu_0+\beta^k\delta\mu_0)}(T)\big) - \\ \qquad -\Psi\big(x^{(\mu_0)}(T)\big) \leq \alpha\beta^k\theta_h\big(x^{(\mu_0)}, \mu_0\big), \\ \quad \Phi\big(x^{(\mu_0+\beta^k\delta\mu_0)}(T)\big) \leq \alpha\beta^k\theta_h\big(x^{(\mu_0)}, \mu_0\big)\}, \\ \qquad\qquad \text{if } \Phi(x^{(\mu_0)}) \leq 0; \\ \min\{k \in \mathbb{N} \,|\, \Phi\big(x^{(\mu_0+\beta^k\delta\mu_0)}(T)\big) - \\ \qquad -\Phi\big(x^{(\mu_0)}(T)\big) \leq \alpha\beta^k\theta_h\big(x^{(\mu_0)}, \mu_0\big)\}, \\ \qquad\qquad \text{if } \Phi(x^{(\mu_0)}) > 0. \end{cases} \tag{7.22}$$

Where $x^{(\mu_0+\beta^k\delta\mu_0)}$ is the trajectory of the dynamics in the problem (7.10) with $\mu_0 + \beta^k\delta\mu_0$.

Now we can show the numerical algorithm in the infinite dimensional continuous space as algorithm 4 and its convergence. Based on [125, Theorem 5.12], we have

Theorem 7.4. *Let $\{\mu_i\}_{i\in\mathbb{N}}$ be a sequence of control processes generated by algorithm 4, and let $\{x^{(\mu_i)}\}_{i\in\mathbb{N}}$ be its corresponding sequence of trajectories in the dynamical system in problem* (7.10)*. Then*

$$lim_{i\to\infty}\,\theta_h\Big(x^{(\mu_i)},\mu_i\Big) \to 0.$$

7.3 Synthesis of relaxed optimal inputs

Now that we have established a theoretical foundation for the equivalence between computing relaxed optimal control inputs and the Pontryagin Minimum Principle, we focus our attention on the development of numerical algorithms to synthesize approximated optimal control inputs. As we show in this section, the use of relaxed inputs is beneficial not only from a theoretical point of view, but also in our numerical algorithms, since the optimal control

Algorithm 4 Optimization algorithm to problem (7.10) in the infinite dimensional space

Require: $\big(x^{(\mu_0)},\mu_0\big)$, $\alpha,\beta\in(0,1)$.

1: $k \leftarrow 0$.
2: **loop**:
3: Compute $\theta_h\big(x^{(\mu_k)},\mu_k\big)$ and $\delta\mu_k$ based on problem (7.13).
4: Compute $\eta(\mu_k)$ based on problem (7.22).
5: **if** $\theta_h\big(x^{(\mu_k)},\mu_k\big) = 0$ **then return** $\big(x^{(\mu_k)},\mu_k\big)$.
6: $\mu_{k+1} \leftarrow \mu_k + \beta^{\eta(\mu_k)}\delta\mu_k$.
7: Update $x^{(\mu_{k+1})}$ based on μ_{k+1} and dynamic system in problem (7.10).
8: $k \leftarrow k+1$.
End loop.

problem becomes equivalent to solving a sequence of convex optimization problems, even when the dynamical system is nonlinear.

7.3.1 Vector field representation

As we show in section 7.2.2, it is possible to formulate an iterative gradient descent method using relaxed inputs that converges to Pontryagin-optimal points. This theoretical iterative method revolves around computing the value of θ_h, as defined in equation (7.13), which aims to find a new stochastic process that locally reduces the cost function of the problem in equation (7.10).

First, it is easy to show that

Proposition 7.4. *The optimization problem in equation* (7.13) *is convex.*

Based on proposition 7.4, we now focus our attention on methods to numerically represent the feasible set of the problem in equation (7.13).

Proposition 7.5. *Let $x \in \mathbb{R}^n$. Then*

$$\left\{ \int_{\mathbb{R}^m} f(x,u)\, \mathrm{d}\mu(u) \mid \mu \in \mathcal{M}(\mathbb{R}^m),\ \mathrm{supp}(\mu) \subset U \right\} = \\ = \mathrm{co}\{ f(x,u) \mid u \in U \}, \quad (7.23)$$

where $\mathrm{co}(S)$ *is the convex hull of a set $S \subset \mathbb{R}^n$.*

We omit a detailed proof, but the result follows since the convex hull is clearly contained in the left-hand side set of all possible expected values, and every expected value can be written

as the limit of a sequence of points in the convex hull since all Lebesgue-Stieltjes integrals can be approximated using finite Riemann integrals [44].

The result in Proposition 7.5 suggests that to synthesize optimal inputs, we need only to be able to compute the convex hull of the vector field at any given state $x \in \mathbb{R}^n$. Now, some points in the convex hull of the vector field have a particular input vector $u \in U$ associated with them, but others cannot be directly realized.

On the other hand, every point in the convex hull is, by definition, a convex combination of a finite set of vectors in the vector field. Hence, we can approximate the convex hull of the vector field at each $x \in \mathbb{R}^n$ with the convex hull of a finite collection of samples of the vector field for a set $\{\hat{u}_i\}_{i=1}^{N_s}$. Moreover, as shown in [125] and [126], we can arbitrarily approximate the trajectories resulting from any convex combination of vectors in a finite vector field by using a projection operation that results in switching between those vectors. In the next section we overview the main results of this method.

7.3.2 Sampled-based synthesis

First we are going to show that by using samples we can obtain approximations of the convex hull and the stochastic process. Given a control's stochastic process, μ, and its trajectory $x^{(\mu)}$ for the system in problem (7.10) at time $t \in [0, T]$, the sampling points for the vector field are $\left\{ f\big(t, x^{(\mu)}(t), u_i\big) \right\}_{i=1}^{N_s}$, where $\{u_i\}_{i=1}^{N_s} \subset U$. Each sampling point has a corresponding

weight, and the sequence of $\{w_i(t)\}_{i=1}^{N_s}$ satisfies

$$\begin{aligned} &\sum_{i}^{N_s} w_i(t) = 1, \\ &w_i(t) \geq 0, \ \forall i \in \{1, \cdots, N_s\}. \end{aligned} \tag{7.24}$$

We use these sampling points and related discrete Borel measures to represent the stochastic process at each time. The approximation converges based on the following proposition.

Proposition 7.6. *If the probability space is a connect and bounded set in $\mathbb{R}^n$, define the approximation process with discrete Borel measure in equation* (7.24) *as μ_{N_s},*

$$\begin{aligned} &\mu_{N_s,t} \to \mu_t, \ \textit{for a. e. } t \in [0,T], \\ &\textit{almost sure (weakly)} \quad N_s \to \infty. \end{aligned}$$

The details of proposition 7.6 is in [42, Section 4] and [51, Chapter 11.4]. A similar result holds for approximating the stochastic process's variance, $\delta\mu$, with sampling points in the vector field.

Since numerically the number of sampling points is finite and, at each time step, the only difference between each samples is the control value in the vector field, we get a relaxed switched system. At time t, the chance to perform control under value u_i is its weight $w_i(t) \in [0,1]$. In order to reconstruct a deterministic control, we need to project the weights $\{w_i(t)\}_{i=1}^{N_s}$ from $[0,1]^{N_s}$ into $\{0,1\}^{N_s}$, and at the same time, preserve the trajectory, $x^{(\mu)}$, and the sum of $w_i(t)$ to be 1. We use wavelet transformation and pulse-width modulation (PWM) to perform the projection. After wavelet transformation, the weight, $w_i(t)$, becomes a piecewise constant in

energy spectrum space, and by using the PWM operator, we project the weight back into time space with only 0/1 values. Details about reconstructing a deterministic control from a relaxed switch system can be found in section 4.4 [125].

Now we present the numerical version of algorithm 4. In the algorithm, the sampling values for the control are fixed as $\{u_i\}_{i=1}^{N_s} \subset U$. At each iteration, the control's stochastic process, μ_k, and its vector field at time t are approximated by the samples' weights, $\{w_{k,i}(t)\}_{i=1}^{N_s}$. Also, we define the approximated weights to $\delta\mu_k$ from equation (7.13) as $\{\hat{w}_{k,j}(t)\}_{j=1}^{N_k}$, which will be derived from the discrete version of equation (7.13).

Then, we are able to present the discrete versions of ζ in equation (7.14), and write the discrete version of θ_h problem in equation (7.13). The regularity term $\|\delta\mu\|$ both is chosen to be l_1-regularity, then θ in equation (7.13) can be discretized into

$$
\begin{aligned}
&\theta_h(\{w_{k,j}\}_{j=1}^{N_s}) = \\
&= \min_{\hat{w}_{k,i}(t)\in\mathbb{R}} \quad \zeta_h(\{w_{k,j}\}_{j=1}^{N_s}; \{\hat{w}_{k,j}\}_{j=1}^{N_s}), \\
&\text{subject to:} \quad \text{for a. e. } t \in [0,T], \\
&\qquad w_{k,i}(t) + \hat{w}_{k,i}(t) \geq 0, \ \forall i \in \{1, \cdots, N_s\}, \\
&\qquad \text{and } \sum_{i=1}^{N_s} \hat{w}_{k,i}(t) = 0,
\end{aligned}
\tag{7.25}
$$

where ζ_h is

$$\begin{aligned}
&\zeta_h(\{w_{k,j}\}_{j=1}^{N_s};\{\hat{w}_{k,j}\}_{j=1}^{N_s}) = \\
&\max\{\max_{(i,t)\in\mathcal{I}\times[0,T]} D\psi_{i,t}(\{w_{k,j}\}_{j=1}^{N_s};\{\hat{w}_{k,j}\}_{j=1}^{N_s}) + \\
&\qquad + \gamma_0\,\mathbf{1}(\Phi(\mu_k)\leq 0)\Phi(\mu_k) + \gamma_1\|\hat{w}_k\|_1, \\
&\quad \Delta H(\{w_{k,j}\}_{j=1}^{N_s};\{\hat{w}_{k,j}\}_{j=1}^{N_s}) + \\
&\qquad - \mathbf{1}(\Phi(\mu_k)>0)\Phi(\mu_k) + \gamma_1\|\hat{w}_k\|_1\}.
\end{aligned} \tag{7.26}$$

$D\psi_{i,t}(\mu_k;\delta\mu)$ and $\Delta H(\mu_k;\delta\mu)$ are respectively,

$$\begin{aligned}
&D\psi_{i,t}(\{w_{k,j}\}_{j=1}^{N_s};\{\hat{w}_{k,j}\}_{j=1}^{N_s}) = \\
&= \int_0^t p'_{i,t}(s)\Big(\sum_{j=1}^{N_s} f\big(s,x^{(\mu_k)}(s),u_j\big)\,\hat{w}_{k,j}(s)\Big)\,ds, \text{ and,}
\end{aligned} \tag{7.27}$$

$$\begin{aligned}
&\Delta H(\{w_{k,j}\}_{j=1}^{N_s};\{\hat{w}_{k,j}\}_{j=1}^{N_s}) = \\
&= \int_0^T p_0(t)'\Big(\sum_{j=1}^{N_s} f\big(t,x^{(\mu_k)}(t),u_j\big)\,\hat{w}_{k,j}(t)\Big)\,dt.
\end{aligned} \tag{7.28}$$

Now we can show the numerical implementation of algorithm 4 as follows:

Algorithm 5 Numerical implementation to the optimization algorithm of problem (7.10)

Require: $\{u_i\}_{i=1}^{N_s}$, $\{w_{0,i}(t)\}_{i=1}^{N_s}$, $x^{(\mu_0)}$, and $\alpha,\beta\in(0,1)$.

1: $k\leftarrow 0$.
2: **loop**:
3: Compute θ_h and $\{\hat{w}_{k,i}(t)\}_{i=1}^{N_s}$ based on problem (7.25).
4: **if** $\theta_h = 0$ **then** Follow the section 4.4 [125] to use wavelet and PWM to reconstruct the optimal $u_o(t)$ from $\{w_{k,i}(t)\}_{i=1}^{N_s}$. **return** $x^{(\mu_k)}$, μ_k and $u_o(t)$.
5: Compute $\eta(\mu_{k,t})$ based on problem (7.22).
6: $w_{k+1,i}(t)\leftarrow w_{k,i}(t)+\beta^{\eta(\mu_{k,t})}\hat{w}_{k,i}(t)$, $\forall i\in\{1,\cdots,N_s\}$.
7: Update $x^{(\mu_{k+1})}$ based on $\{u_i\}_{i=1}^{N_s}$ and $\{w_{k+1,i}(t)\}_{i=1}^{N_s}$ and dynamic system in problem (7.10).
8: $k\leftarrow k+1$.
End loop.

Now, we show that the discrete implementation is weakly consistent to the original problem.

Theorem 7.5. *Define the discrete optimal control problem in equation* (7.10) *with N sampling points in relaxed control space as* $\mathbf{P}_N$ *and related discrete optimality function in equation* (7.25) *as* θ_N*. Also define the original optimal control problem in equation* (7.10) *as* $\mathbf{P}$ *and related optimality function in equation* (7.13) *as* θ*. Then the discrete pair* $(\mathbf{P}_N, \theta_N)$ *is weakly consistent to the original pair* $(\mathbf{P}, \theta)$*, i.e.*

1. $\mathbf{P}_N \rightarrow_{epi.} \mathbf{P}$*, as* $N \rightarrow \infty$*;*
2. *when* $\mu_N \rightarrow \mu$ *weakly,* $\lim_{N\rightarrow\infty} \sup \theta_N(\mu_N) \leq \theta(\mu)$.

The detail of the proof is in appendix D. Theorem 7.5 shows that as the number of sampling points goes to infinity, our discrete implementation and algorithm 5 reaches the same optimal point as the original continuous problem and algorithm 4, moreover, the optimal numerical solution satisfies the Minimum principle.

7.3.3 Parallel computation

For each iteration in numerical algorithm 5, in order to further decrease the computation scale and speed, we show the theoretical foundation to parallel compute θ_h in algorithm 5.

First, we show the min and max symbols in discrete optimality problem (7.25) can be flipped.

Proposition 7.7. *The discrete optimality problem* (7.25) *is equivalent to the following problem,*

$$\begin{aligned} &\theta_h(\{w_{k,j}\}_{j=1}^{N_s}) = \\ &\quad = \max\ \{\zeta_{h,1}(\{w_{k,j}\}_{j=1}^{N_s}),\ \zeta_{h,2}(\{w_{k,j}\}_{j=1}^{N_s}),\} \end{aligned} \tag{7.29}$$

where $\zeta_{h,1}$ *and* $\zeta_{h,2}$ *are*

$$
\begin{aligned}
&\zeta_{h,1}(\{w_{k,j}\}_{j=1}^{N_s}) = \min_{\hat{w}_{k,i}(t)\in\mathbb{R}} \\
&\max_{(i,t)\in\mathcal{I}\times[0,T]} D\psi_{i,t}(\{w_{k,j}\}_{j=1}^{N_s};\{\hat{w}_{k,j}\}_{j=1}^{N_s}) + \\
&\qquad + \gamma_0\, \mathbf{1}(\Phi(\mu_k)\le 0)\Phi(\mu_k) + \gamma_1\|\hat{w}_k\|_1, \\
&\textit{subject to:}\quad \textit{for a. e. } t\in[0,T], \\
&\qquad w_{k,i}(t) + \hat{w}_{k,i}(t) \ge 0,\ \forall i\in\{1,\cdots,N_s\}, \\
&\qquad \textit{and } \sum_{i=1}^{N_s} \hat{w}_{k,i}(t) = 0;\ \textit{and,}
\end{aligned}
\tag{7.30}
$$

$$
\begin{aligned}
&\zeta_{h,2}(\{w_{k,j}\}_{j=1}^{N_s}) = \\
&\min_{\hat{w}_{k,i}(t)\in\mathbb{R}} \quad \Delta H(\{w_{k,j}\}_{j=1}^{N_s};\{\hat{w}_{k,j}\}_{j=1}^{N_s}) + \\
&\qquad - \mathbf{1}(\Phi(\mu_k)>0)\Phi(\mu_k) + \gamma_1\|\hat{w}_k\|_1, \\
&\textit{subject to:}\quad \textit{for a. e. } t\in[0,T], \\
&\qquad w_{k,i}(t) + \hat{w}_{k,i}(t) \ge 0,\ \forall i\in\{1,\cdots,N_s\}, \\
&\qquad \textit{and } \sum_{i=1}^{N_s} \hat{w}_{k,i}(t) = 0.
\end{aligned}
\tag{7.31}
$$

In problems (7.30) and (7.31), $D\Psi_{i,t}$ and ΔH are given as equations (7.16) and (7.15). The proof of proposition 7.7 is in appendix D.

According to proposition 7.7, optimality problem (7.25) can be separated into two independent smaller optimal problems, which are $\zeta_{h,1}$ and $\zeta_{h,2}$, then pick up the larger one. Moreover, both optimal problems can be further parallelized. Take $\zeta_{h,2}$ as an example.

Proposition 7.8. *The optimal problem* (7.31) *is equivalent to*

$$\int_0^T \min_{\hat{w}_{k,i}(t)\in\mathbb{R}} p_0(t)'\Big(\sum_{j=1}^{N_s} f\big(t, x^{(\mu_k)}(t), u_j\big)\,\hat{w}_{k,j}(t)\Big) + \\ + \gamma_1\|\hat{w}_k(t)\|_1\,dt - \mathbf{1}(\Phi(\mu_k)<0)\Phi(\mu_k),$$

subject to: for a. e. $t\in[0,T]$,

$$w_{k,i}(t)+\hat{w}_{k,i}(t)\geq 0,\ \forall i\in\{1,\cdots,N_s\},$$

and $\sum_{i=1}^{N_s}\hat{w}_{k,i}(t)=0.$

The proof of proposition 7.8 is in appendix D. Proposition 7.8 above implies that after discretizing the time, the optimization problem $\min\zeta_{h,2}$ can be separated into smaller problems, which are dependent to different time slides. For example, if the time is evenly discretized in to N_t slides, at time $t_i\in\{t_i\}_{i=1}^{N_t}$, the separated optimization problem is

$$\begin{aligned}&\zeta_{h,2}(\{w_{k,j}\}_{j=1}^{N_s},t_i)=\\ &\min_{\hat{w}_{k,j}(t_i)\in\mathbb{R}} p_0(t_i)'\Big(\sum_{j=1}^{N_s} f\big(t_i,x^{(\mu_k)}(t_i),u_j\big)\,\hat{w}_{k,j}(t_i)\Big)+\\ &\qquad+\gamma_1\|\hat{w}_k(t_i)\|_1,\\ &\text{subject to:}\\ &\qquad w_{k,j}(t_i)+\hat{w}_{k,j}(t_i)\geq 0,\ \forall j\in\{1,\cdots,N_s\},\\ &\qquad\text{and }\sum_{j=1}^{N_s}\hat{w}_{k,j}(t_i)=0.\end{aligned} \tag{7.32}$$

Then $\zeta_{h,2}$ can be computed as

$$\begin{aligned}&\zeta_{h,2}(\{w_{k,j}\}_{j=1}^{N_s}) = \\ &= \Delta t \sum_{i=1}^{N_t} \zeta_{h,2}(\{w_{k,j}\}_{j=1}^{N_s}, t_i) - \mathbf{1}(\Phi(\mu_k) > 0)\Phi(\mu_k),\end{aligned} \tag{7.33}$$

where Δt is the time interval between two time steps.

Now we are able to parallelize the computation of $\zeta_{h,2}$ as algorithm 6. And using the same strategy, it is also possible to parallelize $\zeta_{h,1}$, we do not draw a detailed procedure again.

Algorithm 6 Parallelizing the computation of $\zeta_{h,2}$ in problem (7.29)

Require: $\{w_{k,i}\}_{i=1}^{N_s}$, $x^{(\mu_k)}$, and $p_0^{(\mu_k)}$.

1: Distribute $\{\zeta_{h,2}(t_i)\}_{i=1}^{N_t}$ in problem (7.32) to multi-processors.

2: Collect $\{\zeta_{h,2}(t_i)\}_{i=1}^{N_t}$, compute $\zeta_{h,2}$ as equation (7.33). **return** $\zeta_{h,2}$.

7.4 Simulations

In this section, we apply the sample-based algorithm to solve to nonlinear optimal control problems to validate its performance and way to balance between accuracy and computation complexity.

7.4.1 Plan attack angle control

The initial disturbances in angle of attack of an F-8 in a level trim, the flight at $Mach = 0.85$ and an altitude of 9000 [m], for which the nonlinear equations of motion representing the

dynamics of the aircraft become [61, 38],

$$\begin{aligned}
\dot{x}_1(t) &= -0.877x_1(t) + x_3(t) - 0.088x_1(t)x_3(t) + \\
&\quad + 0.47x_1^2(t) - 0.019x_2^2(t) - x_1^2(t)x_3(t) + 3.846x_1^3(t) + \\
&\quad - 0.215u(t) + 0.28x_1^2(t)u(t) + 0.47x_1(t)u^2(t) + \\
&\quad + 0.63u^3(t), \\
\dot{x}_2(t) &= x_3(t), \\
\dot{x}_3(t) &= -0.4208x_1(t) - 0.396x_3(t) - 0.47x_1^2(t) + \\
&\quad - 3.564x_1^3(t) - 20.967u(t) + 6.265x_1^2(t)u(t) + \\
&\quad + 46x_1(t)u^2(t) + 61.4u^3(t).
\end{aligned} \tag{7.34}$$

Where x_1 is the angle of attack (unit: [rad]), x_2 is the pitch angle (unit: [rad]), x_3 is the pitch rate (unit: $[\mathrm{rad} \cdot \mathrm{s}^{-1}]$) and u is the control input (manipulated variable) provided by the tail deflection (or elevator) angle (unit: [rad]).

The dynamic system in equation (7.34) is highly nonlinear and non-affine, the corresponding attack angle control problem is,

$$\begin{aligned}
&\min_{\substack{x \in L^2([0,2],\mathbb{R}^3) \\ u \in L^2([0,2],\mathbb{R})}} \int_{t=0}^{2} \Big(\sum_{i=1}^{3} x_i^2(t) + 0.1u^2(t) \Big) dt + \sum_{i=1}^{3} x_i^2(2), \\
&\text{subject to:} \quad \text{nonlinear dynamic system in equation (7.34)}, \\
&\qquad\qquad x(0) = \xi, \\
&\qquad\qquad x_1(2) \in [0.0, 0.01], \\
&\qquad\qquad u(t) \in [-0.1, 0.1], \text{ for a. e. } t \in [0, 2].
\end{aligned} \tag{7.35}$$

Where $\xi \in \mathbb{R}^3$ is the value of initial states. The optimal control problem in equation (7.35) tries to make the final attack angle, $x_1(2)$, in to the range $[0.0, 0.01]$ under the elevator control in the constraint range $[-0.1, 0.1]$.

Due to the highly nonlinear property of the problem, usually in order to solve it in real time inside a jet's central control system, the problem (7.35) is approximated into a Linear Quadratic Regularity (LQR) problem. However, the accuracy of simplified LQR problem can be only guaranteed in a small range [38].

We apply our sample-based accelerate algorithm in this paper to solve the problem (7.35). Since the dimension of this optimal control problem is 4, we solve its corresponding discritized optimization problem in IPOPT [127]. We use the comparison results from the sample-based algorithm and IPOPT to numerically show how to balance approximation accuracy and computation speed.

Figure 7.1a shows one simulation result when the initial condition in problem (7.35) is $\xi = (0.56, 0, 0)$. The number of sampling points in this case is 100, the cost function value from IPOPT and sample-based method are 0.168 and 0.171 respectively. Since in all simulation cases, the cost value for IPOPT is lower, we use its solutions as standards to compare the accuracy from sample-based algorithm's results. Figure 7.1b and 7.1c are statistical results based on 10 different initial conditions and 6 different numbers of sampling points. Figure 7.1b shows the relative difference between cost value from IPOPT and sample-based algorithm. Figure 7.1c shows the computation time with different number of sampling points. The average time IPOPT used to solve the problem is 10.43 [sec]. As shown in figure 7.1b and 7.1c, as the number of sampling points increases, the cost difference between two methods decreases, while the computation time increases.

Figure 7.1c also shows the speed performance for parallel computing, based on the slopes of two lines, which represent the computation time for sample-based algorithm with and without parallel computing method, the time computation complexities w.r.t. number of sampling points are $\mathcal{O}(n^1)$ and $\mathcal{O}(n^{0.67})$ respectively.. The time computation complexity shows the potential to apply parallel computing method for further time acceleration.

According to figure 7.1b and 7.1c it is possible to balance approximation accuracy and computation time of sample-based algorithm. For example, if the number of sampling point chosen is 30, the sample-based algorithm will be faster than IPOPT and their approximation difference is around 2%.

7.4.2 Indoor thermal comfort control

We apply the sample-based algorithm to solve the indoor thermal comfort optimal control problem. Define the indoor area as a bounded and connected subset $\Omega \subset \mathbb{R}^2$, the indoor climate consists flow's temperature, $T_e : \Omega \times [0, T] \to \mathbb{R}$, velocity, $u : \Omega \to \mathbb{R}^2$, and pressure, $p : \Omega \to \mathbb{R}$. Given initial condition, time horizon $[0, T]$, the temperature control, $g_{T_e} : [0, T] \to \mathbb{R}$ and the velocity control, $g_u : \Omega \to \mathbb{R}^2$, the indoor climate follows the dynamic system which can be represented by partial differential equations (PDE) in chapter 5, moreover this PDE system is nonlinear. The thermal comfort is quantified by Predicted Mean Vote (PMV) index and approximated by function as in chapter 5, $\text{pmv}^2(T_e(x, t; g_{T_e}, g_u), u(x; g_u))$. Suppose the indoor resident is inside the target area $\Omega_t \subset \Omega$, the corresponding optimal

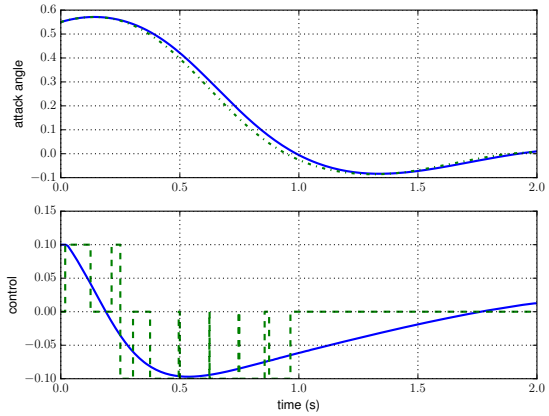

(a) Attack angle trajectory and corresponding control.. Green dashed line: sample-based algorithm; Blue line: IPOPT.

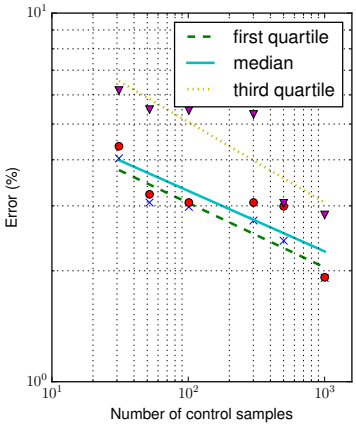

(b) Relative differences to IPOPT with different number of sampling points.

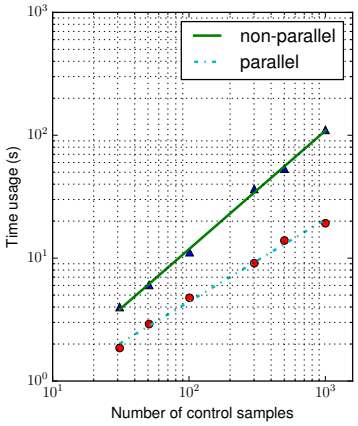

(c) Computation time with different number of sampling points.

Figure 7.1: Simulation results for problem (7.35).

control problem is shown as

$$
\begin{aligned}
&\min_{g_{T_e}, g_u} J_c(g_{T_e}, g_u) = \\
&\quad = \int_0^T \int_{\Omega_t} \mathrm{pmv}^2(T_e(x,t;g_{T_e},g_u), u(x;g_u), M, I_{cl})\mathrm{d}x\mathrm{d}t + \\
&\quad + \eta_0' \left\| g_{T_e} \right\|_{\Omega\times[0,T]} + \eta_1' \left\| g_u \right\|_{\Omega}, \\
&\text{subject to:} \quad \text{the fluid dynamic model,} \\
&\quad \left| \int_{\Omega_t} \mathrm{pmv}(T_e(x,T';g_{T_e},g_u), g_u, M, I_{cl})dx \right| / \|\Omega_t\| \leq 0.5, \\
&\quad \underline{g_{T_e}} \leq g_{T_e}(t) \leq \overline{g_{T_e}}, \text{for a.e. } t \in [0,T], \\
&\quad \underline{g_u} \leq \|g_u\| \leq \overline{g_u}.
\end{aligned}
\tag{7.36}
$$

Where $\underline{g_{T_e}}$, $\overline{g_{T_e}}$, $\underline{g_u}$ and $\overline{g_u}$ are positive and controllers' power limits. The problem (7.36) tries to balance the thermal comfort inside the target area and total energy used by controllers. Moreover, it has a final state constraint for PMV index to guarantee resident's comfort.

After discretizing the PDE dynamic system in space by finite element method [67], the problem (7.36) becomes a large-scale ordinary differential equation based problem with tens of thousands variables in spatial. Previously, the problem is solved by derivative-based algorithm and the computation time is one scale larger than the time horizon [38, 61]. In this section, we apply sample-based algorithm to this optimal control problem and balance between approximation accuracy and speed.

Figure 7.2a shows the final PMV index distribution inside apartment under sample-based optimal solution. The apartment plan used for simulations is given by Washington University in Saint Louis and locates in 749 Westgate, Saint Louis. According to figure 7.2a, the final PMV index inside two target area is close to zero, which makes inside residents comfortable.

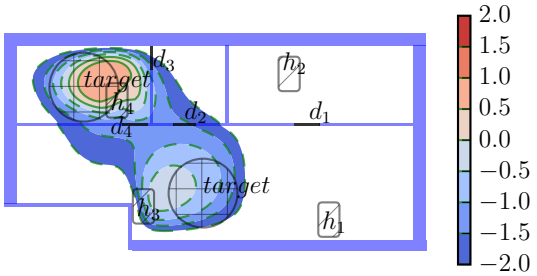

(a) Final state PMV index distribution inside apartment.

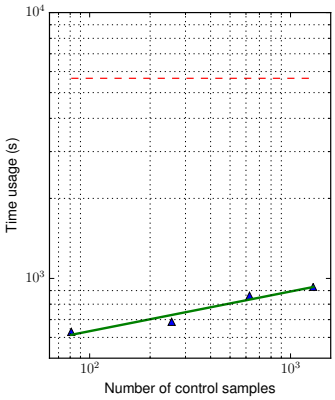

(b) Statistical result for computation times with different number of sampling points.

Figure 7.2: Simulation results for problem (7.36).

Figure 7.2b shows the average time used to solve the optimal control problem (7.36), the red dash line represents the results by derivative-based algorithm and the blue line is based on sample-based algorithm without parallel computation. The statistical results are based on ten different simulation cases, and the PDE solver used is FEniCS [93], which does not support parallel computation in Python. Compare the computation speeds in figure 7.2b, the sample-based algorithm is one scale faster than traditional derivative-based algorithm and its computation time is close to the problem's time horizon, which shows the potential to use this approximation acceleration algorithm to solve large-scale nonlinear optimal control problem in reality.

7.5 Chapter conclusion

In this paper, we show a direct method to find Minimum Principle point for an optimal control problem, its corresponding numerical implementation. We use sample-based approximation to simplify the model to balance between the accuracy of the algorithm's optimal solution and its computation speed, moreover, we prove the consistence of this approximation implementation algorithm. The simulation results show its potential to solve large-scale nonlinear optimal control problems in time. In future, the study will focus on the theoretical analysis to relation between the approximation accuracy and number of sampling points for general problems.

Chapter 8

Conclusions

8.1 Summary and conclustions

In this dissertation, we study about algorithms to control HVAC system and estimate indoor fluid dynamics and building configurations based on nonlinear PDE CFD models.

We first show how accurate a nonlinear PDE-based optimal control algorithm for HVAC system to maintain indoor temperature. This result opens the door to a large number of exiting opportunities to improve the energy efficiency of buildings. The result validates the idea that an accurate distributed indoor climate model is able to improve the HVAC system's efficiency by focusing on local indoor target areas.

Next, we introduce an estimator which is based on our distributed PDE-based model. The estimator is able to estimate the indoor fluid distribution and the doors configurations at the same time, which in turn saves the sensor expense. Due to the application of a gradient-based numerical direct algorithm with the CFD model's co-states, the estimator's corresponding optimization problem is able to solve efficiently both in the aspect of time and memory complexity.

Then, we develop a MPC system to control the thermal comfort around indoor residents based on distributed CFD model, instead of focusing on only temperature control. The simulation results validate the performance of our MPC to adapt its control strategy based on different cases, and reflect the importance of resident's own influence to thermal comfort, which is usually be ignored in control literature.

Finally, in order to make our PDE-based HVAC optimal control problems run in real time, we present a theoretical formulation, and a corresponding numerical algorithm that can find Pontryagin-optimal inputs for general dynamical systems by using a direct method. Simulation results validate the algorithm's performance and its potential fast speed to solve large-scale nonlinear optimal control problems.

The studies in this dissertation validate the idea that by making small improvements to existing HVAC units it is possible to dramatically increase the efficiency of HVAC units without a decrease in human comfort.

8.2 Future directions

Based on this dissertation, there are several potential future research directions.

Online/Cloud control to HVAC system. An accurate CFD model based on physical principle consists of Navier-Stokes equation and even turbulence property. This will generate a large-scale nonlinear optimization problem, in order to solve it in real time to control the HVAC system, it is possible to use parallel computing technology or even cloud server, i.g. AWS, these days. Due to the development of computer engineering, the price of hardware and cloud services these days are available for residents' daily usage.

Model reduction method to simplify CFD model. In order to further speed up the control to HVAC system with distributed model, there is another potential solution which is to reduce the dimension of the nonlinear model, for example proper orthogonal decomposition [112]. Also for the sampling-based numerical algorithm in chapter 6, it is possible to further speed the algorithm by simplifying the representation of the convex hull.

Smart housing system for residential buildings. In chapter 5, we use wearable devices to monitor residents' personal property and adapt the HVAC system to maintain thermal comfort. Furthermore, it is possible to unify all the electrical devices in house to build a smart housing system to help residents take of their home and life. For example, if we connect our HVAC system with home security alerts, since our estimator is able to identify a building's configuration in real-time, it can potentially be applied to monitor an unexpected break-in and inform home security directly.

Appendix A

Proofs in Chapter 2

In this appendix, we are going to show the solution's existence and uniqueness to the CFD model containing equations (2.2), (2.3), (2.4), (2.5), (2.8), (2.6) and (2.7) in chapter 2.

According to [45] and [67, Theorem I.4.1], the solution's existence and uniqueness of the weak formulas in equations (2.9) and (2.10) with boundary condition (2.6) are equivalent to the corresponding problem of the following weak formula,

$$\begin{aligned} &\langle \alpha u, \varphi \rangle_\Omega + \frac{1}{Re} \langle \nabla_x u, \nabla_x \varphi \rangle_\Omega + \langle u \cdot \nabla_x u, \varphi \rangle_\Omega = \\ &= \langle g_u, \varphi \rangle_\Omega \quad \forall \varphi \in V_0 \end{aligned} \tag{A.1}$$

The existence and uniqueness of the CFD system are given as the following,

Theorem A.1 (Equivelent theorem to theorem 2.1)**.** *Let $\Omega \subset \mathbb{R}^2$ be bounded and locally Lipschitz, there exists at least one tuple $(T_e, u, p) \in L^2([t_0, t_0']; H_1) \times (H^1(\Omega) \times H^1(\Omega)) \times L^2(\Omega)$, such that*

- *T_e satisfies the boundary and initial condition in equations* (2.8) *and* (2.3)*, and $\forall \xi \in H_0^1$ the equation* (2.11) *holds.*

- $u \in V_0$ *satisfies the boundary condition in equation* (2.6), (2.7) *and the equation* (A.1).
- p *satisfies the equation* (2.4).

Theorem A.2. *Let* $\Omega \subset \mathbb{R}^2$ *be bounded and locally Lipschitz, define the area of* Ω *as* $|\Omega|$. *For the weak solution tuple* (T_e, u, p) *in the theorem 2.1, if* $|u|_1 = \left(\int_\Omega |\nabla_x u|^2 dx\right)^{1/2} < \frac{1}{C \cdot Re}$, *where* $C = \frac{|\Omega|^{1/2}}{2}$, *Then* (T_e, u, p) *is the only weak solution to the CFD system.*

Since the equation (2.2) is weakly coupled with the fluid's flow equations (2.4) and (2.5). In order to prove theorems A.1 and A.2, we study the weak solution's property of the PDE system with equations (2.4), (2.5) and boundary condition (2.6) first. Then when u is given, equation (2.11) becomes a time-dependent parabolic partial differential equation and we study its solution's property. The technologies used in the proofs are similar to the previous work [67] [45] and [85].

For each $\varepsilon > 0$, according to Hopf extension [67, Lemma I.4.2.3], there exists a function $\bar{u} \in H^1(\Omega) \times H^1(\Omega)$ s.t. $\nabla_x \cdot (\bar{u})(x) = 0$, $\bar{u}|_{\Gamma_w} = 0$, $\bar{u}|_{\Gamma_o} = u_o \hat{n}(x)$, and, $|\langle (v \cdot \nabla_x)\bar{u}, v\rangle_\Omega| \leq \varepsilon |v|_1^2$, $\forall v \in V_0$. Then any functions $u \in H^1(\Omega) \times H^1(\Omega)$ satisfying the boundary condition (2.6) can be represented as $u = w + \bar{u}$, for some $w \in V_0$.

The main technology to show the existence of the weak solution to the equation (A.1) is to use the fix point theory. Firstly, given $\hat{u} = \hat{w} + \bar{u}$, for fixed $\hat{w} \in V_0$, we show the equation

$$\begin{aligned} \langle \alpha(x) w, \varphi\rangle_\Omega + \frac{1}{Re}\langle \nabla_x u, \nabla_x \varphi\rangle_\Omega + \langle \hat{u} \cdot \nabla_x w, \varphi\rangle_\Omega + \\ + \langle u \cdot \nabla_x \bar{u}, \varphi\rangle_\Omega = \langle g_u, \varphi\rangle_\Omega \end{aligned} \tag{A.2}$$

$\forall \varphi \in V_0$, has unique solution. Define the mapping $\mathcal{S}$, from the given $\hat{u}$ to u, the solution to the equation (A.2), as $\mathcal{S}(\hat{u}) = u$, then the fixed point of the mapping $\mathcal{S}$ is one solution to

the equation (A.1). Define bilinear operator $\sigma_0(w,\varphi) = \langle\alpha(x)w,\varphi\rangle_\Omega + \frac{1}{Re}\langle\nabla_x u, \nabla_x\varphi\rangle_\Omega + \langle\hat{u}\cdot\nabla_x w,\varphi\rangle_\Omega + \langle u\cdot\nabla_x\bar{u},\varphi\rangle_\Omega$, $\forall w,\varphi\in V_0$.

Lemma A.1. *σ_0 is bounded.*

Proof of lemma A.1. Holder's inequality directly shows σ_0 is bounded.

$$\begin{aligned}|\sigma_0(w,\varphi)| \le |\langle\alpha(x)w,\varphi\rangle_\Omega| + |\frac{1}{Re}\langle\nabla_x u,\nabla_x\varphi\rangle_\Omega| + \\ +|\langle\hat{u}\cdot\nabla_x w,\varphi\rangle_\Omega| + |\langle w\cdot\nabla_x\bar{u},\varphi\rangle_\Omega| \le \|\alpha(x)w\|_0\|\varphi\|_0 + \\ +\frac{1}{Re}|w|_1|v|_1 + \|\hat{u}\|_1|w|_1\|\varphi\|_1 + \|w\|_1|\bar{u}|_1\|\varphi\|_1.\end{aligned}$$

□

Definition A.3. *A bilinear form $a: V\times V\to\mathbb{R}$ is called* coercive *if there exists a constant $C>0$ such that, $\forall x\in V$, $|a(x,x)|\ge C\|x\|_V^2$.*

Lemma A.2. *σ_0 is coercive.*

Proof of lemma A.2. For arbitrary $w\in V_0$. By Poincare-Friedrichs inequality (Lemma 3.1, Chapter 1, [67]) there exists a constant $C>0$ s.t. $|\frac{1}{Re}\langle\nabla_x w,\nabla_x w\rangle_\Omega| \ge C\|w\|_1^2$. According to Hopf's extension, let $C-\varepsilon\ge 0$, for instance, fix $\varepsilon=\frac{1}{2}C$, and pick up the corresponding $\bar{u}$, s.t. $|\langle w\cdot\nabla_x\bar{u},w\rangle_\Omega|\le\varepsilon|w|_1^2\le\frac{1}{2}C\|w\|_1^2$ Then, $\sigma_0(w,w) = \langle\alpha(x)w,w\rangle_\Omega + \frac{1}{Re}\langle\nabla_x u,\nabla_x w\rangle_\Omega + \langle\hat{u}\cdot\nabla_x w,w\rangle_\Omega + \langle u\cdot\nabla_x\bar{u},w\rangle_\Omega \ge \langle\alpha(x)w,w\rangle_\Omega + \langle u\cdot\nabla_x\bar{u},w\rangle_\Omega \ge \frac{1}{2}C\|w\|_1^2$. Thus σ_0 is coercive. □

Lemma A.3. *$\forall\varphi\in V_0$, the equation* (A.2) *has unique weak solution u. And u can be separated as $u=w+\bar{u}$, for some $w\in V_0$.*

Proof of lemma A.3. According to the Lemma A.1 and A.2, it follows from the Lax-Milgram theorem [67, Chapter 1.2] that the equation, $\sigma_0(w,\varphi) = -\langle\alpha(x)\bar{u},\varphi\rangle_\Omega - \langle\frac{1}{Re}\nabla_x\bar{u},\varphi\rangle_\Omega - \langle\bar{u}\cdot$

$\nabla_x \bar{u}, \varphi\rangle_\Omega + \langle g_u, \varphi\rangle_\Omega$ has a unique solution $w \in V_0$ for all $\varphi \in V_0$. Since $u = w + \bar{u}$, the equation (A.2) has unique solution u. □

Lemma A.4. *$\forall \hat{u} \in V_0$, the solution $u = \mathcal{S}(\hat{u})$ to equation* (A.2) *is always bounded.*

Proof of lemma A.4. Set $\varphi = w$ in equation (A.1), since $u = w + \bar{u}$, we get

$$\begin{aligned}\langle \alpha(x)w, w\rangle_\Omega + \langle \alpha(x)\bar{u}, w\rangle_\Omega + \frac{1}{Re}\langle w, w\rangle_\Omega + \frac{1}{Re}\langle \nabla_x \bar{u}, w\rangle_\Omega + \\ + \langle \hat{u}\cdot\nabla_x w, w\rangle_\Omega + \langle w\cdot\nabla_x \bar{u}, w\rangle_\Omega + \langle \bar{u}\cdot\nabla_x \bar{u}, w\rangle_\Omega = 0,\end{aligned}$$

which is

$$\begin{aligned}\langle \alpha(x)w, w\rangle_\Omega + \frac{1}{Re}\langle w, w\rangle_\Omega + \langle w\cdot\nabla_x \bar{u}, w\rangle_\Omega = \\ = -\langle \alpha(x)\bar{u}, w\rangle_\Omega - \frac{1}{Re}\nabla_x \bar{u}, w\rangle_\Omega - \langle \bar{u}\cdot\nabla_x \bar{u}, w\rangle_\Omega\end{aligned} \tag{A.3}$$

Since $\alpha(x) \in L^\infty(\Omega)$ and non-negative, define the upper bound of $\alpha(x)$ as $\bar{\alpha}$ and lower bound as $\underline{\alpha}$, the Left Half Side (LHS) of the equation (A.3) is

$$\begin{aligned}\langle \alpha(x)w, w\rangle_\Omega + \frac{1}{Re}\langle w, w\rangle_\Omega + \langle w\cdot\nabla_x \bar{u}, w\rangle_\Omega \geq \\ \geq \frac{1}{Re}\langle w, w\rangle_\Omega + \langle w\cdot\nabla_x \bar{u}, w\rangle_\Omega \geq \frac{1}{2}C\|w\|_1^2\end{aligned}$$

While according to Holder Inequality, the Right Half Side (RHS) of (A.3) is

$$\begin{aligned}-\langle \alpha(x)\bar{u}, w\rangle_\Omega - \frac{1}{Re}\langle \nabla_x \bar{u}, w\rangle_\Omega - \langle \bar{u}\cdot\nabla_x \bar{u}, w\rangle_\Omega \leq \\ \leq |\langle \alpha(x)\bar{u}, w\rangle_\Omega| + |\frac{1}{Re}\nabla_x \bar{u}, w\rangle_\Omega| + |\langle \bar{u}\cdot\nabla_x \bar{u}, w\rangle_\Omega| \leq \\ \leq \bar{\alpha}\|\bar{u}\|_0\|w\|_0 + |\bar{u}|_1|w|_1 + \|\bar{u}\|_1|\bar{u}|_1|w|_1 \leq \\ \leq \bar{\alpha}\|\bar{u}\|_0\|w\|_1 + |\bar{u}|_1|w|_1 + \|\bar{u}\|_1|\bar{u}|_1|w|_1\end{aligned}$$

According to Poincare-Friedrichs inequality, in V_0 the norm $|\cdot|_1$ and the norm $\|\cdot\|_1$ are equivalent. There exists a constant $C_1 > 0$ s.t. $\forall w \in V_0$, $|w|_1 \leq C_1\|w\|_1$, then,

$$\begin{aligned} -\langle\alpha(x)\bar{u}, w\rangle_\Omega - \frac{1}{Re}\langle\nabla_x\bar{u}, w\rangle_\Omega - \langle\bar{u}\cdot\nabla_x\bar{u}, w\rangle_\Omega \leq \\ \leq \bar{\alpha}\|\bar{u}\|_0\|w\|_1 + |\bar{u}|_1|w|_1 + \|\bar{u}\|_1|\bar{u}|_1|w|_1 \leq \\ \leq \bar{\alpha}\|\bar{u}\|_0\|w\|_1 + C_1|\bar{u}|_1\|w\|_1 + C_1\|\bar{u}\|_1|\bar{u}|_1\|w\|_1 \end{aligned}$$

Thus, $\|w\|_1$ is bounded by $\|w\|_1 \leq \frac{2}{C}(\bar{\alpha}\|\bar{u}\|_0 + C_1|\bar{u}|_1 + C_1\|\bar{u}\|_1|\bar{u}|_1)$ Define this upper bound as γ, let Σ be a closed convex subset of $H^1(\Omega)$ as $\Sigma = \{u = w + \bar{u}, w \in V_0$ satisfying $\|w\|_1 \leq \gamma\}$ Thus the mapping $\mathcal{S}$ maps from Σ into Σ thus is bounded. □

Lemma A.5. *The mapping $S : \Sigma \to \Sigma$ is compact.*

proof of lemma A.5. A mapping between two norm spaces is said to be compact if it is continuous and maps bounded sets into relatively compact sets. Since $H^1(\Omega)$ is compactly embedded in $L^4(\Omega)$, and Σ is a closed and bounded subset in $H^1(\Omega)$, it is compact. Thus it is only left to show $\mathcal{S}$ is a continuous mapping.

If the sequence $\{\hat{w}_k\}$ converges to $\hat{w}$ in V_0, then $\|\hat{u}_k - \hat{u}\|_{L^4} \to 0$. Suppose the mapping sequence $\{\mathcal{S}(\hat{u}_k)\} = \{u_k\}$ and $S(\hat{u}) = u$. From the equation (A.1), we have

$$\begin{aligned} \langle\alpha(x)u_k - u, \varphi\rangle_\Omega + \frac{1}{Re}\langle\nabla_x u_k - u, \nabla_x\varphi\rangle_\Omega + \\ + \langle u_k - u\cdot\nabla_x\bar{u}, \varphi\rangle_\Omega + \langle\hat{u}_k\cdot\nabla_x u_k - u, \varphi\rangle_\Omega + \\ + \langle\hat{u}_k - \hat{u}\cdot w, \varphi\rangle_\Omega = 0. \end{aligned}$$

Set $\varphi = u_k - u$, we get

$$\begin{aligned}\langle \alpha(x)u_k - u, u_k - u\rangle_\Omega + \frac{1}{Re}\langle \nabla_x u_k - u, \nabla_x u_k - u\rangle_\Omega + \\ + \langle u_k - u\cdot\nabla_x \bar{u}, u_k - u\rangle_\Omega = -\langle \hat{u}_k - \hat{u}\cdot w, u_k - u\rangle_\Omega\end{aligned} \tag{A.4}$$

The LHS of (A.4) has $LHS \geq +\frac{1}{Re}\langle \nabla_x u_k - u, \nabla_x u_k - u\rangle_\Omega + \langle u_k - u\cdot\nabla_x\bar{u}, u_k - u\rangle_\Omega \geq \frac{1}{2}C\|u_k - u\|_1^2$. The RHS of (A.4) has $RHS \leq |w|_1\|u_k - u\|_1\|\hat{u}_k - \hat{u}\|_{L^4}$. Thus as $\|\hat{u}_k - \hat{u}\|_{L^4} \to 0$, $\|u_k - u\|_1 \to 0$. □

Based on these lemmas, we can derive the existence of solution to problem (A.1).

Lemma A.6. *There exists at least one fixed point for the mapping $\mathcal{S}$. Thus $u \in V_0 + \bar{u}$ exists as the solution to problem* (A.1)*.*

Proof of lemma A.6. According to Lemma A.5, the existence of the weak solution to equation (A.1) can be shown by the Theorem 1.J in [119]. □

In order to study the existence and uniqueness of weak solution of temperature, let us define bilinear operator σ_1 as $\sigma_1(T_e, \xi) = \langle \kappa(x)\nabla_x T_e, \nabla_x \xi\rangle_\Omega + \langle u\cdot\nabla_x T_e, \xi\rangle_\Omega$, $\forall t \in [t_0, t_0 + T]$. Then at an arbitrary time $t \in [t_0, t_0 + T]$, equation (2.11) can be written as, $\forall \xi \in V_1$, $\langle \dot{T}_e, \xi\rangle_\Omega + \sigma_1(T_e, \xi) = \langle g_{T_e}, \xi\rangle_\Omega$.

Similarly, we prove that σ_1 is bounded and coercive.

Lemma A.7. *σ_1 is bounded.*

Since $\kappa(x)$ and $u(x)$ are bounded, by Holder inequality, we can show that σ_1 is bounded through a similar way as the proof of Lemma A.1

Lemma A.8. *σ_1 is coercive.*

Proof of lemma A.8. By Poincare-Friedrichs inequality, there exists $C > 0$, s.t. $|\sigma_1(T_e, T_e)| = |\langle \kappa(x)\nabla_x T_e, \nabla_x T_e\rangle_\Omega + \langle u \cdot \nabla_x T_e, T_e\rangle_\Omega| = |\langle \kappa(x)\nabla_x T_e, \nabla_x T_e\rangle_\Omega| \geq C\|T_e\|_1^2$. □

Lemma A.9. *There exists a unique solution, $T_e \in L^2([t_0, t_0']; H^1(\Omega))$, to the equation* (2.11).

Proof of lemma A.9. According to Lemma A.7 and A.8 and [107, Theorem 11.1.1], the lemma A.9 holds. □

Now, we can prove the theorem A.1.

Proof of theorem A.1 (theorem 2.1). According to lemmas A.6 and A.9, the target theorem holds. □

Finally, we are going to study the uniqueness of the weak solution to CFD system. For the uniqueness of the solution to equation (A.1), here we derive a sufficient condition.

Lemma A.10. *Let $\Omega \subset \mathbb{R}^2$ be bounded and locally Lipschitz, define the area of Ω as $|\Omega|$, if the solution u's norm $|u|_1 < \frac{1}{C \cdot Re}$, where $C = \frac{|\Omega|^{1/2}}{2}$, the weak formula* (A.1) *has only one solution.*

Proof of lemma A.10. Given fixed α and boundary conditions, suppose u_1 and u_2 are two different solutions to the equation (A.1). Let $\tilde{u} = u_1 - u_2$, we have $\forall \varphi \in V_0$, $\langle \alpha(x)\tilde{u}, \varphi\rangle_\Omega + \frac{1}{Re}\langle \nabla_x \tilde{u}, \nabla_x \varphi\rangle_\Omega + \langle u_1 \cdot \nabla_x \tilde{u}, \varphi\rangle_\Omega + \langle \tilde{u} \cdot \nabla_x u_2, \varphi\rangle_\Omega = 0$. Then set $\varphi = \tilde{u}$, we get $\langle \alpha(x)\tilde{u}, \tilde{u}\rangle_\Omega +$

$\frac{1}{Re}\langle\nabla_x\tilde{u},\nabla_x\tilde{u}\rangle_\Omega + \langle u_1\cdot\nabla_x\tilde{u},\tilde{u}\rangle_\Omega + \langle\tilde{u}\cdot\nabla_x u_2,\tilde{u}\rangle_\Omega = 0$. Thus we can bound the norm of $\tilde{u}$ as

$$\begin{aligned}\frac{1}{Re}\langle\nabla_x\tilde{u},\nabla_x\tilde{u}\rangle_\Omega = -\langle\alpha(x)\tilde{u},\tilde{u}\rangle_\Omega - \langle\tilde{u}\cdot\nabla_x u_2,\tilde{u}\rangle_\Omega \leq \\ \leq |\langle\tilde{u}\cdot\nabla_x u_2,\tilde{u}\rangle_\Omega| \leq C|u_2|_1|\tilde{u}|_1^2\end{aligned} \tag{A.5}$$

Where $C = \frac{|\Omega|^{1/2}}{2}$ for $\Omega\subset\mathbb{R}^2$ [60, Lemma 9.1.2].

Equation (A.5) derives $\left(\frac{1}{Re} - C|u_2|_1\right)|\tilde{u}|_1^2 \leq 0$. Thus if $\frac{1}{Re} - C|u_2|_1 \geq 0$, $|\tilde{u}|_1 = 0$, then weak formulation has unique solution u. □

Proof of theorem A.2 (theorem 2.2). According to lemmas A.10 and A.9, the target theorem holds. □

Appendix B

Derivations in Chapter 4

In this appendix, we give the derivativations of adjoint equations and Fréchet derivatives.

B.1 Derivation of adjoint equations

Consider the Lagrangian function in equation (4.3). For each set of functions (w, v, q) in the respective dual space of the tuple (Te, u, p), we can write $\left\langle \frac{\partial L}{\partial T_e}, w \right\rangle_{\Omega\times[0,T]} = 0$ as follows:

$$\begin{aligned}\left\langle \frac{\partial L}{\partial T_e}, w \right\rangle_{\Omega\times[0,T]} = \left\langle \frac{\partial J}{\partial T_e}, w \right\rangle_{\Omega\times[0,T]} + \left\langle \lambda_1, \frac{\partial w}{\partial t} - \nabla_x\cdot(\kappa\,\nabla_x w) + u\cdot\nabla_x w \right\rangle_{\Omega\times[0,T]} + \\ + \langle \lambda_4, w\rangle_{\partial\Omega\times[0,T]} + \langle \lambda_6, w(0,\cdot)\rangle_{\Omega} = 0.\end{aligned} \tag{B.1}$$

Similarly, we can write $\left\langle \frac{\partial L}{\partial u}, v \right\rangle_{\Omega} = 0$ as

$$\begin{aligned}\left\langle \frac{\partial L}{\partial u}, v \right\rangle_{\Omega} = \left\langle \lambda_1, v\cdot\nabla_x T_e \right\rangle_{\Omega\times[0,T]} + \\ + \left\langle \lambda_2, -\frac{1}{Re}\Delta_x v + (u\cdot\nabla_x)v + (v\cdot\nabla_x)u + \alpha\, v \right\rangle_{\Omega} + \\ + \langle \lambda_3, \nabla_x\cdot v\rangle_{\Omega} + \langle \lambda_5, v\rangle_{\Gamma_w} = 0,\end{aligned} \tag{B.2}$$

and we can write $\left\langle \frac{\partial L}{\partial p}, q \right\rangle_{\Omega} = 0$ as $\left\langle \lambda_2, \nabla_x q \right\rangle_{\Omega} = 0$.

Applying integration by parts and Green's formula, equations (B.1) and (B.2) become

$$\begin{aligned} &\left\langle \frac{\partial J}{\partial T_e}, w \right\rangle_{\Omega\times[0,T]} - \left\langle \frac{\partial \lambda_1}{\partial t} + \nabla_x\cdot(\kappa\,\nabla_x\lambda_1) + u\cdot\nabla_x\lambda_1, w \right\rangle_{\Omega\times[0,T]} + \\ &+ \left\langle \lambda_1(\cdot,T), w(\cdot,T) \right\rangle_{\Omega} + \left\langle \lambda_6 - \lambda_1(\cdot,0), w(\cdot,0) \right\rangle_{\Omega} + \\ &+ \left\langle \kappa\,\frac{\partial \lambda_1}{\partial \vec{n}} + \lambda_4 + \vec{n}\cdot u\lambda_1, w \right\rangle_{\partial\Omega\times[0,T]} - \left\langle \kappa\,\lambda_1, \frac{\partial w}{\partial \vec{n}} \right\rangle_{\partial\Omega\times[0,T]} = 0, \end{aligned} \tag{B.3}$$

$$\begin{aligned} &\left\langle \lambda_1, v\cdot\nabla_x T_e \right\rangle_{\Omega\times[0,T]} + \left\langle \alpha\,\lambda_2 - \frac{1}{Re}\Delta_x\lambda_2 + \nabla_x u\cdot\lambda_2 - u\cdot\nabla_x\lambda_2 - \nabla_x\lambda_3, v \right\rangle_{\Omega} + \\ &\quad - \frac{1}{Re}\left\langle \lambda_2, \frac{\partial v}{\partial \vec{n}} \right\rangle_{\partial\Omega} + \left\langle \frac{1}{Re}\frac{\partial \lambda_2}{\partial \vec{n}} + \lambda_3\,\vec{n} + (u\cdot\vec{n})\lambda_2, v \right\rangle_{\partial\Omega} + \left\langle \lambda_5, v \right\rangle_{\Gamma_w} = 0. \end{aligned} \tag{B.4}$$

Where $\vec{n}$ is the vector normal to the boundary at $x \in \partial\Omega$.

From the identities above it follows that, in order to make $\left\langle \frac{\partial L}{\partial T_e}, w \right\rangle_{\Omega\times[0,T]}$, $\left\langle \frac{\partial L}{\partial u}, v \right\rangle_{\Omega}$, and $\left\langle \frac{\partial L}{\partial p}, q \right\rangle_{\Omega}$ all equal to 0 for any set of functions (w, v, q), a sufficient condition for the dual variables $\lambda_{1,2,3,6}$ is to satisfy the differential equations (4.4) to (4.7) and their boundary conditions.

B.2 Derivation of Fréchet derivatives

As explained in Section 4.2.1, if we take variations $(\delta\pi_0, \delta\theta)$ of our optimization variables, they will induce variations $\delta\alpha$, $\delta\kappa$, δT_e, δu, and δp. Then, from equations (2.2), (2.4),

and (2.5), it follows that the variations satisfy the following differential equations:

$$\frac{\partial \delta T_e}{\partial t} - \nabla_x \cdot (\delta\kappa \, \nabla_x T_e) - \nabla_x \cdot (\kappa \, \nabla_x \delta T_e) + \delta u \cdot \nabla_x T_e + u \cdot \nabla_x \delta T_e = 0, \tag{B.5}$$

$$\delta\alpha \, u + \alpha \, \delta u - \frac{1}{Re} \, \Delta_x \delta u + \delta u \cdot \nabla_x u + u \cdot \nabla_x \delta u + \nabla \delta p = 0, \tag{B.6}$$

$$\nabla_x \cdot \delta p = 0, \tag{B.7}$$

with the following boundary and initial conditions: $\delta T_e(x,t) = 0$ for each $x \in \partial\Omega$ and $t \in [0,T]$, $\delta T_e(x,0) = \delta\pi_0(x)$ for each $x \in \Omega$, and $\delta u(x) = 0$ for each $x \in \Gamma_w$.

Now, using equations (4.2), (B.5), (B.6) and (B.7) and their boundary and initial conditions, we get

$$\begin{aligned}
&J(\theta + \delta\theta, \pi_0 + \delta\pi_0) - J(\theta, \pi_0) = \left\langle \frac{\partial J}{\partial T_e}, \delta T_e \right\rangle_{\Omega\times[0,T]} + \left\langle \frac{\partial J}{\partial T_e}, \delta\pi_0 \right\rangle_{\Omega} + \\
&+ \left\langle \lambda_1, \frac{\partial \delta T_e}{\partial t} - \nabla_x \cdot (\delta\kappa \, \nabla_x T_e) - \nabla_x \cdot (\kappa \, \nabla_x \delta T_e) + \delta u \cdot \nabla_x T_e + u \cdot \nabla_x \delta T_e \right\rangle_{\Omega\times[0,T]} + \\
&+ \left\langle \lambda_2, \delta\alpha \, u + \alpha \, \delta u - \frac{1}{Re} \Delta_x \delta u + \delta u \cdot \nabla_x u + u \cdot \nabla_x \delta u + \nabla_x \delta p \right\rangle_{\Omega} + \left\langle \lambda_3, \nabla_x \cdot \delta u \right\rangle_{\Omega} + \\
&+ \left\langle \lambda_4, \delta T_e \right\rangle_{\partial\Omega\times[0,T]} + \left\langle \lambda_5, \delta u \right\rangle_{\Gamma_w} + \left\langle \lambda_6, \delta Te(\cdot, 0) - \delta\pi_0 \right\rangle_{\Omega}.
\end{aligned} \tag{B.8}$$

Where $\{\lambda_i\}_{i=1}^{6}$ are the adjoint variables defined in Section 4.2.1. Then, applying integration by parts and Green's formula to equation (B.8), and after canceling terms using the identities in equations (4.4) to (4.7), we can get

$$\begin{aligned}
&J(\theta + \delta\theta, \pi_0 + \delta\pi_0) - J(\theta, \pi_0) = \left\langle \nabla_{\pi_0} J - \lambda_6, \delta\pi_0 \right\rangle_{\Omega} + \\
&+ \left\langle \nabla_x \lambda_1 \cdot \nabla_x T_e, \delta\kappa \right\rangle_{\Omega\times[0,T]} + \left\langle \lambda_2 \cdot u, \delta\alpha \right\rangle_{\Omega}.
\end{aligned} \tag{B.9}$$

Which are equivalent to the directional derivatives in equations (4.8) and (4.9), as desired.

Appendix C

Proofs in Chapter 5

In this appendix, we show the proofs to the theorems in chapter C.

C.1 Existence of Lagrange Multipliers

In this section, we are going to show the existence of Lagrange multipliers to our optimization problems in equations (5.6) and (5.7).

First, we focus on the estimation problem in equation (5.6). Define the space for π_0, κ, α and θ as $C_e = \{(\pi_0, \theta) \in H^1(\Omega) \times [0,1]^{n_d}\}$. Define the space for weak solutions to the PDE equations (2.2) to (2.6) as $X = L^2([t_0, t_0']; H^1(\Omega)) \times \big(H^1\big(\Omega\big) \times H^1\big(\Omega\big)\big) \times L^2\big(\Omega\big)$ and the space $Z = \{L^2([t_0, t_0']; H^1(\Omega)) \times \Big(H^{-1}\big(\Omega\big) \times H^{-1}\big(\Omega\big)\Big) \times L^2\big(\Omega\big) \times H^1\big(\Omega\big) \times L^2\big(\partial\Omega\big) \times L^2\big(\partial\Gamma_w\big)\}$. Define the mapping $\mathcal{S}_e : X \times C_e \to Z$, such that for the tuple $\big(T_e, u, p, \pi_0, \theta\big) \in X \times C_e$ and

$\mathcal{S}_e\big(T_e, u, p, \pi_0, \theta\big) = \big(v_1, v_2, v_3, v_4, v_5, v_6\big) \in Z$, we have the formulas,

$$\begin{aligned}
&\langle \frac{\partial T_e(x,t)}{\partial t}, \xi(x)\rangle_\Omega - \langle \nabla_x \cdot \Big(\kappa(x,\theta)\nabla T_e(x,t)\Big), \xi(x)\rangle_\Omega + \\
&+ \langle u(x)\cdot\nabla_x T_e(x,t), \xi(x)\rangle_\Omega - \langle g_{T_e}(x,t), \xi(x)\rangle_\Omega = \\
&= \langle v_1(x,t), \xi(x)\rangle_\Omega, \quad \forall \xi(x) \in H_0^1(\Omega),
\end{aligned} \tag{C.1}$$

$$\begin{aligned}
&\langle \alpha(x,\theta)u(x), \varphi(x)\rangle_\Omega + \frac{1}{Re}\langle \nabla_x u(x), \nabla_x \varphi(x)\rangle_\Omega + \\
&+ \langle u(x)\cdot\nabla_x u(x), \varphi(x)\rangle_\Omega - \langle p(x), \nabla_x \cdot \varphi(x)\rangle_\Omega + \\
&- \langle g_u(x), \varphi(x)\rangle_\Omega = \langle v_2(x), \varphi(x)\rangle_\Omega, \\
&\forall \varphi(x) \in H_0^1(\Omega) \times H_0^1(\Omega),
\end{aligned} \tag{C.2}$$

$$\langle \nabla_x \cdot u(x), \psi(x)\rangle_\Omega = \langle v_3(x), \psi(x)\rangle_\Omega, \; \forall \psi(x) \in L^2(\Omega) \tag{C.3}$$

$$T_e(x, t_0) - \pi_0(x) = v_4(x), \quad \text{for } x \in \Omega. \tag{C.4}$$

$$T_e(x) - T_A = v_5(x), \quad \text{for } x \in \partial\Omega, \text{ and} \tag{C.5}$$

$$u(x) = v_6(x), \quad \text{for } x \in \Gamma_w. \tag{C.6}$$

Then the weak solutions to PDE equations (2.2) to (2.6) satisfy the equality, $\mathcal{S}_e\big(T_e, u, p, \pi_0, \theta\big) = 0 \in Z$.

Suppose $(T_e^\star, u^\star, p^\star, \pi_0^\star, \theta^\star)$ is the optimal point to the problem (5.6), define the first derivative of S_e w.r.t. X at the optimal point as $\mathcal{S}'_{e,x^\star} : X \to Z$. For the point $(w_t, w_u, w_p) \in X$,

$\mathcal{S}'_{e,x^\star}(w_t, w_u, w_p) = (v_1, v_2, v_3, v_4, v_5, v_6)$ has the formula,

$$\begin{aligned}
&\langle \frac{\partial w_t(x,t)}{\partial t}, \xi(x)\rangle_\Omega - \langle \nabla_x \cdot \Big(\kappa^\star(x,\theta)\nabla w_t(x,t)\Big), \xi(x)\rangle_\Omega + \\
&+ \langle u^\star(x)\cdot\nabla_x w_t(x,t), \xi(x)\rangle_\Omega + \\
&+ \langle w_u(x)\cdot\nabla_x T_e^\star(x,t), \xi(x)\rangle_\Omega = \langle v_1(x), \xi(x)\rangle_\Omega, \\
&\forall \xi(x) \in H_0^1(\Omega),
\end{aligned} \tag{C.7}$$

$$\begin{aligned}
&\langle \alpha(x,\theta) w_u(x), \varphi(x)\rangle_\Omega + \\
&+ \frac{1}{Re}\langle \nabla_x w_u(x), \nabla_x \varphi(x)\rangle_\Omega + \\
&+ \langle w_u(x)\cdot\nabla_x u^\star(x), \varphi(x)\rangle_\Omega + \\
&+ \langle u^\star(x)\cdot\nabla_x w_u(x), \varphi(x)\rangle_\Omega - \langle w_p(x), \nabla_x\cdot\varphi(x)\rangle_\Omega + \\
&= \langle v_2(x), \varphi(x)\rangle_\Omega, \ \forall \varphi(x) \in H_0^1(\Omega)\times H_0^1(\Omega),
\end{aligned} \tag{C.8}$$

$$\langle \nabla_x \cdot w_u(x), \psi(x)\rangle_\Omega = \langle v_3(x), \psi(x)\rangle_\Omega, \ \forall \psi(x) \in L^2(\Omega) \tag{C.9}$$

$$w_t(x, t_0) = v_4(x), \quad \text{for } x \in \Omega. \tag{C.10}$$

$$w_t(x) = v_5(x), \quad \text{for } x \in \partial\Omega, \text{ and} \tag{C.11}$$

$$w_u(x) = v_6(x), \quad \text{for } x \in \Gamma_w. \tag{C.12}$$

Lemma C.1. *$\mathcal{S}'_{e,x^\star} : X \to Z$ is a closed operator.*

Proof to lemma C.1. Since $\mathcal{S}'_{e,x^\star}$ is a linear operator w.r.t. (w_t, w_u, w_p), it is sufficient to show that, for arbitrary sequence in X, $\{(w_{t,i}, w_{u,i}, w_{p,i})\}_{i=1}^\infty \to 0 \in X$, $\mathcal{S}'_{e,x^\star}(w_{t,i}, w_{u,i}, w_{p,i}) \to 0 \in Z$. According to appendix A and Lax-Milgram theorem [67, Chapter 1.2], the only solution to $\mathcal{S}'_{e,x^\star} = 0$ is $(w_t, w_u, w_p) = 0$, thus operator $\mathcal{S}'_{e,x^\star}$ is closed. □

Lemma C.2. *Define the adjoint operator for* $\mathcal{S}'_{e,x^\star}$ *as* $\mathcal{S}'^{,\star}_{e,x^\star} : Z^\star \to X^\star$. $\mathcal{S}'^{,\star}_{e,x^\star}$ *is surjective.*

Proof to lemma C.2. Since $\mathcal{S}'_{e,x^\star}$ is closed and its domain is the whole X, it is sufficient to show the kernel of $\mathcal{S}'_{e,x^\star}$ is $\{0\}$. According to the proof of Lemma C.1, the only solution to $\mathcal{S}'_{e,x^\star} = 0$ is $(w_t, w_u, w_p) = 0$. □

Theorem C.1. *If* $(T_e^\star, u^\star, p^\star, \pi_0^\star, \theta^\star)$ *is the optimal point to the problem* (5.6)*, then there exist Lagrange multipliers,* $\{\lambda_i\}_{i=1}^6$*, which are corresponding to PDE-constraints, such that* $\forall (w, v, q) \in L^2\big([t_0, t_0']; H^1(\Omega)\big) \times \big(H^1(\Omega) \times H^1(\Omega)\big) \times L^2(\Omega)$*, the Lagrange function's variation w.r.t.* (w, v, q) *is zero, and* $\lambda_{1,2,3,6}$ *satisfy,*

$$\begin{aligned} &-\frac{\partial J}{\partial T_e} + \frac{\partial \lambda_1}{\partial t}(x,t) + \nabla_x \cdot (\kappa(x)\, \nabla_x \lambda_1(x,t)) + \\ &+ u(x) \cdot \nabla_x \lambda_1(x,t) = 0, \end{aligned} \tag{C.13}$$

$$\lambda_6(x) = \lambda_1(x, 0), \tag{C.14}$$

$$\begin{aligned} &\int_{t_0}^{t_0'} \lambda_1(x,t)\, \nabla_x T_e(x,t)\, \mathrm{d}t + \alpha(x)\, \lambda_2(x) - \frac{1}{Re} \Delta_x \lambda_2(x) + \\ &- u(x) \cdot \nabla_x \lambda_2(x) + \lambda_2(x) \cdot \nabla_x u(x) - \nabla_x \lambda_3(x) = 0, \quad \textit{and,} \end{aligned} \tag{C.15}$$

$$\nabla_x \cdot \lambda_2(x) = 0, \tag{C.16}$$

with boundary conditions $\lambda_1(x,t) = 0$ *and* $\lambda_2(x) = 0$ *for each* $x \in \partial\Omega$ *and* $t \in [t_0, t_0']$*, together with final condition* $\lambda_1(x, T) = 0$ *for each* $x \in \Omega$*. The adjoint functions* λ_4 *and* λ_5 *are irrelevant to our Fréchet derivative calculation, therefore we omit them from this presentation.*

If $\big(T_e^\star, u^\star, p^\star, g_{T_e}^\star, g_u^\star\big)$ *is the optimal point to the problem* (5.7)*, its Lagrange multipliers,* $\lambda_{1,2,3,6}$*, also satisfy the above ajoint PDE system.*

Proof to theorem C.1. According to subsection C.2 below, (T_e, u, p) are Gateaux differentiable w.r.t. $(\theta, \alpha, \kappa, \pi_0)$. Furthermore, according to Lemma C.1 and C.2, $\mathcal{S}'_{e,x^\star}$ is continuous and $\mathcal{S}'^{,\star}_{e,x^\star}$ is surjective, then the Lagrange multipliers exist. According to [76], the Lagrange multipliers, $\{\lambda_i\}_{i=1,2,3,6}$ satisfy equations (4.4), (4.5) and (4.7) hold [86, Theorem 1.17].

Similarly, we can prove the existence of Lagrange multipliers to the problem 5.7. □

C.2 Proof of Fréchet Derivatives

In this section, we prove the directional derivatives in equations (5.17) (5.18) and (5.19) are Fréchet derivatives. We are going to show these derivatives are Gateaux derivatives and then extend to show they are Fréchet derivatives.

Theorem C.2. *Given variables $\pi_0 \in H^1(\Omega)$, $\theta \in \mathbb{R}^{n_d}$ and $\alpha, \kappa \in L^2(\Omega) \cap L^\infty(\Omega)$. The directional derivatives in equations* (4.8) *and* (4.9) *are Fréchet derivatives of cost function J_e to corresponding variables.*

Lemma C.3. *The solution to the CFD model in equations* (2.2) *to* (2.6)*, (T_e, u, p), has a Gateaux derivative $\big(w_t[\delta\kappa], w_u[\delta\kappa], w_p[\delta\kappa]\big)$ in every direction $\delta\kappa \in L^\infty(\Omega) \cap L^2(\Omega)$ w.r.t. $\kappa \in L^\infty(\Omega) \cap L^2(\Omega)$. Furthermore, the Gateaux Derivatives, $w_u[\delta\kappa] = 0$, $w_p[\delta\kappa] = 0$ and $w_t[\delta\kappa]$ is the solution to the PDE:*

$$\begin{aligned} &\frac{\partial w_t[\delta\kappa]}{\partial t}(x,t) - \nabla_x\cdot\big(\delta\kappa\,\nabla_x T_e(x,t;\kappa)\big) + \\ &-\nabla_x\cdot\big(\kappa\,\nabla_x w_t[\delta\kappa](x,t)\big) + u(x)\cdot\nabla_x w_t[\kappa](x,t) = 0, \end{aligned} \tag{C.17}$$

With initial condition,

$$w_t[\delta\kappa](x,t_0) = 0, \quad \text{for } x \in \Omega. \tag{C.18}$$

and boundary condition,

$$w_t[\delta\kappa](x) \equiv 0, \quad \textit{for } x \in \partial\Omega. \tag{C.19}$$

Proof to lemma C.3. Since κ does not relate to Navier-Stokes equations (2.4), (2.5) and (2.8), $w_u[\delta\kappa] = 0$ and $w_p[\delta\kappa] = 0$.

Define the weak solution to temperature with given κ as $T_e(x,t;\kappa)$. Define $\tilde{T}_e(x,t) = T_e(x,t;\kappa+s\delta\kappa) - T_e(x,t;\kappa) - sw_t[t_0,t_0']$, then for $w_t[\delta\kappa]$, it is sufficient to show for $w_t[\delta\kappa]$ satisfying the following,

$$\lim_{s\to 0}\Big(\frac{\|\tilde{T}_e\|_{\Omega\times[t_0,t_0']}}{|s|}\Big) = 0 \tag{C.20}$$

Define $\hat{T}_e = T_e(\kappa+s\delta\kappa) - T_e(\kappa)$, then $\tilde{T}_e$ satisfies the following PDE

$$\begin{aligned}&\frac{\partial\tilde{T}_e}{\partial t}(x,t) + u(x)\cdot\nabla_x\tilde{T}_e(x,t) - \nabla_x\cdot\big(\kappa\,\nabla_x\tilde{T}_e(x,t)\big)\\ &= s\nabla_x\cdot(\delta\kappa\,\nabla_x(\hat{T}_e(x,t))),\end{aligned} \tag{C.21}$$

with homogeneous zero initial and boundary conditions. $\hat{T}_e$ satisfies the following PDE

$$\begin{aligned}&\frac{\partial\hat{T}_e}{\partial t}(x,t) + u(x)\cdot\nabla_x\hat{T}_e(x,t) - \nabla_x\cdot\big(\kappa\,\nabla_x\hat{T}_e(x,t)\big) =\\ &= s\nabla_x\cdot\Big(\delta\kappa\,\nabla_x T_e(x,t;\kappa+s\delta\kappa)\Big),\end{aligned} \tag{C.22}$$

also with homogeneous zero initial and boundary conditions. According to the energy estimation inequality [107, Chapter 11.1], we can bound $\hat{T}_e$ and $\tilde{T}_e$,

$$\Big\|\hat{T}_e\Big\|_{\Omega\times[t_0,t_0']} \le sC_1\|T_e(x,t;\kappa+s\delta\kappa)\|_{\Omega\times[t_0,t_0']}, \tag{C.23}$$

$$\begin{aligned}\left\|\tilde{T}_e\right\|_{\Omega\times[t_0,t_0']} \leq sC_2\left\|\hat{T}_e\right\|_{\Omega\times[t_0,t_0']} \leq \\ \leq s^2C_1C_2\|T_e(x,t;\kappa+s\delta\kappa)\|_{\Omega\times[t_0,t_0']},\end{aligned} \tag{C.24}$$

where $C_{1,2} > 0$ are two independent parameters. Thus equation (C.20) holds and $w_t[\delta\kappa]$ is T_e Gateaux derivative w.r.t. $\delta\kappa$. □

Lemma C.4. *The solution to the CFD model in equations* (2.2) *to* (2.6)*,* (T_e, u, p) *has a Gateaux derivative in every direction* $\delta\alpha \in L^\infty(\Omega)\cap L^2(\Omega)$ *w.r.t.* $\alpha \in L^\infty(\Omega)\cap L^2(\Omega)$*. Furthermore, the Gateaux Derivatives of* T_e *and* u*,* $w_t[\delta\alpha]$ *and* $w_u[\delta\alpha]$ *are the solution to the PDE:*

$$\begin{aligned}&\frac{\partial w_t[\delta\alpha](x)}{\partial t} - \nabla_x\cdot(\kappa\,\nabla_x w_t[\delta\alpha](x))+ \\ &+ u(x;\alpha)\cdot\nabla_x w_t[\delta\alpha](x)+ \\ &+ w_u[\delta\alpha](x)\cdot\nabla_x T_e(x;\alpha) = 0,\end{aligned} \tag{C.25}$$

$$\begin{aligned}&\alpha w_u[\delta\alpha](x) + \delta\alpha u(x;\alpha)+ \\ &- \frac{1}{Re}\Delta_x w_u[\delta\alpha] + u(x;\alpha)\cdot\nabla_x w_u[\delta\alpha](x)+ \\ &+ w_u[\delta\alpha]\cdot\nabla_x u(x;\alpha) + \nabla_x w_p(x) = 0, \quad \textit{and,}\end{aligned} \tag{C.26}$$

$$\nabla_x\cdot w_u[\delta\alpha](x) = 0, \tag{C.27}$$

with homogeneous zero initial and boundary conditions.

Proof to lemma C.4. First, We prove $w_u[\delta\alpha]$ above is the Gateaux derivative. Define $\tilde{u}(x) = u(x;\alpha+s\delta\alpha) - u(x;\alpha) - sw_u[\delta\alpha](x)$, then it is sufficient to show that,

$$\lim_{s\to 0}\Big(\frac{\|\tilde{u}(x)\|_1}{|s|}\Big) = 0 \tag{C.28}$$

According to [71], $\tilde{u}$ satisfies the PDE

$$\begin{aligned}&\alpha\tilde{u}(x) - \frac{1}{Re}\Delta\tilde{u}(x) + u(x;\alpha)\cdot\nabla\tilde{u}(x) + \tilde{u}(x)\cdot\nabla u(x;\alpha) = \\ &= -s\delta\alpha\big(u(x;\alpha+s\delta\alpha) - u(x;\alpha)\big) + k_u,\end{aligned} \tag{C.29}$$

with zero homogeneous boundary condition, and k_u is defined as

$$\begin{aligned}k_u &= -u(x;\alpha+s\delta\alpha)\cdot\nabla_x u(x;\alpha+s\delta\alpha) + \\ &+ u(x;\alpha)\cdot\nabla_x u(x;\alpha+s\delta\alpha) + \\ &+ u(x;\alpha+s\delta\alpha)\cdot\nabla_x u(x;\alpha) - u(x;\alpha)\cdot\nabla_x u(x;\alpha).\end{aligned} \tag{C.30}$$

Multiply both sides of (C.29) with $\tilde{u}$ and integrate in Ω, by the notations and calculations from appendix A, we get

$$\begin{aligned}&\langle\alpha\tilde{u},\tilde{u}\rangle_\Omega - \left\langle\frac{1}{Re}\Delta_x\tilde{u},\tilde{u}\right\rangle_\Omega + \langle u(x;\alpha)\cdot\nabla_x\tilde{u},\tilde{u}\rangle_\Omega + \\ &+ \langle\tilde{u}\cdot\nabla_x u(x,\alpha),\tilde{u}\rangle_\Omega = \sigma_0(\tilde{u},\tilde{u}) = \\ &= \big\langle -s\delta\alpha\big(u(\alpha+s\delta\alpha) - u(\alpha)\big) + k_u,\tilde{u}\big\rangle_\Omega\end{aligned} \tag{C.31}$$

According to appendix A, σ_0 is a coercive bilinear operator, thus there exists a positive real number C_1 s.t

$$\begin{aligned}&0 \le \|\tilde{u}\|_1^2 \le C_1\sigma_0(\tilde{u},\tilde{u}) = \\ &= C_1\big\langle -s\delta\alpha\big(u(x;\alpha+s\delta\alpha) - u(x;\alpha)\big) + k_u,\tilde{u}\big\rangle_\Omega \le \\ &\le C_1\big|\big\langle -s\delta\alpha\big(u(x;\alpha+s\delta\alpha) - u(x;\alpha)\big),\tilde{u}\big\rangle_\Omega\big| + \\ &+ C_1|\langle k_u,\tilde{u}\rangle_\Omega|.\end{aligned} \tag{C.32}$$

In order to prove the equation (C.28), it is sufficient to prove that the two terms,

$$|\big\langle -s\delta\alpha\big(u(x;\alpha+s\delta\alpha)-u(x;\alpha)\big),\tilde{u}\big\rangle_{\Omega}|$$

and $|\langle k_u,\tilde{u}\rangle_{\Omega}|$ are bounded by higher order of s. Define $\hat{u}=u(x;\alpha+\delta\alpha)-u(x;\alpha)$, then $|\langle k_u,\tilde{u}\rangle_{\Omega}|$ can be bounded as,

$$\begin{aligned}
&\langle k_u,\tilde{u}\rangle_{\Omega}=|-\langle u(x;\alpha+s\delta\alpha)\cdot\nabla_x u(x;\alpha+s\delta\alpha),\tilde{u}\rangle_{\Omega}+\\
&+\langle u(x;\alpha)\cdot\nabla_x u(x;\alpha+s\delta\alpha),\tilde{u}\rangle+\\
&+\langle u(x;\alpha+s\delta\alpha)\cdot\nabla_x u(x;\alpha),\tilde{u}\rangle_{\Omega}+\\
&-\langle u(x;\alpha)\cdot\nabla_x u(x;\alpha),\tilde{u}\rangle_{\Omega}|=\\
&=|-\langle\hat{u}\cdot\nabla_x u(x;\alpha+s\delta\alpha),\tilde{u}\rangle_{\Omega}+\langle\hat{u}\cdot\nabla_x u(x;\alpha),\tilde{u}\rangle_{\Omega}|=\\
&=|\langle\hat{u}\cdot\nabla_x\hat{u},\tilde{u}\rangle_{\Omega}|\leq\\
&\leq C_2|\hat{u}|_1\|\hat{u}\|_1\|\tilde{u}\|_1\leq C_3\|\hat{u}\|_1^2\|\tilde{u}\|_1,
\end{aligned}\tag{C.33}$$

where $C_{2,3}>0$ and independent of s. $\hat{u}$ is the solution to the PDE

$$\begin{aligned}
&\alpha\hat{u}(x)+s\delta\alpha u(x;\alpha+s\delta\alpha)-\frac{1}{Re}\Delta_x\hat{u}(x)+\\
&+u(x;\alpha)\cdot\nabla_x\hat{u}(x)+\hat{u}(x)\cdot\nabla_x u(x;\alpha)+\\
&+\hat{u}(x)\cdot\nabla_x\hat{u}(x)+\nabla_x\hat{p}(x)=0,\quad\text{and,}
\end{aligned}\tag{C.34}$$

$$\nabla_x\cdot\hat{u}=0.\tag{C.35}$$

with zero homogeneous boundary condition.

In order to bound $\hat{u}$, we separate it into two values, $\hat{u} = \hat{u}_1 + \hat{u}_2$, s.t.,

$$\alpha\hat{u}_1(x) - \frac{1}{Re}\Delta_x\hat{u}_1(x) + \nabla_x\hat{p}(x) = -s\delta\alpha u(x;\alpha+\delta\alpha), \tag{C.36}$$

$$\nabla_x \cdot \hat{u}_1(x) = 0, \tag{C.37}$$

$$\begin{aligned}
&\alpha\hat{u}_2(x) - \frac{1}{Re}\Delta_x\hat{u}_2(x) + (u(x;\alpha) + \hat{u}_1(x)) \cdot \nabla_x\hat{u}_2(x) + \\
&+ \hat{u}_2(x) \cdot \nabla_x(u(x;\alpha) + \hat{u}_1(x)) + \hat{u}_2(x) \cdot \nabla_x\hat{u}_2(x) = \\
&= -\hat{u}_1(x) \cdot \nabla_x u(x;\alpha) - u(x;\alpha) \cdot \nabla_x\hat{u}_1(x) + \\
&- \hat{u}_1(x) \cdot \nabla_x\hat{u}_1(x), \quad \text{and}
\end{aligned} \tag{C.38}$$

$$\nabla \cdot \hat{u}_2 = 0. \tag{C.39}$$

Both $\hat{u}_1$ and $\hat{u}_2$ are with zero homogeneous boundary conditions.

Similar to the strategy to bound $\tilde{u}$ in equation (C.32), we can bound $\hat{u}_1$ by s and $\|u(x;\alpha+s\delta\alpha)\|$ as $\|\tilde{u}_1\|_1 \leq C_4|s\delta\alpha|\|u(x;\alpha+s\delta\alpha)\|_1$, where $C_4 > 0$ is independent of s. Then for $\hat{u}_2$, we can bound it by s as well, $\|\tilde{u}_2\|_1 \leq C_5\|-\tilde{u}_1 \cdot \nabla u(x;\alpha) - u(x;\alpha) \cdot \nabla_x\tilde{u}_1 - \tilde{u}_1 \cdot \nabla_x\tilde{u}_1\|_1 \leq C_6|s|\|u(x;\alpha)\|_1$, where $C_{5,6} > 0$ are independent to s.

Thus the limitation in equation (C.28) holds. Then we are going to talk about $w_t[\delta\alpha]$, define $\tilde{T}_e = T_e(x,t;\alpha+s\delta\alpha) - Te(x,t;\alpha) - sw_t$, it is sufficient to show that

$$\lim_{s\to 0}\Big(\frac{\left\|\tilde{T}_e\right\|_{L^2(0,T;H^1(\Omega))}}{|s|}\Big) = 0 \tag{C.40}$$

$\tilde{T}_e$ follows

$$\begin{aligned}&\frac{\partial \tilde{T}_e}{\partial t}(x,t) - \nabla_x \cdot \Big(\kappa \nabla_x \tilde{T}_e(x,t)\Big) + \\ &- u(x;\alpha) \cdot \nabla_x (\tilde{T}_e(x,t)) = k_t,\end{aligned} \tag{C.41}$$

with zero boundary and initial conditions, where $k_t = -\tilde{u} \cdot \nabla_x T_e(x,t;\alpha + s\delta\alpha) - s w_u[\delta\alpha] \cdot \big(\nabla_x T_e(x,t;\alpha + s\delta\alpha) - T_e(x,t;\alpha)\big)$. Then according to [107, Theorem 11.1.1], we can bound $\left\|\tilde{T}_e\right\|_{\Omega \times [t_0, t_0']}$ by $\|k_t\|_\Omega$, it is sufficient to show that $\|k_t\|_\Omega$ can be bounded by higher order of $|s|$.

Define $\hat{T}_e = T_e(x,t;\alpha + s\delta\alpha) - T_e(x,t;\alpha)$, it follows the PDE

$$\begin{aligned}&\frac{\partial \hat{T}_e}{\partial t}(x,t) - \nabla_x \Big(\kappa \nabla_x \hat{T}_e(x,t)\Big) + \\ &+ u(x;\alpha + s w_u) \cdot \nabla_x \hat{T}_e(x,t) = -\hat{u} \cdot \nabla T_e(\alpha)\end{aligned} \tag{C.42}$$

with zero homogeneous boundary and initial conditions. Since $\|\hat{u}\|_1$ is bounded by $|s|$, so does $\left\|\hat{T}_e\right\|_{\Omega \times \left[t_0, t_0'\right]}$. Thus the limitation in equation (C.40) holds as well. □

Lemma C.5. *The solution to the CFD model in equations* (2.2) *to* (2.6)*, (T_e, u, p) has a Gateaux derivative in every direction $\delta\pi_0 \in H^1(\Omega)$ w.r.t. $\pi_0 \in H^1(\Omega)$. Furthermore, the Gateaux Derivatives of T_e, $w_t[\delta\pi_0]$ is the solution to the PDE:*

$$\begin{aligned}&\frac{\partial w_t[\delta\pi_0]}{\partial t}(x,t) - \nabla_x \cdot (\kappa\, \nabla_x w_t[\delta\pi_0])(x,t) + \\ &+ u(x;\pi_0) \cdot \nabla_x w_t[\delta\pi_0](x,t) = 0\end{aligned} \tag{C.43}$$

with homogeneous zero boundary conditions and initial condition,

$$w_t[\delta\pi_0](x,t_0) = \delta\pi_0, \ \textit{for } x \in \Omega. \tag{C.44}$$

The Gateaux Derivatives of u and p are zero.

Proof to lemma C.5. Since the equation (2.2) is weakly coupled with the fluid's flow equations (2.4) and (2.5). The variation of initiation condition, π_0, does not influence u and p. Thus their related derivatives are zeros.

Then we study $w_t[\delta\alpha]$, Define $\tilde{T}_e(x,t) = T_e(x,t;\pi_0 + s\delta\pi_0) - T_e(x,t;\pi_0) - sw_t(x,t)$, it is sufficient to show that

$$\lim_{s\to 0}\Big(\frac{\left\|\tilde{T}_e\right\|_{L^2(0,T;H^1(\Omega))}}{|s|}\Big) = 0 \tag{C.45}$$

$\tilde{T}_e$ satisfies

$$\begin{aligned}&\frac{\partial \tilde{T}_e}{\partial t}(x,t) - \nabla_x\cdot(\kappa\nabla_x\tilde{T}_e)(x,t) + \\ &- u(x;\alpha)\cdot\nabla_x(\tilde{T}_e(x,t)) = 0\end{aligned} \tag{C.46}$$

with zero boundary and initial conditions.

Since $\tilde{T}_e$ is the solution to the parabolic PDE equation (C.46) with zero boundary and initial conditions, then according to Lemma A.7 and A.8 and Theorem 11.1.1 in [107], the only solution, $\tilde{T}_e$, is zero. Thus the limitation in equation (C.46) holds, and $w_t[\delta\pi_0]$ is the target Gateaux Derivative. □

Proof of theorem C.2. As a result of lemma C.3, according to the chain rule we have the Gateaux derivative of cost function, J_e, w.r.t. κ in direction $\delta\kappa$ as,

$$\begin{aligned}
&\left\langle \mathcal{D}_\kappa J_e, \delta\kappa \right\rangle_\Omega = \left\langle \frac{\partial J_e}{\partial T_e}, w_t[\delta\kappa] \right\rangle_{\Omega\times\left[t_0,t_0'\right]} + \\
&+ \left\langle \frac{\partial J_e}{\partial u}, w_u[\delta\kappa] \right\rangle_\Omega + \\
&+ \left\langle \frac{\partial J_e}{\partial p}, w_p[\delta\kappa] \right\rangle_\Omega = \left\langle \frac{\partial J_e}{\partial T_e}, w_t[\delta\kappa] \right\rangle_{\Omega\times\left[t_0,t_0'\right]} + \\
&+ \langle \lambda_1, \frac{\partial w_t[\delta\kappa]}{\partial t} - \nabla_x\cdot\big(\delta\kappa\,\nabla_x T_e\big) + \\
&- \nabla_x\cdot\big(\kappa\,\nabla_x w_t[\delta\kappa]\big) + u(x)\cdot\nabla_x w_t[\kappa]\rangle_{\Omega\times\left[t_0,t_0'\right]} + \\
&+ \langle \lambda_4, w_t[\kappa]\rangle_{\partial\Omega\times\left[t_0,t_0'\right]} + \langle \lambda_6, w_t[\kappa](x,0)\rangle_\Omega = \\
&= \int_{t_0}^{t_0'} \left\langle \nabla_x\lambda_1\cdot\nabla_x T_e, \delta\kappa \right\rangle_\Omega \mathrm{d}t,
\end{aligned} \tag{C.47}$$

where $\lambda_{1,4,6}$ are adjoint variables with equations (4.4) to (4.7).

Then similar to the equation (C.47), based on lemmas C.4 and C.5, with the help with adjoint variables, the Gateaux derivative of cost function, J_e, w.r.t. α in direction $\delta\alpha$ can be derived as shown in equation (4.8), also the Gateaux derivative of cost function, J_e, w.r.t. π_0 in direction $\delta\pi_0$ can be derived as shown in equation (4.9). Then by the chain rule, the Gateaux derivatives of J_e w.r.t. θ in direction $\delta\theta$ is as shown in equation (4.9).

Then we extend the derivatives above to Fréchet derivatives. It is sufficient to show they are linear and bounded.

Since ajoint variables are not related to variations, the derivatives in equation (4.8) and (4.9) are linear w.r.t. variations.

Then in order to show the derivatives are bounded, it is sufficient to show all the adjoint variables are bounded. Since the adjoint variables satisfies the linear PDE system of equations (4.4) to (4.7) and related boundary initial conditions in section 4.2.1, according to the energy study for linear PDEs on the Theory 7.4.1 [107], the adjoint variables are bounded.

Thus the derivatives in equation (4.8) and (4.9) are Fréchet derivatives. □

Theorem C.3. *Given variables,* $g_{T_e} \in L^2([t_0, t_0'] \times \Omega)$ *and* $g_u \in L^2(\Omega) \times L^2(\Omega)$*, the directional derivatives in equation* (5.19) *are Fréchet derivatives of cost function* J_c *to corresponding variables.*

The process to prove the theorem C.3 is similar to the proof of the theorem C.2, thus we skip it in this appendix.

C.3 Convergence of the Algorithm

In this section we are going to show the convergence of the algorithms 1 in section 5.2.3.

Theorem C.4. *Suppose the cost functions in problem* (5.6) *and* (5.7) *are bounded from below, and* $\beta_e, \beta_c \in (0, 1)$ *in algorithm 1 and 5.6 satisfy respectively, when* $V_e(\theta, \pi_0), V_c(g_{T_e}, g_u) < 0$*,* $a \in (0, 1)$

$$J_e(\theta + \beta_e \delta\theta, \pi_0 + \beta_e \delta\pi_0) - J_e(\theta, \pi_0) \leq a\, \beta_e V_e(\theta, \pi_0), \tag{C.48}$$

$$\begin{aligned} &J_c(g_{T_e} + \beta_c \delta g_{T_e}, g_u + \beta_c \delta g_u) - J_c(g_{T_e}, g_u) \leq \\ &\leq a\, \beta_c V_c(g_{T_e}, g_u). \end{aligned} \tag{C.49}$$

where $(\delta\theta, \delta\pi_0)$ *are derived from problem* (5.20)*,* $(\delta g_{T_e}, \delta g_u)$ *are derived from problem* (5.21)*. Then for arbitrary sequence generated by the algorithm 1 or 5.6, its accumulate point satisfies* $V_e(\pi_0, \theta) = 0$ *or* $V_c(g_{T_e}, g_u) = 0$*.*

Proof to theorem C.4. It is trivial to show that $V_e(\pi_0, \theta)$ and $V_c(g_{T_e}, g_u)$ are optimality functions. And under the assumption in equations (C.48) and (C.49), the updating step satisfies the uniform sufficient descent property. Thus using the same contradiction strategy in [125, Theorem 5.12], the accumulate point of every sequence generated by algorithm 1 and 5.6 satisfies $V_e(\pi_0, \theta) = 0$ and $V_c(g_{T_e}, g_u) = 0$ respectively. □

C.4 Finite Element Approximation

The finite element discretization of a partial derivative is defined as follows. Define a discritized and finite dimensional subspace for a space, $S(\Omega)$, as $S^h(\Omega)$. Define $L_0^2(\Omega) = \{q \in L^2(\Omega);\ \int_\Omega q = 0\}$. These subspaces are parameterized by a parameter, h, which represents the average size of all discritized elements. The subspaces usually can be chosen arbitrarily, while there are some standard discretization assumptions, especially for Navier-Stokes equations.

First, the discrete subspaces should satisfy the assumptions, there exist an integer k and a constant C, which are independent of each element in the space, such that, for integer $m \in [1, k]$,

$$\inf_{t^h \in H^{m+1,h}(\Omega)} \|t - t^h\|_1 \leq C h^m \|t\|_{m+1},\ \forall t \in H^{m+1}(\Omega), \tag{C.50}$$

$$\inf_{v^h \in H^{m+1,h}(\Omega)\times H^{m+1,h}(\Omega)} \|v - v^h\|_1 \leq Ch^m \|v\|_{m+1}, \quad \forall v \in H^{m+1}(\Omega) \times H^{m+1}(\Omega), \tag{C.51}$$

$$\inf_{q^h \in H^{m,h}(\Omega)\cap L_0^{2,h}(\Omega)} \|q - q^h\|_0 \leq Ch^m \|q\|_m, \quad \forall q \in H^m(\Omega) \cap L_0^2(\Omega), \tag{C.52}$$

Next, we assume the Ladyzhenskaya-Babuska-Brezzi (LBB) condition holds, such that there exists a constant C, independent of h, such that for non-zero $q^h \in H^{m,h}(\Omega) \cap L_0^{2,h}(\Omega)$, and non-zero $v^h \in H^{m+1,h}(\Omega) \times H^{m+1,h}(\Omega)$

$$\inf_{q^h} \sup_{v^h} \frac{b(v^h, q^h)}{\|v^h\|_1 \|q^h\|_0} \geq C \tag{C.53}$$

Once we have those assumptions, we can discretize the system. For the heat transfer equation, we discretize the temperature in space first, then it becomes a series of ODEs. Here we only estimate the finite element approximation error, and the time discretized error is not studied. The discritized system satisfies the discritized weak formulas,

$$\begin{aligned} &\langle \frac{\partial T_e^h(x,t)}{\partial t}, \xi^h(x)\rangle_\Omega - \langle \nabla_x \cdot \Big(\kappa \nabla T_e^h(x,t)\Big), \xi^h(x)\rangle_\Omega + \\ &+ \langle u^h(x) \cdot \nabla_x {T_e}^h(x,t), \xi^h(x)\rangle_\Omega - \langle g_{T_e}(x,t), \xi^h(x)\rangle_\Omega = \\ &= 0, \quad \forall \xi^h(x) \in H^{1,h}(\Omega), \end{aligned} \tag{C.54}$$

$$\begin{aligned} &\langle \alpha u^h(x), \varphi^h(x)\rangle_\Omega + \frac{1}{Re}\langle \nabla_x u^h(x), \nabla_x \varphi^h(x)\rangle_\Omega + \\ &+ \langle u^h(x) \cdot \nabla_x u^h(x), \varphi^h(x)\rangle_\Omega - \langle p^h(x), \nabla_x \cdot \varphi^h(x)\rangle_\Omega + \\ &- \langle g_u(x), \varphi^h(x)\rangle_\Omega = 0, \ \forall \varphi^h(x) \in H^{1,h}(\Omega) \times H^{1,h}(\Omega), \end{aligned} \tag{C.55}$$

$$\langle \nabla_x \cdot u^h(x), \psi^h(x) \rangle_\Omega = 0, \, \forall \psi^h(x) \in L^{2,h}(\Omega) \tag{C.56}$$

with boundary and initial conditions in equations (2.8), (2.6) and (2.3).

Theorem C.5. *Suppose* $(T_e(x,t), u(x), p(x))$ *is the solution to the weak form of CFD system with equations* (2.2) *to* (2.6) *in chapter 2, during the time period* $t \in [t_0, t_0']$. *Assume that the finite element spaces* $H^{1,h}(\Omega)$, $H^{1,h}(\Omega) \times H^{1,h}(\Omega)$ *and* $L^{2,h}(\Omega)$ *satisfy the conditions* (C.50) *to* (C.53). *Then, for* h *small enough, there exists a tuple* $\big(T_e^h(x,t), u^h(x), p^h(x)\big)$ *such that* $T_e^h(x,t) \in L^2\big([t_0, t_0'], H^{1,h}(\Omega)\big)$, $u^h(x) \in H^{1,h}(\Omega) \times H^{1,h}(\Omega)$, $p^h(x) \in L^{2,h}(\Omega)$ *and* $\big(T_e^h(x,t), u^h(x), p^h(x)\big)$ *are the solutions to the discrete system* (C.54) *to* (C.55) *with corresponding initial and boundary conditions.*

Moreover, as $h \to 0$,

$$\begin{aligned} &\int_{t_0}^{t_0'} \|T_e(\cdot,t) - T_e^h(\cdot,t)\|_1 dt \to 0, \\ &\|u(x) - u^h(x)\|_1 \to 0, \ \textit{and} \\ &\|p(x) - p^h(x)\|_0 \to 0. \end{aligned} \tag{C.57}$$

If, in addition, the solution tuple $(T_e(x,t), u(x), p(x))$ *satisfies,*

$$u(x) \in H^{m+1}(\Omega) \times H^{m+1}(\Omega)$$
$$p(x) \in L^2(\Omega) \cap H^m(\Omega)$$

then there exists constants $C_{1,2,3}$, which are independent of h, such that

$$\begin{aligned}
&\int_{t_0}^{t_0'} \|T_e(\cdot,t) - T_e^h(\cdot,t)\|_1 dt \leq C_1 \max\big(h^m, h^2\big), \\
&\|u(x) - u^h(x)\|_1 \leq C_2 h^m, \ \textit{and} \\
&\|p(x) - p^h(x)\|_0 \leq C_3 h^m.
\end{aligned} \tag{C.58}$$

Proof to theorem C.5. Since the temperature and Navier-stokes are weakly coupled, the discretization algorithm works as, first, we solved the approximated Navier-stokes equation, u^h and p^h. Then, substitute the u^h into heat transfer equation and get the discrete temperature, T_e^h. As the strategy above, we first estimate the discrete Navier-Stokes. The error estimation results can be derived directly from [72] and [31], concerning the approximation of a class of stationary nonlinear problems.

Then we are going to bound the approximation for T_e. Substitute u^h into the weak formula for equation (2.2), we get

$$\begin{aligned}
&\langle \frac{\partial T_e(x,t)}{\partial t}, \xi(x)\rangle_\Omega - \langle \nabla_x \cdot \Big(\kappa \nabla_x T_e(x,t)\Big), \xi(x)\rangle_\Omega + \\
&+ \langle u^h(x) \cdot \nabla_x T_e(x,t), \xi(x)\rangle_\Omega - \langle g_{T_e}(x,t), \xi(x)\rangle_\Omega = \\
&= 0, \quad \forall \xi \in H^1(\Omega).
\end{aligned} \tag{C.59}$$

with initial and boundary condition (2.3) and (2.8). According to theorem A.1, there exists a solution to the equation (C.59), define as $T_e^{\tilde{h}}$. Then $\forall t \in (0, T)$,

$$\begin{aligned}&\|T_e(\cdot,t) - T_e^h(\cdot,t)\|_1 \leq \\ &\|T_e(\cdot,t) - T_e^{\tilde{h}}(\cdot,t)\|_1 + \|T_e^{\tilde{h}}(\cdot,t) - T_e^h(\cdot,t)\|_1\end{aligned}$$

Define $e_{t,\tilde{h}}(x,t) = T_e(x,t) - T_e^{\tilde{h}}(x,t)$, Substract the weak formula to the equation (2.2) with the equation (C.59), $\forall \xi \in H^1(\Omega)$,

$$\begin{aligned}&\langle \frac{\partial e_{t,\tilde{h}}(x,t)}{\partial t}, \xi(x)\rangle_\Omega - \langle \nabla_x \cdot \Big(\kappa \nabla e_{t,\tilde{h}}(x,t)\Big), \xi(x)\rangle_\Omega + \\ &+ u(x) \cdot \nabla_x e_{t,\tilde{h}}(x,t) = \\ &- \langle \Big(u(x) - u^{\tilde{h}}(x)\Big) \cdot \nabla_x Te(x,t)^{\tilde{h}}, \xi(x)\rangle_\Omega,\end{aligned} \tag{C.60}$$

with zero boundary and initial condition.

According to linear PDE's energy estimation in [107, Theorem 11.1.1],

$$\|e_{t,\tilde{h}}(\cdot,t)\|_1 \to 0. \tag{C.61}$$

And if the system satisfies the additional assumptions in theorem C.5, there exist constants C, which is independent of h, such that,

$$\|e_{t,\tilde{h}}(\cdot,t)\|_1 \leq Ch^m(t)(\|u\|_{m+1}), \tag{C.62}$$

For $\forall t \in [t_0, t_0']$, in order to study the error $\|T_e^{\tilde{h}}(\cdot,t) - T_e^h(\cdot,t)\|_1$, define $e_{t,h}(x,t) = T_e^{\tilde{h}}(x,t) - T_e^h(x,t)$. Substract equation (C.59) with (C.54),

$$\begin{aligned}
&\langle \frac{\partial e_{t,h}(x,t)}{\partial t}, \xi^h(x)\rangle_\Omega - \langle \nabla_x \cdot \Big(\kappa \nabla e_{t,h}(x,t)\Big), \xi^h(x)\rangle_\Omega + \\
&+ \langle u^{\tilde{h}}(x) \cdot \nabla_x e_{t,h}(x,t), \xi^h(x)\rangle_\Omega = 0,\ \forall \xi^h(x) \in H^{1,h}(\Omega),
\end{aligned} \tag{C.63}$$

With zero boundary and initial conditions.

For $e_{t,h}(x,t)$, choose $\xi^h(x) = T_e^h(x,t) - w^h(x)$, $w^h(x) \in T^h$, then $\xi^h(x) = \Big(T_e^{\tilde{h}}(x,t) - w^h(x)\Big) - e_{t,h}(x,t)$, separate the equation (C.63) and according to Schwartz inequality,

$$\begin{aligned}
&\langle \frac{\partial e_{t,h}(x,t)}{\partial t}, e_{t,h}(x,t)\rangle_\Omega - \langle \nabla_x \cdot \Big(\kappa \nabla e_{t,h}(x,t)\Big), e_{t,h}(x,t)\rangle_\Omega + \\
&+ \langle u^{\tilde{h}}(x) \cdot \nabla_x e_{t,h}(x,t), e_{t,h}(x,t)\rangle_\Omega = \\
&\langle \frac{\partial e_{t,h}(x,t)}{\partial t}, e_{t,h}(x,t)\rangle_\Omega - \langle \nabla_x \cdot \Big(\kappa \nabla_x e_{t,h}(x,t)\Big), \\
&e_{t,h}(x,t)\rangle_\Omega = -\langle \frac{\partial e_{t,h}(x,t)}{\partial t}, T_e^{\tilde{h}}(x,t) - w^h(x)\rangle_\Omega + \\
&+ \langle \nabla_x \cdot \Big(\kappa \nabla_x e_{t,h}(x,t)\Big), T_e^{\tilde{h}}(x,t) - w^h(x)\rangle_\Omega + \\
&- \langle u^{\tilde{h}}(x) \cdot \nabla_x e_{t,h}(x,t), T_e^{\tilde{h}}(x,t) - w^h(x)\rangle_\Omega \leq \\
&\leq \|\frac{\partial e_{t,h}(x,t)}{\partial t}\|_0 \|T_e^{\tilde{h}}(x,t) - w^h(x)\|_0 + \\
&+ \lambda_1 \|e_{t,h}(x,t)\|_1 \|T_e^{\tilde{h}}(x,t) - w^h(x)\|_1 + \\
&+ \lambda_2 \|u^{\tilde{h}}(x)\|_\infty \|e_{t,h}(x,t)\|_1 \|T_e^{\tilde{h}}(x,t) - w^h(x)\|_1 \leq \\
&\leq \|\frac{\partial e_{t,h}(x,t)}{\partial t}\|_0 \|T_e^{\tilde{h}}(x,t) - w^h(x)\|_0 + \\
&+ \lambda \|e_{t,h}(x,t)\|_1 \|T_e^{\tilde{h}}(t) - w^h(x)\|_1 \leq \\
&\leq \|\frac{\partial e_{t,h}(x,t)}{\partial t}\|_0 \|T_e^{\tilde{h}}(x,t) - w^h(x)\|_0 + \\
&+ \frac{\lambda^2}{4\varepsilon} \|e_{t,h}(x,t)\|_1^2 + \varepsilon \|T_e^{\tilde{h}}(x,t) - w^h(x)\|_1^2
\end{aligned} \tag{C.64}$$

where λ is independent from h, and $\forall \varepsilon > 0$.

According to lemma A.8, there exists a constant k, independent of h, s.t,

$$
\begin{aligned}
&- \langle \nabla_x \cdot \Big(\kappa \nabla_x e_{t,h}(x,t) \Big), e_{t,h}(x,t) \rangle_\Omega = \\
&= \langle \kappa \nabla_x e_{t,h}(x,t), \nabla_x e_{t,h}(x,t) \rangle_\Omega \geq \\
&\geq k \| e_{t,h}(\cdot,t) \|_1^2
\end{aligned}
$$

According to [107, Corollary 11.1.1], it follows that $T_e^{\tilde{h}}, w_t \in L^2([t_0, t_0']; H^2(\Omega))$. Hence, choosing for almost any $t \in [t_0, t_0']$ $w^h = \pi^h(T_e^{\tilde{h}}(t))$, the projection of $T_e^{\tilde{h}}(x,t)$ into $H^{1,h}(\Omega)$, then,

$$
\begin{aligned}
\| T_e^{\tilde{h}}(\cdot,t) - w^h \|_0^2 &\leq C_{\pi,1} h^2 \| T_e^{\tilde{h}}(\cdot,t) \|_2^2 \\
\| T_e^{\tilde{h}}(\cdot,t) - w^h \|_1^2 &\leq C_{\pi,2} h^2 \| T_e^{\tilde{h}}(\cdot,t) \|_2^2
\end{aligned}
$$

The initial estimation is zero, i.e., $\| e_{t,h}(\cdot,0) \|_0^2 = 0$. Choose $\varepsilon = k/(2\lambda^2)$, integrate (C.64) from t_0 to t_0', there exists a constant, $\tilde{C}_3$, independent of h,

$$
\begin{aligned}
&k \int_{t_0}^{t_0'} \| e_{t,h}(\cdot,\tau) \|_1^2 \leq \| e_{t,h}(\cdot,t) \|_0^2 + k \int_{t_0}^{t_0'} \| e_{t,h}(\cdot,\tau) \|_1^2 \leq \\
&\leq \tilde{C}_3 h^2 \int_{t_0}^{t_0'} (\| \frac{\partial T_e^{\tilde{h}}}{\partial t}(\cdot,\tau) \|_0^2 + \| \frac{\partial T e^h}{\partial t}(\cdot,\tau) \|_0^2) + \\
&+ \| T_e^{\tilde{h}}(\cdot,\tau) \|_2^2) d\tau
\end{aligned}
$$

By [107, Proposition 11.1.1], $\|\frac{\partial T_e^h}{\partial t}(\cdot,t)\|_0^2$ is bounded, thus, there exists a constant, C_3, which is independent of h, such that,

$$\int_{t_0}^{t_0'} \|e_{t,h}(\cdot,\tau)\|_1^2 \leq C_3 h^2 \tag{C.65}$$

Thus, if the system satisfies the additional assumptions in the theorem C.5,

$$\int_{t_0}^{t_0'} \|T_e(\cdot,t) - T_e^h(\cdot,t)\|_1 dt \leq C \max\left(\tilde{h}^m, h^2\right) \tag{C.66}$$

□

Appendix D

Proofs in Chapter 7

In this appendix, we give the detailed proofs of propositions and theorems mentioned in sections 7.2 and 7.3.

Proof to theorem 7.3. Compare problems (7.13) and (7.18), it is sufficient to show the following two optimal problems are equivalent,

$$\begin{aligned}
&\min_{\delta\mu\colon [0,T]\to\mathcal{M}(\mathbb{R}^m)} D\Psi(\mu_0;\delta\mu)+\\
&\qquad -\mathbf{1}(\Phi(\mu_0)>0)\Phi(\mu_0)+\gamma_1\|\delta\mu\|\\
&\text{subject to:}\\
&\qquad \dot{\delta x}(t)=\int_{\mathbb{R}^m}\frac{\partial f}{\partial x}\big(t,x^{(\mu_0)}(t),u\big)\mathrm{d}\mu_{0,t}(u)\delta x(t)+\\
&\qquad\qquad +\int_{\mathbb{R}^m} f\big(t,x^{(\mu_0)}(t),u\big)\mathrm{d}\delta\mu_t(u), \qquad \text{(D.1)}\\
&\qquad \delta x(0)=0,\\
&\qquad \mathrm{supp}(\delta\mu_t+\mu_{0,t})\subset U,\\
&\qquad \delta\mu_t+\mu_{0,t}\geq 0,\\
&\qquad \int_{\mathbb{R}^m}\mathrm{d}\delta\mu_t(u)=0 \text{ for a. e. } t\in[0,T];
\end{aligned}$$

and,

$$\begin{aligned}
&\min_{\delta\mu\colon [0,T]\to\mathcal{M}(\mathbb{R}^m)} \Delta H(\mu_0;\delta\mu) - \mathbf{1}(\Phi(\mu_0)>0)\Phi(\mu_0)+\\
&\qquad + \gamma_1\|\delta\mu\|\\
&\text{subject to:}\\
&\qquad \operatorname{supp}(\delta\mu_t+\mu_{0,t})\subset U,\\
&\qquad \delta\mu_t+\mu_{0,t}\geq 0,\\
&\qquad \int_{\mathbb{R}^m} \mathrm{d}\delta\mu_t(u) = 0 \text{ for a. e. } t\in[0,T].
\end{aligned} \tag{D.2}$$

For the linear system in problem (D.1), define its transition matrix as Φ_{μ_0}, then $\delta x(t)$ follows

$$\delta x(t) = \int_0^t \Phi_{\mu_0}(t,\tau)\int_{\mathbb{R}^m} f\big(\tau, x^{(\mu_0)}(\tau), u\big)\mathrm{d}\delta\mu_\tau(u)d\tau. \tag{D.3}$$

Transition matrix $\Phi_{\mu_0}(t,\tau)$ follows

$$\begin{aligned}
&\frac{\partial\Phi_{\mu_0}}{\partial t}(t,\tau) = \int_{\mathbb{R}^m}\frac{\partial f}{\partial x}\big(t, x^{(\mu_0)}(t), u\big)\mathrm{d}\mu_{0,t}(u)\Phi_{\mu_0}(t,\tau),\\
&\Phi_{\mu_0}(\tau,\tau) = I,\ \forall t,\tau\in[0,T].
\end{aligned} \tag{D.4}$$

Thus the cost function in problem (D.1) can be rewritten as,

$$\begin{aligned}
&D\Psi(\mu_0;\delta\mu) - \mathbf{1}(\Phi(\mu_0)>0)\Phi(\mu_0) + \gamma_1\|\delta\mu\| =\\
&= \frac{\partial\Psi}{\partial x}(x^{\mu_0}(T))'\\
&\qquad \int_0^T \Phi_{\mu_0}(T,\tau)\int_{\mathbb{R}^m} f\big(\tau, x^{(\mu_0)}(\tau), u\big)\mathrm{d}\delta\mu_\tau(u)d\tau.
\end{aligned} \tag{D.5}$$

On the other hand, for problem in equation (D.2), with the help of $\Phi_{\mu_0}(t,\tau)$ in equation (D.4), first we are going to show the adjoint variable, $p_0(t)$, can be written as

$$p_0(t) = \Phi'_{\mu_0}(T,t)p_0(T). \tag{D.6}$$

Since $\forall t, \tau \in [0,T]$, the transition matrix has $\Phi_{\mu_0}(t,\tau)\Phi_{\mu_0}(\tau,t) = I$, thus,

$$\frac{\partial \Phi_{\mu_0}}{\partial \tau}(t,\tau)\Phi_{\mu_0}(\tau,t) + \Phi_{\mu_0}(t,\tau)\frac{\partial \Phi_{\mu_0}}{\partial \tau}(\tau,t) = 0.$$

Then,

$$\begin{aligned}\frac{\partial \Phi_{\mu_0}}{\partial \tau}(t,\tau) &= -\Phi_{\mu_0}(t,\tau)\frac{\partial \Phi}{\partial \tau}(\tau,t)\Phi^{-1}_{\mu_0}(t,\tau) = \\ &= -\Phi_{\mu_0}(t,\tau)\int_{\mathbb{R}^m}\frac{\partial f}{\partial x}\big(\tau, x^{(\mu_0)}(\tau), u\big)\mathrm{d}\mu_{0,\tau}(u)\end{aligned}$$

Consider equation (D.6),

$$\begin{aligned}\dot{p_0}(t) &= \frac{\partial \Phi'_{\mu_0}}{\partial t}(T,t)p_0(T) = \\ &= -\int_{\mathbb{R}^m}\frac{\partial f'}{\partial x}\big(t, x^{(\mu_0)}(t), u\big)\mathrm{d}\mu_{0,t}(u)(t)p_0(t), \\ p_0(T) &= \frac{\partial \Psi}{\partial x}\big(x^{(\mu_0)}\big)(T).\end{aligned}$$

Since it shares the same dynamic and end point value with $p(t)$ in the equation (7.12), $p_0(t)$ in equation (D.6) is the solution to adjoint variable $p(t)$.

Thus the cost function of problem (D.2) can be rewritten as

$$\begin{aligned}&\Delta H(\mu_0;\delta\mu) - \mathbf{1}(\Phi(\mu_0) > 0)\Phi(\mu_0) + \gamma_1\|\delta\mu\| = \\ &= \int_0^T p'_0(T)\Phi_{\mu_0}(T,t)\int_{\mathbb{R}^m} f\big(t, x^{(\mu_0)}(t), u\big)\mathrm{d}\delta\mu_t(u)dt + \\ &\quad - \mathbf{1}(\Phi(\mu_0) > 0)\Phi(\mu_0) + \gamma_1\|\delta\mu\|\end{aligned} \tag{D.7}$$

Based on the rewritten cost functions in equations (D.5) and (D.7), the two optimality functions are equivalent. □

Proof of proposition 7.3. It is sufficient to show when $\Phi(x^{\mu_0}) \leq 0$, there exists $\lambda \in [0,1]$, such that

$$\Psi\big(x^{\mu_0+\lambda\delta\mu_0}(T)\big) - \Psi(x^{\mu_0}(T)) \leq 0,$$

which is equivalent to show

$$\begin{aligned} &\Psi\big(x^{\mu_0+\lambda\delta\mu_0}(T)\big) - \Psi\big(x^{\mu_0}(T) + \lambda\delta x^{\delta\mu_0}(T)\big) + \\ &+ \Psi\big(x^{\mu_0}(T) + \lambda\delta x^{\delta\mu_0}(T)\big) - \Psi(x^{\mu_0}(T)) \leq 0. \end{aligned} \tag{D.8}$$

According to the assumption 7.1, the Lipschitz constant of the system is L, then according to the difference between $x^{\mu_0+\lambda\delta\mu_0}(t)$ and $x^{\mu_0}(t) + \lambda\delta x^{\delta\mu_0}(t)$ in equation (D.8),

$$\begin{aligned} &\Psi\big(x^{\mu_0+\lambda\delta\mu_0}(T)\big) - \Psi\big(x^{\mu_0}(T) + \lambda\delta x^{\delta\mu_0}(T)\big) \leq \\ &\leq L\big|x^{\mu_0+\lambda\delta\mu_0}(T) - x^{\mu_0}(T) - \lambda\delta x^{\delta\mu_0}(T)\big| \leq \\ &\leq \lambda^2 e^{LT} L^2\, T\big\|\delta x^{\delta\mu_0}\big\|_2^2. \end{aligned} \tag{D.9}$$

According to the mean value theorem, $\exists s \in [0,1]$ such that

$$\begin{aligned} &\Psi\big(x^{\mu_0}(T) + \lambda\delta x^{\delta\mu_0}(T)\big) - \Psi(x^{\mu_0}(T)) = \\ &= \lambda\frac{\partial\Psi}{\partial x}(x^{\mu_0}(T))'\delta x^{\delta\mu_0}(T) + \\ &\quad + \lambda^2\delta x^{\delta\mu_0}(T)'\frac{\partial^2\Psi}{\partial x^2}\big(x^{\mu_0}(T) + s\lambda\delta x^{\delta\mu_0}(T)\big)\delta x^{\delta\mu_0}(T) \leq \\ &\leq \lambda\theta_l(\mu_0) + \lambda^2 C_p\big\|\delta x^{\delta\mu_0}(T)\big\|^2. \end{aligned} \tag{D.10}$$

Where we assume the cost function's second derivative is bounded by C_p uniformly. Also we define

$$C_f = \lambda^2 e^{LT} L^2 \, T \big\| \delta x^{\delta\mu_0} \big\|_2^2,$$

according to equation (D.9) and (D.10), the difference between $\Psi\big(x^{\mu_0+\lambda\delta\mu_0}(T)\big)$ and $\Psi(x^{\mu_0}(T))$ is

$$\begin{aligned} &\Psi\big(x^{\mu_0+\lambda\delta\mu_0}(T)\big) - \Psi(x^{\mu_0}(T)) \leq \\ &\leq \lambda\theta(\mu_0) + \lambda^2\Big(C_f + C_p\big\|\delta x^{\delta\mu_0}(T)\big\|^2\Big). \end{aligned} \tag{D.11}$$

Since $\theta(\mu_0) \leq 0$, if

$$\lambda \leq \frac{|\theta(\mu_0)|}{C_f + C_p\|\delta x^{\delta\mu_0}(T)\|^2},$$

$\Psi\big(x^{\mu_0+\lambda\delta\mu_0}(T)\big) - \Psi(x^{\mu_0}(T)) \leq 0.$ □

Proof to proposition 7.7. In the cost function of the discrete optimality problem (7.25), the two terms inside the min and max symbols are both convex, according to Slater's condition, we are able to flip the order of min and max. Then we are able to derive the two separate min-problems (7.30) and (7.31), finally compare and pick the larger one as the result to problem (7.25). □

Proof to proposition 7.8. First, it is easy to show that

$$\begin{aligned} \int_0^T \min_{\hat{w}_{k,i}(t)\in\mathbb{R}} p_0(t)'\Big(\sum_{j=1}^{N_s} f\big(t, x^{(\mu_k)}(t), u_j\big)\,\hat{w}_{k,j}(t)\Big) + \\ + \gamma_1\|\hat{w}_k(t)\|_1\,dt - \mathbf{1}(\Phi(\mu_k) < 0)\Phi(\mu_k) \leq \\ \min_{\hat{w}_{k,i}(t)\in\mathbb{R}} \int_0^T p_0(t)'\Big(\sum_{j=1}^{N_s} f\big(t, x^{(\mu_k)}(t), u_j\big)\,\hat{w}_{k,j}(t)\Big) + \\ + \gamma_1\|\hat{w}_k(t)\|_1\,dt - \mathbf{1}(\Phi(\mu_k) < 0)\Phi(\mu_k). \end{aligned}$$

Suppose the inequality holds strictly, define the optimal solution in proposition 7.8 as $\hat{w}$ and the optimal process in problem (7.31) as $\hat{\omega}$. Then these exists a non-zero measurable set $S \subset [0,T]$, such that

$$\begin{aligned}
&\int_{t\in S} p_0(t)'\Big(\sum_{j=1}^{N_s} f\big(t, x^{(\mu_k)}(t), u_j\big)\, \hat{w}_{k,j}(t)\Big) + \\
&\qquad + \gamma_1 \|\hat{w}_k(t)\|_1 \, dt - \mathbf{1}(\Phi(\mu_k) < 0)\Phi(\mu_k) < \\
&\int_{t\in S} p_0(t)'\Big(\sum_{j=1}^{N_s} f\big(t, x^{(\mu_k)}(t), u_j\big)\, \hat{\omega}_{k,j}(t)\Big) + \\
&\qquad + \gamma_1 \|\hat{\omega}_k(t)\|_1 \, dt - \mathbf{1}(\Phi(\mu_k) < 0)\Phi(\mu_k).
\end{aligned}$$

Then substitute $\hat{\omega}$ with $\hat{w}$ when $t \in S$ make a new feasible candidate to problem (7.31), moreover the cost function of the new candidate is strictly smaller than the cost under $\hat{\omega}$. Which comes to a contradiction. Thus the $\int$ and min in problem (7.31) can be flipped. □

Proof to theorem 7.5. We are going to separate the proof into two lemmas and prove those lemmas.

Lemma D.1. *Follow the notation in theorem 7.5,* $\mathbf{P}_N \to_{epi.} \mathbf{P}$*, as* $N \to \infty$*, i.e. if* $\mu_N \to \mu$ *weakly as* $N \to \infty$*, the cost,* $\Psi(x^{\mu_N}(T)) \to \Psi(x^{\mu}(T))$*.*

Proof. According to the Lipschitz assumption 7.1,

$$\begin{aligned}
&|\Psi(x^{\mu_N}(T)) - \Psi(x^{\mu}(T))| \le L\|x^{\mu_N}(T) - x^{\mu}(T)\| \le \\
&\qquad \le L\ T\ C_f\ \|\mu_N - \mu\|_1,
\end{aligned}$$

where $C_f = sup_{u\in U, t\in[0,T]} f(t, x^u(t), u)$, since control and time is bounded and vector field f is Lipschitz, $C_f < \infty$. According to proposition 7.6, $\|\mu_N - \mu\|_1 \to 0$ as $N \to \infty$. □

Lemma D.2. *Follow the notation in theorem 7.5, if $\mu_N \to \mu$ weakly,* $\lim_{N\to\infty} \sup \theta_N(\mu_N) \leq \theta(\mu)$.

Proof. Define the cost function of discrete problem (7.25) as $\zeta_N(\mu_N; \delta\mu)$, and $\delta\mu_N = \arg\min \zeta_N(\mu_N; \delta\mu)$. Also for the original optimality function in problem (7.13), define $\delta\mu = \arg\min \zeta(\mu_N; \delta\mu)$. Define the discrete representation of $\delta\mu$ with N samples as $S_N(\delta\mu)$.

According to problems (7.13) and (7.25), define

$$C_\zeta = \max_{u\in U, s\in[0,T]} \{ \max_{(i,t)\in\mathcal{I}\times[0,T]} p'_{i,t}(s) f(s, x^\mu(s), u), \\ p'_0(s) f(s, x^\mu(s), u)\},$$

similarly define $C_{N,\zeta}$ as

$$C_{N,\zeta} = \max_{u\in U, s\in[0,T]} \{ \max_{(i,t)\in\mathcal{I}\times[0,T]} p'_{i,t}(s) f(s, x^{\mu_N}(s), u), \\ p'_0(s) f(s, x^{\mu_N}(s), u)\},$$

Since the system is Lipschitz with bounded control and time series, C_ζ and $C_{N,\zeta}$ are bounded,

Then for the difference between $\zeta_N(\mu_N; \delta\mu_N)$ and $\zeta(\mu_N; \delta\mu)$ is

$$\begin{aligned}
&\zeta_N(\mu_N; \delta\mu_N) - \zeta(\mu_N; \delta\mu) \leq \\
&\quad \leq \zeta_N(\mu_N; S_N(\delta\mu)) - \zeta(\mu_N; \delta\mu) \leq \\
&\quad \leq \zeta_N(\mu_N; S_N(\delta\mu)) - \zeta(\mu_N; S_N(\delta\mu)) + \\
&\quad + \zeta(\mu_N; S_N(\delta\mu)) - \zeta(\mu_N; \delta\mu) \leq \\
&\quad \leq \zeta(\mu_N; S_N(\delta\mu)) - \zeta(\mu_N; \delta\mu) \leq \\
&\quad \leq (\max C_\zeta, C_{N,\zeta} + \gamma_1) \| S_N(\delta\mu) - \delta\mu \|_1.
\end{aligned}$$

According to theorem (7.6), as $N \to \infty$, $\|S_N(\delta\mu) - \delta\mu\| \to 0$.

Similarly, we can show as $N \to \infty$,

$$\theta(\mu_N) - \theta(\mu) \to 0.$$

If $\mu_N \to \mu$ as $N \to \infty$, $\lim_{N\to\infty} \theta_N(\mu_N) = \theta(\mu)$. □

Based on the above two lemmas, theorem 7.5 holds. □

References

[1] Robert A Adams and John JF Fournier. *Sobolev spaces*, volume 140. Academic press, 2003.

[2] Abdul Afram and Farrokh Janabi-Sharifi. Theory and applications of HVAC control systems—a review of model predictive control (MPC). *Building and Environment*, 72:343–355, 2014.

[3] Imran Akhtar, Jeff Borggaard, and John A. Burns. High Performance Computing for Energy Efficient Buildings. In *Proceedings of the 8th International Conference on Frontiers of Information Technology*, 2010.

[4] Martin Alnas, Jan Blechta, Johan Hake, August Johansson, Benjamin Kehlet, Anders Logg, Chris Richardson, Johannes Ring, Marie Rognes, and Garth Wells. The fenics project version 1.5. *Archive of Numerical Software*, 3(100), 2015.

[5] Christophe Andrieu, Nando De Freitas, Arnaud Doucet, and Michael I Jordan. An introduction to mcmc for machine learning. *Machine learning*, 50(1-2):5–43, 2003.

[6] ANSI/ASHRAE. *Standard 55–2010 — Thermal Environmental Conditions for Human Occupancy*. ANSI/ASHRAE, 2010.

[7] ANSI/ASHRAE. *Standard 55-2013 — Thermal Environmental Conditions for Human Occupancy*. ANSI/ASHRAE, 2013.

[8] Larry Armijo. Minimization of functions having lipschitz continuous first partial derivatives. *Pacific Journal of mathematics*, 16(1):1–3, 1966.

[9] M Sanjeev Arulampalam, Simon Maskell, Neil Gordon, and Tim Clapp. A tutorial on particle filters for online nonlinear/non-gaussian bayesian tracking. *IEEE Transactions on signal processing*, 50(2):174–188, 2002.

[10] A. Aswani, N. Master, J. Taneja, D. Culler, and C. Tomlin. Reducing transient and steady state electricity consumption in hvac using learning-based model-predictive control. *Proceedings of the IEEE*, 100(1):240–253, Jan 2012.

[11] Anil Aswani, Humberto Gonzalez, Shankar S. Sastry, and Claire J. Tomlin. Provably Safe and Robust Learning-based Model Predictive Control. *Automatica*, 49(5):1216–1226, 2013.

[12] Anil Aswani, Neal Master, Jay Taneja, Andrew Krioukov, David Culler, and Claire J. Tomlin. Energy-efficient Building HVAC Control using Hybrid System LBMPC. In *Proceedings of the 4th IFAC Nonlinear Model Predictive Control Conference*, pages 496–501, 2012.

[13] Hazim B. Awbi. Application of Computational Fluid Dynamics in Room Ventilation. *Building and Environment*, 24(1):73–84, 1989.

[14] Hazim B. Awbi. *Ventilation of Buildings*. Routledge, 2 edition, 2003.

[15] H.B. Awbi and S.J. Allwinkle. Domestic ventilation with heat recovery to improve indoor air quality. *Energy and Buildings*, 9(4):305 – 312, 1986.

[16] Wolfgang Bangerth, Ralf Hartmann, and Guido Kanschat. deal. ii—a general-purpose object-oriented finite element library. *ACM Transactions on Mathematical Software (TOMS)*, 33(4):24, 2007.

[17] H Thomas Banks and Kathleen L Bihari. Modelling and estimating uncertainty in parameter estimation. *Inverse Problems*, 17(1), 2001.

[18] Harvey Thomas Banks, Kathleen Holm, and Franz Kappel. Comparison of optimal design methods in inverse problems. *Inverse Problems*, 27(7), 2011.

[19] Viorel Barbu, Irena Lasiecka, and Roberto Triggiani. Abstract settings for tangential boundary stabilization of navier–stokes equations by high-and low-gain feedback controllers. *Nonlinear Analysis: Theory, Methods & Applications*, 64(12):2704–2746, 2006.

[20] Klaus-Jürgen Bathe and Hou Zhang. Finite Element Developments for General Fluid Flows with Structural Interactions. *International Journal for Numerical Methods in Engineering*, 60(1):213–232, 2004.

[21] Richard Bellman. Dynamic programming and lagrange multipliers. *Proceedings of the National Academy of Sciences*, 42(10):767–769, 1956.

[22] Richard E Bellman and Stuart E Dreyfus. *Applied dynamic programming*. Princeton University Press, 1962.

[23] Sorin C Bengea and Raymond A DeCarlo. Optimal control of switching systems. *automatica*, 41(1):11–27, 2005.

[24] Leonard David Berkovitz. *Optimal control theory*, volume 12. Springer Science & Business Media, 1974.

[25] Dimitri P Bertsekas, Dimitri P Bertsekas, Dimitri P Bertsekas, and Dimitri P Bertsekas. *Dynamic programming and optimal control*. Athena Scientific Belmont, MA, 1995.

[26] J. T. Betts, S. L. Campbell, and N. N. Kalla. Initialization of direct transcription optimal control software. In *42nd IEEE International Conference on Decision and Control*, volume 4, pages 3802–3807, Dec 2003.

[27] John T. Betts. *Practical Methods for Optimal Control and Estimation Using Nonlinear Programming*. Society for Industrial and Applied Mathematics, 2nd edition, 2010.

[28] John T Betts and William P Huffman. Mesh refinement in direct transcription methods for optimal control. *Optimal Control Applications and Methods*, 19(1):1–21, 1998.

[29] Jeff Borggaard, John Allen Burns, Amit Surana, Lizette Zietsman, et al. Control, Estimation and Optimization of Energy Efficient Buildings. In *Proceedings of the 2009 American Control Conference*, pages 837–841, 2009.

[30] Stephen P Boyd and Craig H Barratt. *Linear Controller Design: Limits of Performance*. Prentice hall New Jersey, 1991.

[31] F Brezzi, J Rappaz, and PA Raviart. Finite dimensional approximation of nonlinear problems. *Numerische Mathematik*, 36(1):1–25, 1980.

[32] Arthur Earl Bryson. *Applied optimal control: optimization, estimation and control*. CRC Press, 1975.

[33] John Allen Burns, Xiaoming He, and Weiwei Hu. Control of the Boussinesq Equations with Implications for Sensor Location in Energy Efficient Buildings. In *Proceedings of the 2012 American Control Conference*, pages 2232–2237, 2012.

[34] John Allen Burns and Weiwei Hu. Approximation Methods for Boundary Control of the Boussinesq Equations. In *Proceedings of the 52nd IEEE Conference on Decision and Control*, pages 454–459, 2013.

[35] Claudio Canuto, M Yousuff Hussaini, Alfio Quarteroni, and Thomas A Zang. *Spectral Methods: Fundamentals in Single Domains*. Springer Science & Business Media, 2006.

[36] Xiao Chen, Qian Wang, and Jelena Srebric. Occupant feedback based model predictive control for thermal comfort and energy optimization: A chamber experimental evaluation. *Applied Energy*, 164:341 – 351, 2016.

[37] Jiří Cigler, Samuel Prívara, Zdeněk Váňa, Eva Žáčeková, and Lukáš Ferkl. Optimization of predicted mean vote index within model predictive control framework: computationally tractable solution. *Energy and Buildings*, 52:39 – 49, 2012.

[38] Tayfun Cimen and Stephen P Banks. Global optimal feedback control for general nonlinear systems with nonquadratic performance criteria. *Systems & Control Letters*, 53(5):327–346, 2004.

[39] Joe A. Clarke. *Energy Simulation in Building Design*. Routledge, 2 edition, 2001.

[40] Ian Cleland, Basel Kikhia, Chris Nugent, Andrey Boytsov, Josef Hallberg, Kåre Synnes, Sally McClean, and Dewar Finlay. Optimal placement of accelerometers for the detection of everyday activities. *Sensors*, 13(7):9183–9200, 2013.

[41] J Colin and Y Houdas. Experimental determination of coefficient of heat exchanges by convection of human body. *Journal of Applied Physiology*, 22(1):31–38, 1967.

[42] Dan Crisan and Arnaud Doucet. A survey of convergence results on particle filtering methods for practitioners. *IEEE Transactions on signal processing*, 50(3):736–746, 2002.

[43] Cornelis Cuvelier, August Segal, and Anton A. van Steenhoven. *Finite Element Methods and Navier-Stokes Equations*. Mathematics and Its Applications. D. Reidel Publishing Company, 1986.

[44] Philip J Davis and Philip Rabinowitz. *Methods of numerical integration*. Academic Press, 1984.

[45] Mihir Desai and Kazufumi Ito. Optimal controls of navier–stokes equations. *SIAM Journal on Control and Optimization*, 32(5):1428–1446, 1994.

[46] C. Dobrzynski, Olivier Pironneau, and P. Frey. Numerical Coupling for Air Flow Computations in Complex Architectures. In *Proceedings of the European Congress on Computational Methods in Applied Sciences and Engineering (ECCOMAS)*, 2004.

[47] Charles R Doering and John D. Gibbon. *Applied Analysis of the Navier-Stokes Equations*. Cambridge University Press, 1995.

[48] Alexander Domahidi, Fabian Ullmann, Manfred Morari, and Colin Jones. Learning Near-optimal Decision Rules for Energy Efficient Building Control. In *Proceedings of the 51st IEEE Conference on Decision and Control*, pages 7571–7576, 2012.

[49] Alexander Domahidi, Fabian Ullmann, Manfred Morari, and Colin N Jones. Learning Decision Rules for Energy Efficient Building Control. *Journal of Process Control*, 24(6):763–772, 2014.

[50] Anastasios I Dounis and Christos Caraiscos. Advanced control systems engineering for energy and comfort management in a building environment—A review. *Renewable and Sustainable Energy Reviews*, 13(6):1246–1261, 2009.

[51] Richard M Dudley. *Real analysis and probability*, volume 74. Cambridge University Press, 2002.

[52] Lawrence C. Evans. *Partial Differential Equations*. Graduate Studies in Mathematics. American Mathematical Society, 2 edition, 2010.

[53] Audun Faanes and Sigurd Skogestad. Offset-free tracking of model predictive control with model mismatch: Experimental results. *Industrial & engineering chemistry research*, 44(11):3966–3972, 2005.

[54] Poul O Fanger et al. Thermal comfort analysis and applications in environmental engineering. *Thermal Comfort Analysis and Applications in Environmental Engineering.*, 1970.

[55] Clifford C. Federspiel and Haruhiko Asada. User-adaptable comfort control for hvac systems. *American Control Conference*, 29:2312 – 2319, 1992.

[56] P.M. Ferreira, A.E. Ruano, S. Silva, and E.Z.E. Conceição. Neural networks based predictive control for thermal comfort and energy savings in public buildings. *Energy and Buildings*, 55:238 – 251, 2012. Cool Roofs, Cool Pavements, Cool Cities, and Cool World.

[57] Ciprian Foias, Oscar Manley, Ricardo Rosa, and R. Temam. *Navier-Stokes Equations and Turbulence*. Cambridge University Press, 2001.

[58] Roberto Z. Freire, Gustavo H.C. Oliveira, and Nathan Mendes. Predictive controllers for thermal comfort optimization and energy savings. *Energy and Buildings*, 40(7):1353 – 1365, 2008.

[59] Samuel F. Fux, Araz Ashouri, Michael J. Benz, and Lino Guzzella. EKF Based Self-adaptive Thermal Model for a Passive House. *Energy and Buildings*, 68:811–817, 2014.

[60] Giovanni P Galdi. *An introduction to the mathematical theory of the Navier-Stokes equations: Steady-state problems*. Springer Science & Business Media, 2011.

[61] William L Garrard and John M Jordan. Design of nonlinear automatic flight control systems. *Automatica*, 13(5):497–505, 1977.

[62] Arthur Gelb. *Applied optimal estimation*. MIT press, 1974.

[63] Allan Gersborg-Hansen, Ole Sigmund, and Robert B. Haber. Topology Optimization of Channel Flow Problems. *Structural and Multidisciplinary Optimization*, 30(3):181–192, 2005.

[64] Allan Gersborg-Hansen, Ole Sigmund, and Robert B Haber. Topology optimization of channel flow problems. *Structural and Multidisciplinary Optimization*, 30(3):181–192, 2005.

[65] Michael B Giles and Niles A Pierce. Adjoint equations in CFD: duality, boundary conditions and solution behaviour. In *Proceedings of the 13th Computational Fluid Dynamics Conference*, 1997.

[66] Philip E. Gill, Walter Murray, and Michael A. Saunders. SNOPT: An SQP Algorithm for Large-Scale Constrained Optimization. *SIAM Journal on Optimization*, 12(4):979–1006, 2002.

[67] Vivette Girault and Pierre-Arnaud Raviart. *Finite element methods for Navier-Stokes equations: Theory and algorithms*, volume 5. Springer Science & Business Media, 2012.

[68] Qi Gong, Wei Kang, and I. M. Ross. A pseudospectral method for the optimal control of constrained feedback linearizable systems. *IEEE Transactions on Automatic Control*, 51(7):1115–1129, July 2006.

[69] Humberto Gonzalez, Ram Vasudevan, Maryam Kamgarpour, S Shankar Sastry, Ruzena Bajcsy, and Claire Tomlin. A numerical method for the optimal control of switched systems. In *Decision and Control (CDC), 2010 49th IEEE Conference on*, pages 7519–7526. IEEE, 2010.

[70] Siddharth Goyal and Prabir Barooah. A Method for Model-reduction of Non-linear Thermal Dynamics of Multi-zone Buildings. *Energy and Buildings*, 47:332–340, 2012.

[71] Max Gunzburger. Adjoint equation-based methods for control problems in incompressible, viscous flows. *Flow, Turbulence and Combustion*, 65(3-4):249–272, 2000.

[72] MD Gunzburger, LS Hou, and Th P Svobodny. Analysis and finite element approximation of optimal control problems for the stationary navier-stokes equations with dirichlet controls. *RAIRO-Modélisation mathématique et analyse numérique*, 25(6):711–748, 1991.

[73] S Gutman. Identification of discontinuous parameters in flow equations. *SIAM Journal on Control and Optimization*, 28(5):1049–1060, 1990.

[74] Ion Hazyuk, Christian Ghiaus, and David Penhouet. Optimal Temperature Control of Intermittently Heated Buildings Using Model Predictive Control: Part I – Building Modeling. *Building and Environment*, 51:379–387, 2012.

[75] Ion Hazyuk, Christian Ghiaus, and David Penhouet. Optimal Temperature Control of Intermittently Heated Buildings Using Model Predictive Control: Part II – Control Algorithm. *Building and Environment*, 51:388–394, 2012.

[76] Runxin He and Humberto Gonzalez. Gradient-based estimation of air flow and geometry configurations in a building using fluid dynamic adjoint equations. Proceedings of the 2016 International Compressor, Refrigeration and Air Conditioning, and High Performance Buildings Conferences. arXiv preprint arXiv:1605.05339, 2016.

[77] Runxin He and Humberto Gonzalez. Zoned hvac control via pde-constrained optimization. In *American Control Conference (ACC), 2016*, pages 587–592. IEEE, 2016.

[78] Runxin He and Humberto Gonzalez. Numerical Synthesis of Pontryagin Optimal Control Minimizers Using S ampling-Based Methods. *ArXiv e-prints*, 2017.

[79] L Steven Hou and SS Ravindran. A penalized neumann control approach for solving an optimal dirichlet control problem for the navier–stokes equations. *SIAM Journal on Control and Optimization*, 36(5):1795–1814, 1998.

[80] Gongsheng Huang. Model predictive control of VAV zone thermal systems concerning bi-linearity and gain nonlinearity. *Control Engineering Practice*, 19(7):700–710, 2011.

[81] Hao Huang, Lei Chen, and Eric Hu. A neural network-based multi-zone modelling approach for predictive control system design in commercial buildings. *Energy and Buildings*, 97:86 – 97, 2015.

[82] Runxin He Humberto Gonzalez. OptWrapper Python Library, March 2016.

[83] Victor Isakov. *Inverse problems for partial differential equations*. Springer, 2006.

[84] K. Ito and S. S. Ravindran. Optimal Control of Thermally Convected Fluid Flows. *SIAM Journal on Scientific Computing*, 19(6):1847–1869, 1998.

[85] K. Ito and S. S. Ravindran. Optimal control of thermally convected fluid flows. *SIAM Journal on Scientific Computing*, 19(6):1847–1869, 1998.

[86] Kazufumi Ito and Karl Kunisch. *Lagrange multiplier approach to variational problems and applications*, volume 15. SIAM, 2008.

[87] M. Jin, H. Zou, K. Weekly, R. Jia, A. M. Bayen, and C. J. Spanos. Environmental sensing by wearable device for indoor activity and location estimation. In *IECON 2014 - 40th Annual Conference of the IEEE Industrial Electronics Society*, pages 5369–5375, Oct 2014.

[88] J Jorgensen, J Rawlings, and S Jorgensen. Numerical methods for large-scale moving horizon estimation and control. In *Proceedings of Int. Symposium on Dynamics and Control Process Systems (DYCOPS)*, volume 7, 2004.

[89] Anthony Kelman and Francesco Borrelli. Bilinear Model Predictive Control of a HVAC System Using Sequential Quadratic Programming. In *Proceedings of the 18th IFAC World Congress*, pages 9869–9874, 2011.

[90] Peter Kühl, Moritz Diehl, Tom Kraus, Johannes P Schlöder, and Hans Georg Bock. A real-time algorithm for moving horizon state and parameter estimation. *Computers & chemical engineering*, 35(1):71–83, 2011.

[91] P. R. Kumar and Pravin Varaiya. *Stochastic Systems: Estimation, Identification, and Adaptive Control*. SIAM, 2015.

[92] Lev D. Landau and Evgeny M. Lifshitz. *Fluid Mechanics: Course of Theoretical Physics, Volume 6*. Butterworth-Heinemann, 2 edition, 1987.

[93] Anders Logg, Kent-Andre Mardal, and Garth Wells. *Automated solution of differential equations by the finite element method: The FEniCS book*. Springer, 2012.

[94] Anders Logg, Kent-Andre Mardal, and Garth N. Wells. *Automated Solution of Differential Equations by the Finite Element Method: The FEniCS Book*. Lecture Notes in Computational Science and Engineering. Springer, 2012.

[95] Yudong Ma, J Matusko, and Francesco Borrelli. Stochastic Model Predictive Control for Building HVAC Systems: Complexity and Conservatism. *IEEE Transactions on Control Systems Technology*, 23(1):101–116, 2013.

[96] David Q Mayne, James B Rawlings, Christopher V Rao, and Pierre OM Scokaert. Constrained model predictive control: Stability and optimality. *Automatica*, 36(6):789–814, 2000.

[97] Petru-Daniel Moroşan, Romain Bourdais, Didier Dumur, and Jean Buisson. Building temperature regulation using a distributed model predictive control. *Energy and Buildings*, 42(9):1445–1452, 2010.

[98] Kevin P Murphy. *Machine learning: a probabilistic perspective*. MIT press, 2012.

[99] Jorge Nocedal and Stephen Wright. *Numerical optimization*. Springer, 2006.

[100] F. Oldewurtel, C. N. Jones, A. Parisio, and M. Morari. Stochastic model predictive control for building climate control. *IEEE Transactions on Control Systems Technology*, 22(3):1198–1205, May 2014.

[101] Frauke Oldewurtel, Alessandra Parisio, Colin N. Jones, Dimitrios Gyalistras, Markus Gwerder, Vanessa Stauch, Beat Lehmann, and Manfred Morari. Use of model predictive control and weather forecasts for energy efficient building climate control. *Energy and Buildings*, 45:15 – 27, 2012.

[102] Georg Pingen, Anton Evgrafov, and Kurt Maute. Topology Optimization of Flow Domains Using the Lattice Boltzmann Method. *Structural and Multidisciplinary Optimization*, 34(6):507–524, 2007.

[103] Elijah Polak. *Optimization: algorithms and consistent approximations*, volume 124. Springer Science & Business Media, 1997.

[104] Lev Semenovich Pontryagin. *Mathematical theory of optimal processes*. CRC Press, 1987.

[105] Paul Pounds, Robert Mahony, and Peter Corke. Modelling and control of a quadrotor robot. In *Proceedings Australasian Conference on Robotics and Automation 2006*. Australian Robotics and Automation Association Inc., 2006.

[106] Samuel Prívara, Jan Širokỳ, Lukáš Ferkl, and Jiří Cigler. Model predictive control of a building heating system: The first experience. *Energy and Buildings*, 43(2):564–572, 2011.

[107] Alfio Quarteroni and Alberto Valli. *Numerical approximation of partial differential equations*, volume 23. Springer Science & Business Media, 2008.

[108] Anil V Rao. A survey of numerical methods for optimal control. *Advances in the Astronautical Sciences*, 135(1):497–528, 2009.

[109] Christopher V Rao, James B Rawlings, and Jay H Lee. Constrained linear state estimation—a moving horizon approach. *Automatica*, 37(10):1619–1628, 2001.

[110] Christopher V Rao, James B Rawlings, and David Q Mayne. Constrained state estimation for nonlinear discrete-time systems: Stability and moving horizon approximations. *Automatic Control, IEEE Transactions on*, 48(2):246–258, 2003.

[111] Jean-Pierre Raymond. Feedback boundary stabilization of the two-dimensional navier–stokes equations. *SIAM Journal on Control and Optimization*, 45(3):790–828, 2006.

[112] Clarence W Rowley. Model reduction for fluids, using balanced proper orthogonal decomposition. *International Journal of Bifurcation and Chaos*, 15(03):997–1013, 2005.

[113] Angela Sasic Kalagasidis. *HAM-tools an integrated simulation tool for heat, air and moisture transfer analyses in building physics*. Chalmers University of Technology, 2004.

[114] Adam Lowell Schwartz. *Theory and implementation of numerical methods based on Runge-Kutta integration for solving optimal control problems*. PhD thesis, University of California at Berkeley, 1996.

[115] Pervez Hameed Shaikh, Nursyarizal Bin Mohd Nor, Perumal Nallagownden, Irraivan Elamvazuthi, and Taib Ibrahim. A review on optimized control systems for building energy and comfort management of smart sustainable buildings. *Renewable and Sustainable Energy Reviews*, 34:409 – 429, 2014.

[116] Zhenjun Ma Shengwei Wang. Supervisory and optimal control of building hvac systems: A review. *HVAC&R Research*, 14(1):3–32, 2008.

[117] S. L. Sinha, R. C. Arora, and Subhransu Roy. Numerical Simulation of Two-Dimensional Room Air Flow with and without Buoyancy. *Energy and Buildings*, 32(1):121–129, 2000.

[118] H. Sun, R. R. Stowell, H. M. Keener, and F. C. Michel. Two-dimensional Computational Fluid Dynamics (CFD) Modeling of Air Velocity and Ammonia Distribution in a High-Rise Hog Building. *Transactions of the ASAE*, 45(5):1559–1568, 2002.

[119] Giovanni Maria Troianiello. *Elliptic differential equations and obstacle problems*. Springer Science & Business Media, 2013.

[120] U.S. Department of Energy. 2011 Buildings Energy Data Book, March 2012.

[121] U.S. Green Building Council. Better Buildings, Better Policy: A compilation of green building policy adoptions in the United States, 2011-2014, 2014.

[122] Héctor Valdés-González, Jean-Marie Flaus, and Gonzalo Acuña. Moving horizon state estimation with global convergence using interval techniques: application to biotechnological processes. *Journal of process control*, 13(4):325–336, 2003.

[123] Erwin P. van der Poel, Richard J. A. M. Stevens, and Detlef Lohse. Comparison Between Two- and Three-Dimensional Rayleigh–Bénard Convection. *Journal of Fluid Mechanics*, 736:177–194, 2013.

[124] A. W. M. van Schijndel. Multiphysics Modeling of Building Physical Constructions. *Building Simulation*, 4(1):49–60, 2011.

[125] Ramanarayan Vasudevan, Humberto Gonzalez, Ruzena Bajcsy, and S. Shankar Sastry. Consistent Approximations for the Optimal Control of Constrained Switched Systems—Part 1: A Conceptual Algorithm. *SIAM Journal on Control and Optimization*, 51(6):4463–4483, 2013.

[126] Ramanarayan Vasudevan, Humberto Gonzalez, Ruzena Bajcsy, and S. Shankar Sastry. Consistent Approximations for the Optimal Control of Constrained Switched Systems—Part 2: An Implementable Algorithm. *SIAM Journal on Control and Optimization*, 51(6):4484–4503, 2013.

[127] Andreas Wächter and Lorenz T. Biegler. On the implementation of an interior-point filter line-search algorithm for large-scale nonlinear programming. *Mathematical Programming*, 106(1):25–57, Mar 2006.

[128] Nadine Walikewitz, Britta Jänicke, Marcel Langner, Fred Meier, and Wilfried Endlicher. The difference between the mean radiant temperature and the air temperature within indoor environments: A case study during summer conditions. *Building and Environment*, 84:151 – 161, 2015.

[129] J. Warga. Relaxed variational problems. *Journal of Mathematical Analysis and Applications*, 4(1):111 – 128, 1962.

[130] Jack Warga. *Optimal control of differential and functional equations*. Academic press, 1972.

[131] M. S. Waring and J. A. Siegel. Particle Loading Rates for HVAC Filters, Heat Exchangers, and Ducts. *Indoor Air*, 18:209–224, 2008.

[132] Stephen Wright and Jorge Nocedal. Numerical optimization. *Springer Science*, 35:67–68, 1999.

[133] Xue-Cheng Xi, Aun-Neow Poo, and Siaw-Kiang Chou. Support vector regression model predictive control on a HVAC plant. *Control Engineering Practice*, 15(8):897–908, 2007.

[134] Che-Chang Yang and Yeh-Liang Hsu. A review of accelerometry-based wearable motion detectors for physical activity monitoring. *Sensors*, 10(8):7772–7788, 2010.

[135] Insoon Yang and Claire J Tomlin. Reaction–diffusion systems in protein networks: Global existence and identification. *Systems & Control Letters*, 74:50–57, 2014.

[136] Baris Yuce, Haijiang Li, Yacine Rezgui, Ioan Petri, Bejay Jayan, and Chunfeng Yang. Utilizing artificial neural network to predict energy consumption and thermal comfort level: An indoor swimming pool case study. *Energy and Buildings*, 80:45 – 56, 2014.

[137] Victor M Zavala, Carl D Laird, and Lorenz T Biegler. A fast computational framework for large-scale moving horizon estimation. In *Proceedings of 8th International Symposium on Dynamics and Control of Process Systems, Cancun, Mexico*, 2007.

[138] Kemin Zhou, John Comstock Doyle, Keith Glover, et al. *Robust and optimal control*, volume 40. Prentice hall New Jersey, 1996.

[139] William P. Ziemer. *Weakly Differentiable Functions*. Graduate Texts in Mathematics. Springer, 1989.

[140] Olgierd Cecil Zienkiewicz, Robert Leroy Taylor, and Robert Lee Taylor. *The finite element method*, volume 3. McGraw-hill London, 1977.

Vita

Runxin He

Degrees

Ph.D., Electrical Engineering, Washington University in St. Louis, Missouri, USA, August 2017
M.S., Electrical Engineering, Washington University in St. Louis, Missouri, USA, May 2017
M.S., Data Analysis and Statistics, Washington University in St. Louis, Missouri, USA, May 2017
B.S., Electrical Engineering, Fudan University, Shanghai, China, July 2012

Professional Memberships

The Institute of Electrical and Electronics Engineers (IEEE)

Publications

Journal Publications:

R. He and H. Gonzalez, "Model Predicted Controller for Indoor Thermal Comfort based on Fluid Dynamics' Adjoint Equations," submitted.

R. He and H. Gonzalez, "Numerical Sampling-based Method to Pontryagin Optimal Control Minimizers in State-constrained Problems," preparing.

Conference Publications:

R. He and H. Gonzalez, "Numerical Synthesis of Pontryagin Optimal Control Minimizers Using Sampling-Based Methods," submitted.

R. He and H. Gonzalez, "Gradient-Based Estimation of Air Flow and Geometry Configurations in a Building Using Fluid Dynamic Adjoint Equations," in *2016 International High Performance Buildings Conference*, pp.3446.1–3446.10, Purdue University, USA, July. 2016.

R. He and H. Gonzalez, "Zoned HVAC Control via PDE-Constrained Optimization," in *2016 American Control Conference*, Boston, USA, July. 2015, pp. 587–592.

August 2017